THE SPECTROSCOPIC STUDY OF AN ELECTRODELESS DISCHARGE IN ARGON AT ATMOSPHERIC PRESSURE

P. D. Johnston, B.Sc., A.R.C.S.
Imperial College, London

A THESIS SUBMITTED FOR THE DEGREE OF DOCTOR OF PHILOSOPHY

ABSTRACT

The determination of temperature in discharge sources such as plasma jets, arcs, and shock tubes, can be made by a simple method involving the measurement of the relative intensities of spectral lines emitted by the discharge, provided their transition probabilities are known and the conditions of local thermodynamic equilibrium, (L.T.E), pertain to the discharge. The more transition probabilities available and the greater the spread of the appropriate upper energy levels, the better the accuracy of the temperature determination.

With a view to measuring transition probabilities in neutral argon, a new type of discharge, the radio-frequency discharge at atmospheric pressure was investigated. A previous temperature measurement of a similar discharge operating under similar conditions was shown to be incorrect by a factor of 2 owing to an erroneous interpretation of the results of a method inapplicable to this type of discharge.

The radio-frequency discharge was shown to operate within the conditions of local thermodynamic equilibrium and was proved to be eminently suitable for the measurement of transition probabilities.

A reversal technique for temperature determination was adapted to this discharge and, once the temperature had been obtained to a high degree of accuracy, the intensities of 116 neutral argon lines were measured and their transition probabilities determined. Many of these lines had never been measured before, consequently, to afford some comparison, the transition probabilities were calculated in LS, J_1 and intermediate coupling. These calculations considerably extended any previous calculations and, where there was duplication with the only previous calculation, eight significant discrepancies were found.

C O N T E N T S

ILLUSTRATIONS AND TABLES

PHOTOGRAPHS

P A R T I

THE SPECTROSCOPIC PROPERTIES OF THE R.F. DISCHARGE IN ARGON AT ATMOSPHERIC PRESSURE

CHAPTER 1

The Radio-frequency Discharge

Introduction

Induced discharges in static gases at atmospheric pressure were first reported by Babat (ref. 1) and a "plasma-torch", based on inductive coupling between a radio-frequency field and a flowing ionised gas, was developed by Reed (ref. 2). Temperature and electron density measurements were, up to 1964, sketchy, assumed from other people's work, or incorrect. The work described in the first part of this thesis was performed (cf Chapter 2) to remedy this, and to investigate the possible spectroscopic uses of this newly-developed, high-intensity discharge.

In the course of this preliminary survey, the need for neutral argon transition probabilities became apparent. Those already available, either as experimental or theoretical values were few and clustered in two distinct energy ranges (cf Chapter 4). In discharges such as arcs, plasma jets, and shock-tubes, where local thermodynamic equilibrium obtains, a measurement of the relative line intensities of spectral line intensities from the neutral species will give the temperature pertaining to the discharge, provided the transition probabilities of the lines involved are known. The more transition probabilities available and the greater the energy spread of their appropriate upper levels, the greater the accuracy of the temperature determination. Also, with more values available, deviations from thermal equilibrium would become apparent so that corresponding corrections could be made.

The preliminary survey of the discharge showed it to be in local thermodynamic equilibrium (cf Chapter 3) and comparison with other

discharge source proved it to be eminently suitable for measuring transition probabilities in neutral argon (cf Chapter 4).

To effect an accurate temperature determination for this purpose, a reversal method , which takes into account spatial inhomogeneities but had only previously been applied to a low temperature sodium seeded brush discharge, was applied to this discharge. This method was chosen for its independence of any transition probability, the requirement of local thermodynamic equilibrium between the states involved in the transition being the only stipulation (cf Chapter 5).

The temperature was determined accurately and with this knowledge, the transition probabilities of 116 neutral argon lines obtained by measurement of their intensities (cf Chapter 6). No comparison could be made with previous measurements for most of these values since only 36 neutral lines had previously been measured, consequently values were computed in LS, J_1 j, and intermediate coupling (cf Chapter 7). A discussion of these results is presented in Chapter 8.

Throughout the thesis, mention is made of various topics or methods which will be familiar to the spectroscopist or "plasma diagnostician". However, for those not familiar with terms such as 'local thermodynamic equilibrium' or 'Abel inversion' for example, either a description is given in the appendices, or a reference is given from which details can be obtained. This avoids digression and, I hope, promotes the continuity of the thesis.

Historical Background

The first reported work on electrodeless discharges at pressures up to one atmosphere was that of Babat (ref. 1), who, in 1941 investigated the operating characteristics of capacitively and inductively coupled discharges. In his paper, published in 1947, he reported studies made on electrodeless discharges of different configurations at frequencies from 10^6 Hz to 10^8 Hz and for powers up to 100 KW. He discussed 'E' field discharges and 'H' field discharges. The investigations were carried out over a wide range of pressure with air as the discharge gas.

No description was given by Babat of any temperature measurement, although temperature profiles across the discharges, (in arbitrary units) were given, deduced from the electrical characteristics.

The next reported work was that of Reed (refs. 2, 3) who developed the atmospheric-pressure radio-frequency discharge for crystal growing. This was the first reported instance in which gas flowed through the discharge and generated an 'arc-jet'. The electrodeless discharges of Babat were, although similar, entirely enclosed.

Reed used a simple quartz tube with a single tangential gas inlet at one end and, near the other open end, the radio-frequency coil was wound around the tube. He operated the discharge at 4 MHZ and at powers up to 10 KW. To start the discharge, a pilot arc was formed upstream by a conventional 30 amp, D.C. arc, the R-F power was then switched on, the R-F discharge formed and the D.C. arc switched off. He found later that the R-F discharge could be initiated by an earthed carbon rod, placed in the tube within the coils, which started a brush discharge; increasing the power to the

coil caused the R-F discharge to form suddenly from this preliminary discharge. Reed's experiments were conducted in argon and argon/oxygen mixtures. He measured the temperature of the discharge by the Fowler-Milne method which had been used by Olsen (ref. 4) to measure the temperature of a DC arc. This method relies on the fact that the intensity of a given spectral line increases with increasing temperature, reaches a maximum, and then decreases owing to depopulation of the neutral atom ground state as ionisation becomes extensive. When the population of the levels is governed by Boltzmann's equation, this maximum occurs at a known temperature for a given pressure. If pressure balance in the discharge is assumed, the intensity of the spectral line thus becomes a function of the discharge temperature only.

Reed measured the intensity of the 7635Å line of neutral argon across a diameter of the discharge, and converted the observed integrated distribution into a radial distribution by means of the "Abel inversion technique" (cf Appendix 5). This radial profile exhibited off-axis peaks in intensity which he then identified with the aforementioned intensity maximum (corresponding to 16,000°K), and, assuming a monatonic increase in temperature to the centre of the discharge obtained the radial temperature-profile shown in fig. 1.1. Using this measurement as an intensity calibration he obtained the temperature throughout the discharge as shown in fig. 1.2. The justification for invoking local thermodynamic equilibrium, LTE, was the similarity of the results with those obtained by Olsen (ref. 4) for the D.C. arc.

The next reported work was that of Galtier (ref. 5) who described an induction discharge similar to that of Reed's. He states, without mentioning how it was obtained, that a maximum

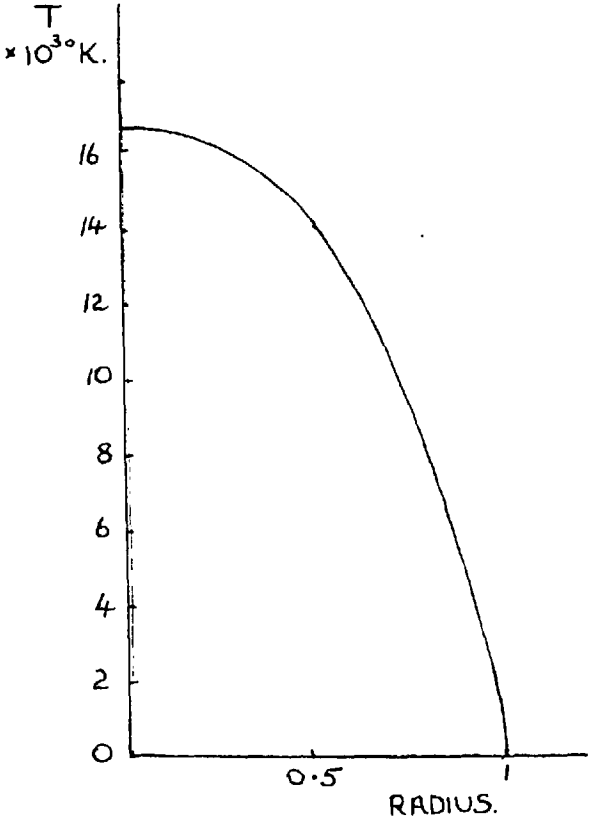

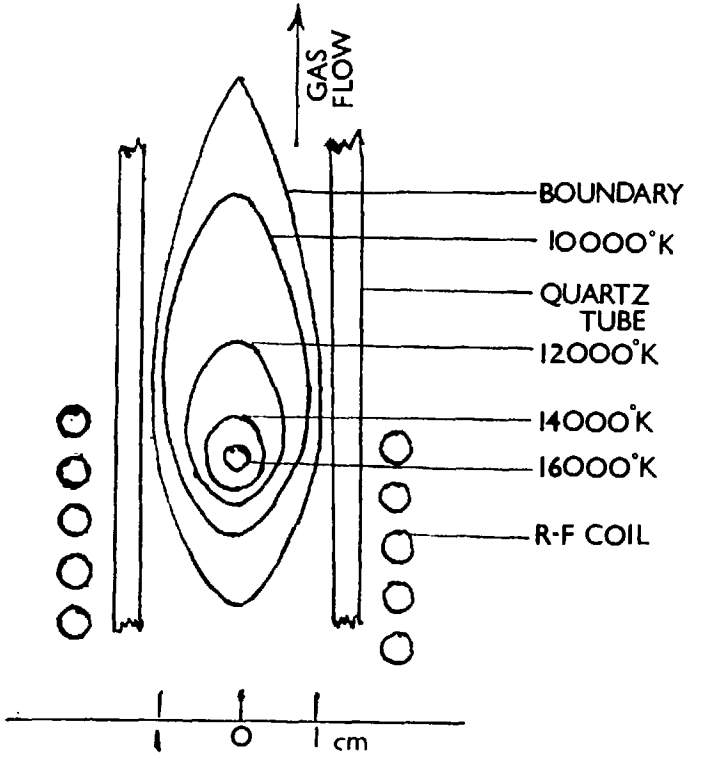

FIG 1.1 & 1.2 Reed's temperature measurement

temperature of 20,000°C was reached at the centre of the discharge.

In 1963, Reboux (ref. 6) Marynowski and Munroe (ref. 7) Mironer and Hushfar (ref. 8) and Clement and Consoli (ref. 9) all described work done on radio-frequency induction discharges. The first of these papers, a review of applications of inductive discharges, again quotes axial temperatures of the order of 20,000°K, although no description is given of how, or from whom, this value is obtained. The first part of the symposium paper by Marynowski deals with the applications of the "plasma torch", describes the equipment, the initiation and stabilisation of the discharge, and givesoperating results of power versus argon gas flow for stable operation. The second part of the paper, by Munroe, compares DC arc and RF discharge heating, and here, an axial temperature of 15,000°K is quoted without justification. Mironer and Hushfar (ref. 8) describe basic theoretical and experimental work done on "radio-frequency energy addition" to a dense moving plasma stream. Both the "E" and "H" type of discharge are discussed and a one-dimensional flow analysis performed for an ionised flowing gas undergoing energy addition. The experimental part of the paper discusses coil configurations and efficiency curves obtained for them. No discharge diagnostics were performed by these authors.

Clement et al (ref. 9) measured the temperature of an induction-coupled discharge by three different spectroscopic methods, and studied the reflection of 8.52 mm. waves, and the scattering of ruby-laser light, by the discharge. This discharge, in a quartz tube 27 mm. in diameter with an argon flow rate of 6 to 10 litres/minute was excited by 2 KW of 3 MH_z radio-frequency

power. The temperature of the discharge was measured by a relative line intensity method (cf Chapter 2), by the Stark broadening of H_β by adding a small amount of hydrogen to the argon (cf Chapter 5) and by measuring the absolute intensities of neutral argon lines. The first method gave a value of 7,550°K, the second 9,800°K and the third 8,600°K for the maximum temperature. These values are significantly different from the others quoted above.

During this period, various papers appeared in journals concerned with analytical chemistry by chemists using inductive discharges, "plasma torches", for the chemical analysis of powders and aerosols. None of these papers described temperature or electron density determinations and few described operating characteristics of the discharge, so, for the purposes of this review, they are ignored.

Description of the Apparatus

The generator of radio-frequency power was a Radyne C155/P power unit, which had a self-oscillating Colpitts-type output circuit using two air-cooled silica-enveloped triodes in parallel. The oscillatory circuit comprised the induction coil and the tank capacitance, which, together, determined the operating frequency. The tank capacitance, divided into three sections, between the valve grids and earth, anodes and earth, and output terminals to the coil and anodes, was altered, together with the coil configuration, to achieve maximum stability of the discharge with the correct load matching of the power unit.

The loading of the oscillator was affected by the configuration of the discharge tube, the type and flow of gas, and the size and number of turns of the discharge coil. Consequently, each time a different form of discharge tube was used, the tank circuit capacitance had to be changed.

The discharge tube itself consisted of a quartz tube, open at one end, with the argon gas feed at the other, around which the induction coil was placed. This quartz tube could be water-cooled or air-cooled.

There are six different methods for starting the discharge:-

1. Pilot arc discharge:- as employed initially by Reed (ref. 2). This consists of a small DC or AC pilot arc, started upstream and then withdrawn and extinguished, after the r-f discharge has coupled with it and formed.
2. Low-pressure breakdown:- attaching the open end of the discharge tube to a pumping line and reducing the pressure in the discharge tube to 1 mm. will allow the r-f discharge to form spontaneously on application of power to the induction coil. Once the discharge is formed the pressure and power input to the coil can be increased until the required operating regime is reached.
3. Pointed conductors:- introducing a sharp pointed conductor into the quartz tube within the r-f coils causes corona breakdown at the tip owing to the convergence there of the field flux lines. This corona breakdown then leads to a spark-type breakdown which in turn leads to a stable r-f discharge once the power level and gas flow are suitable.

4. Heated conductor:- if, instead of being sharp, the conductor in the above case is any shape, when left for several seconds in the r-f field within the coil, inductive heating will raise its temperature to a point where thermal emission of electrons can be sufficient to start a pilot discharge.

   In this and the previous case, the conductor is removed once the main discharge has formed.

5. Tesla coil:- a Tesla coil, placed outside the quartz tube and downstream from the r-f coil can initiate a pilot discharge and thus avoid putting anything into the discharge tube which could affect the discharge by contamination as in the case of the earthed conductors or by r-f sputtering from electrodes as in the case of the pilot arc.

6. Laser induced breakdown:- although rather exotic in nature there is no reason why the r-f discharge could not be initiated by a plasma formed at the focus of a pulsed ruby laser. As with the last method, this would avoid any possible contamination and would be eminently suitable for an enclosed discharge system.

The method used by Babat (ref. 1) was the second. Reed (ref. 2,3) at first used the pilot arc but found that an earthed conductor, using a combination of methods 3 and 4, was far simpler and just as effective. To the author's knowledge, no-one has yet used the last method to initiate the r-f discharge.

In the work described here, the discharge was initiated by introducing an earthed carbon rod into the end of the discharge tube (method 3) with argon flowing through the tube and about 5 KV anode potential on the work coil. This causes a corona discharge at the end of the conductor, which then produces electrical discharges

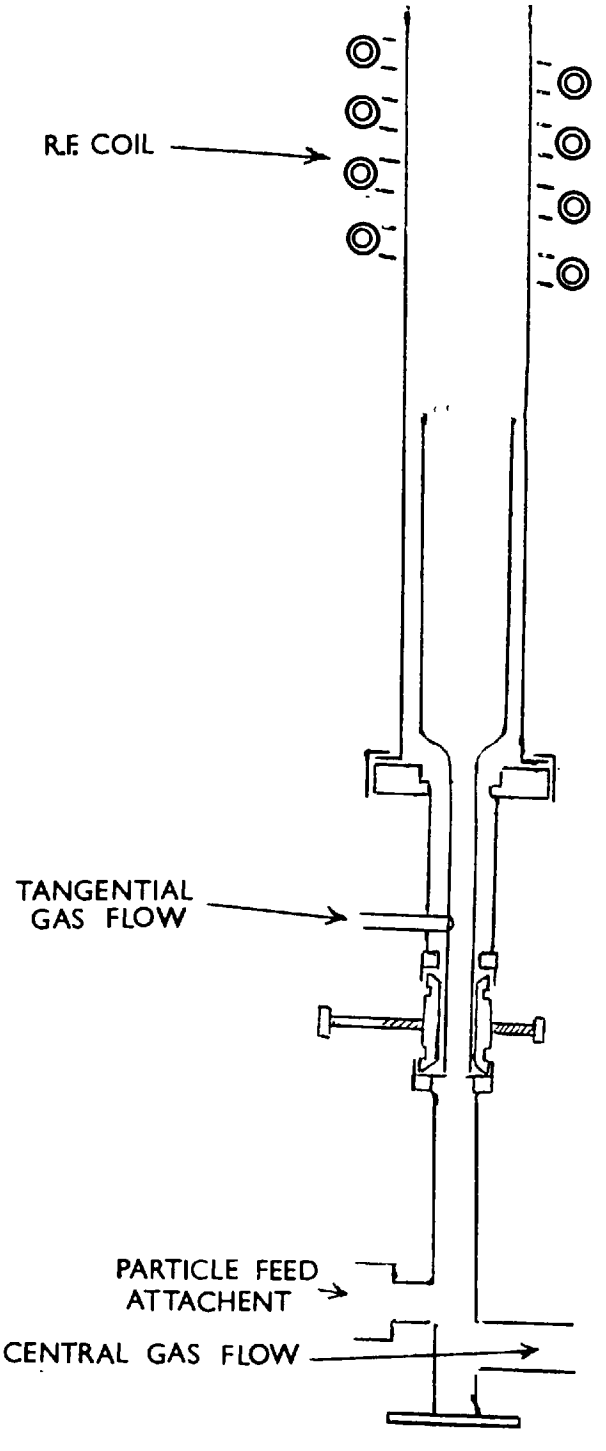

Fig 1.3 Discharge tube.

streaming up the discharge tube along the argon flow lines. By adjusting the power input and gas flow rate, this electrical discharge suddenly avalanched to the r-f discharge.

Initially a quartz tube 24 mm. in diameter with a side-arm for gas feed and a five turn coil around it was tried. The discharge formed in this tube immediately started to heat the quartz walls which collapsed. Increasing the gas flow caused the discharge to become unstable and oscillate in the tube while higher flows caused it to be extinguished. To prevent the overheating, a water jacket was attached below the coil, but overheating still occurred at the junction between the water jacket and the tube. A pyrex tube, watercooled its entire length, was unsuccessful, since pyrex was unable to stand the thermal shock of the discharge forming in the first place.

Two configurations of discharge tube proved successful - a 25 mm. diameter quartz tube, watercooled its entire length with the r-f coil outside the waterjacket, and a 48 mm. diameter uncooled quartz tube. The second of these two was chosen here since a waterjacket not only reduces the power input to the discharge but also creates focussing problems in optical diagnostics.

The chosen configuration is shown in fig. 1.3 and photo 1. A tangential gas flow of 1 litre/sec. with 3 K.V. and 2 amps at 4.5 MHZ. was used in all the experiments described here. No centre flow was used, the centre tube acted as a baffle since the discharge required a turbulent flow for operating; consequently the part of the tangential gas flow adjacent to the centre tube became turbulent while that adjacent to the quartz tube stayed against the walls and kept them cool. This tube was operated for several hours continuously without any damage to the quartz wall. The centre tube could be used for introducing other gases or solids in particle form into the discharge.

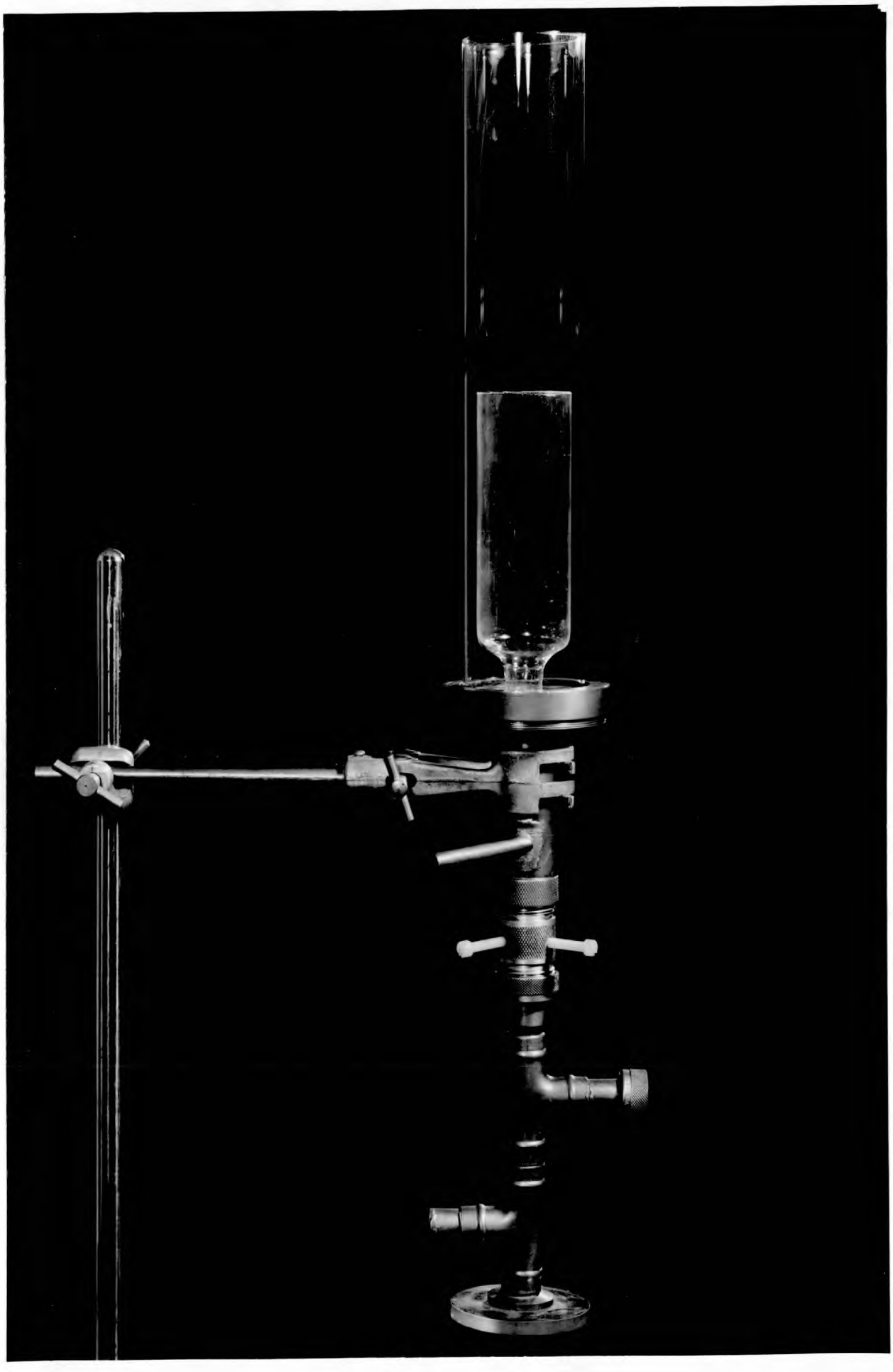

I

With every change of discharge tube configuration described above, the oscillator circuit had to be re-adjusted for optimum load-matching.

Preliminary Survey of the Discharge

The first experiment performed on the stable discharge was that of photographing its spectrum. The discharge was set up in front of a 10 ft. normal incidence Eagle spectrograph and plates taken in the first order of a 10,000 line per inch grating over the range 3,000 - 8,000Å using Ilford LRS, Astra III and Kodak II-N plates. The plates were developed in the usual manner and a recording trace obtained from them by means of a microdensitometer.

If the temperature of the discharge was of the order of 15,000°K or more, as measured by Reed (ref. 2), one would expect a considerable number of argon II lines to be emitted by the discharge and some of them would have intensities comparable to those of argon I lines. However, not a single argon II line could be detected from the plates or the micro-densitometer traces - an example of one of the traces is shown in fig. 1.4 with the expected positions of argon II lines noted on it. This indicated that the temperature within the discharge must be lower than about 10,000°K since above this temperature argon II emission should become detectable. To make sure that this was not a local effect, plates were taken from sample portions of the discharge throughout its entirety. No argon II emission was detected.

When monitoring the frequency of the applied radio-frequency power on a Tektronix 551 oscilloscope, it was noted that the applied

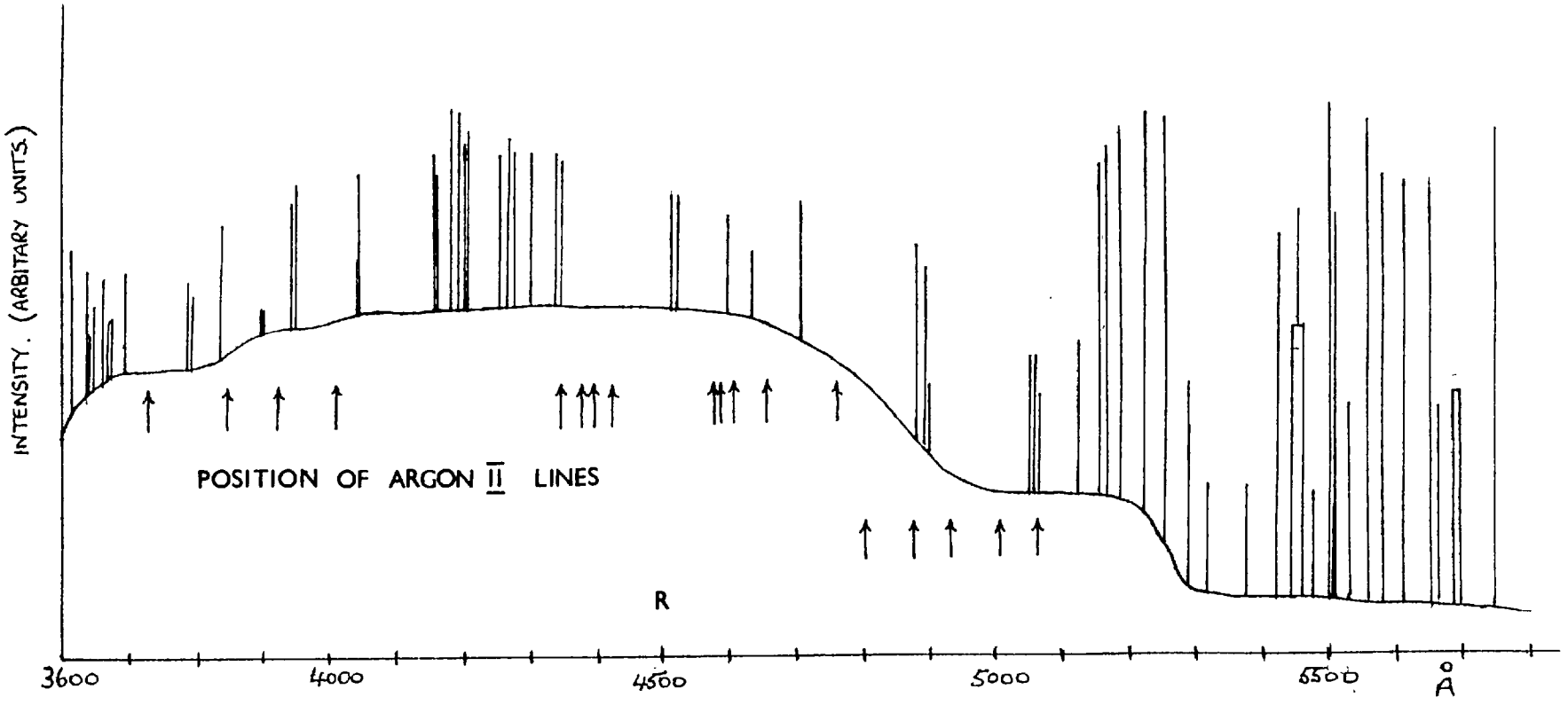

FIG 1.4 Emission from the R-F discharge

voltage and current both fluctuated at 300 HZ with a peak.to peak variation of about 5% of the total 4.5 MHZ oscillation. Also the 4.5 MHZ frequency of the generator had a superimposed ripple of 30 MHZ. To determine whether these had any effect on the discharge light output, a constant deviation spectrograph with an RCA 931A side-window photomultiplier attached behind the exit slit, was used to investigate any frequency dependence of the emission from the discharge. The Tektronix 551 oscilloscope was used to measure the output from the photomultiplier. No variation of light output at the 4.5 or 30 MHZ frequency was detected but both the spectral lines and the continuum varied at 300 HZ. The degree of the peak to peak variation was ± 20% for both the spectral lines and the continuum. This 300 HZ light intensity variation could be caused by one of two different effects. Either -

a) the discharge volume was fluctuating due to the power input to it fluctuating, and causing a fluctuating integrated intensity, or

b) the discharge volume was remaining constant and the temperature varying, causing the line and continuum emission to vary.

The first of these two possibilities was the one expected since the size of the discharge was dependent on the power input.

Since the edges of the discharge were well defined, c.f. photo 2, any fluctuation in size should have been easily detectable, whereas a variation in temperature, which would amount to only a few per cent to cause 20% emission variation, would not cause the luminous zone to increase in volume appreciably since the temperature gradient at the edges must have been very steep.

Consequently, to decide between these effects, a rotating drum camera was used to see if there was any variation in the diametrical size of the discharge. A Robot camera shutter was placed in

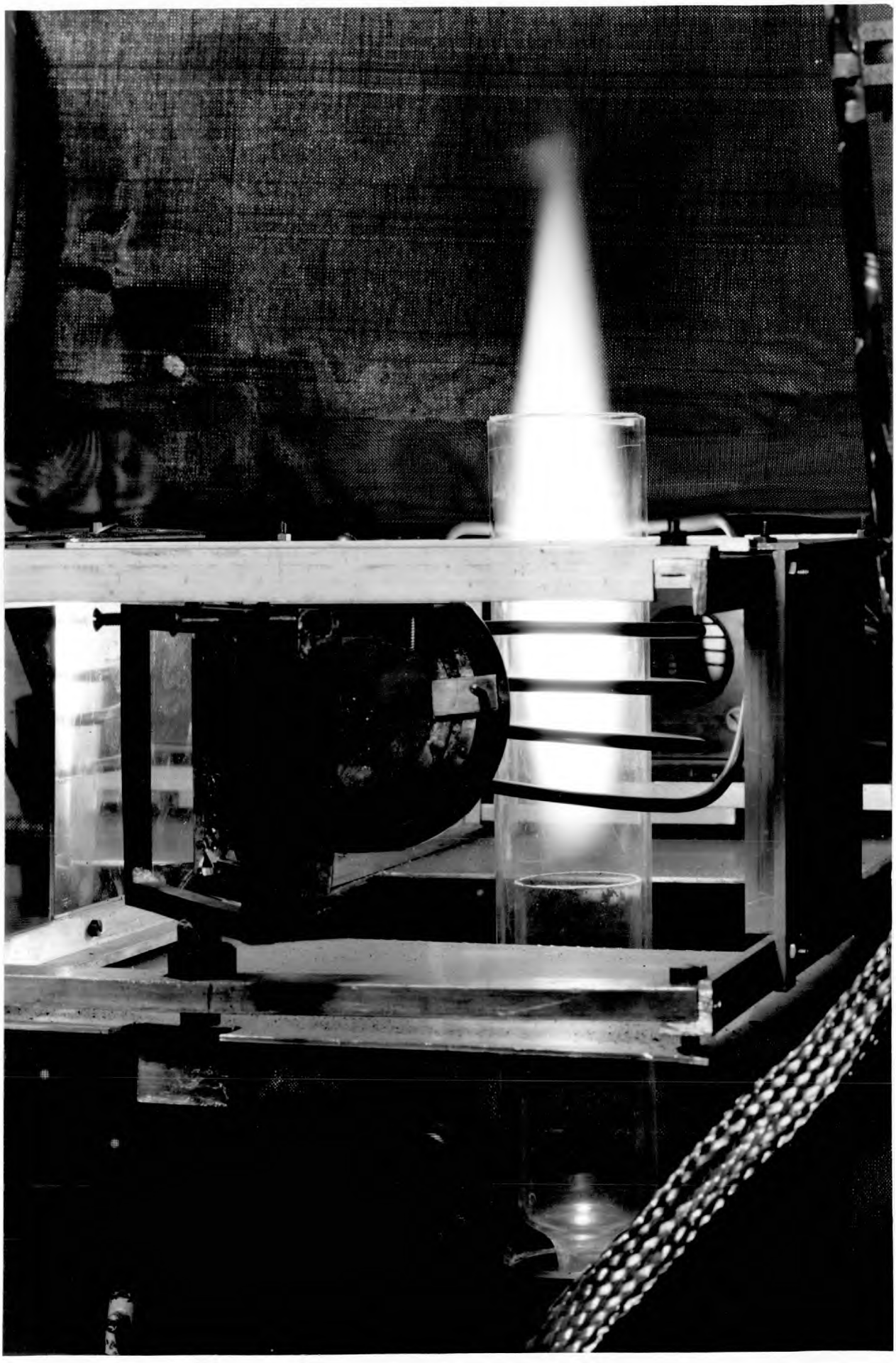

2

front of the drum aperture and an exposure which gave approximately one inch of film for 3 m. secs. taken. No variation of diameter could be determined. If the effect was due to a), a 20% variation in diameter would be expected, whereas if the effect was due to b) only a 1% or so variation would be seen.

It would therefore appear that the temperature of the discharge was fluctuating at 300 HZ. In the next chapter the proof of this is given.

CHAPTER 2

Determination of Discharge Temperature

Introduction

In this chapter measurements of the temperature of the whole discharge are presented. As mentioned in chapter 1, all lines and continuum emitted by the discharge fluctuate at 300 HZ, although a rotating drum camera photograph revealed no fluctuation in size of the discharge, therefore temperature measurements were also made at different points within the cycle.

The temperatures obtained for the discharge were in complete disagreement with those previously presented by Reed (ref. 2); to check on the validity of the measurements made here, the temperature was measured by another method, the line to continuum ratio method.

Temperature Measurement

Method To measure the temperature of the discharge simply, the method of relative intensities was used. Since spectra taken of the discharge had not shown any ArII emission, the relative intensities of ArI lines only could be used. To use this method, the concept of local thermodynamic equilibrium, LTE, (discussed in the next chapter), is assumed to pertain to the discharge and the assumption checked later.

Now the intensity of a spectral line emitted by the discharge, $I(\nu) = \frac{h\nu}{4\pi} n_s A_{sm}$ where n_s is the number of atoms in the state s per cc, Asm is the spontaneous transition probability from a level s to a level m where the energy of the state, E_s is $> E_m$

Now, under the assumption of LTE, n_s can be related to the ground state density by

$$n_s = \frac{n_o gs}{U_o(T)} \exp\left[\frac{-E_s}{kT}\right]$$

where gs is the statistical weight of level s and $U_o(T)$ is the partition function and is equal to $\sum gs \exp\left[\frac{-En}{kT}\right]$ i.e. a function of temperature. However, in the temperature range considered here, the partition function is nearly constant and equal to one.

Thus $I(\nu) = \frac{h\nu}{4\pi} \frac{gs}{Uo(T)} n_o Asm \exp\left[\frac{-Es}{kT}\right]$

Now, if Asm is known for each line measured, and E_s is documented (ref. 10), since gs and ν are known, the measurement of $I(\nu)$ will enable T to be determined.

i.e. $\text{Log} \frac{I(\nu)\ 4\pi U_o(T)}{h\nu gs\ n_o\ Asm} = -\frac{Es}{kT}$

For two lines, $I(\nu_1)$ and $I(\nu_2)$, the ratio,

$$\log \frac{I(\nu_1)\ \nu_2\ gs_1\ Asm_1}{I(\nu_2)\ \nu_1\ gs_2\ Asm_2} = \frac{-Es_1 + Es_2}{kT}$$

Thus a graph of $\log \frac{I\lambda}{gA}$ versus Es will give a straight line with slope inversely proportioned to the temperature.

Apparatus

To facilitate line intensity measurements and to make calibration easier, a photomultiplier technique of measurement was used. To obtain the dispersion necessary to resolve the lines concerned a 10 ft. normal incidence Eagle spectrograph was chosen, and a photomultiplier attachment, built and described by Steers (ref. 11) was used in conjunction with it. Since full details of the photomultiplier attachment and ancillary recording apparatus have already been given by Steers, no further description is necessary here.

Since transition probability values were available only for the $3p^5 4s - 3p^5 4p$ and $3p^5 4s - 3p^5 5p$ transitions, these two groups were chosen for the intensity measurements. These groups lie in the regions 7,600 - 6,900Å and 3,900 - 4,300Å. The reciprocal dispersion of the spectrograph with a 15,000 line per inch grating was approximately 5Å per mm. This meant that, in any position of the grating, approximately 2,000Å could be scanned without altering the grating position and focus. By using the grating in the second order, the two groups of lines, the blue in the second order and the red in the first order could be viewed simultaneously. An EMI 9664B photomultiplier with an S-11 cathode and an EMI 9661B photomultiplier with an S-5 cathode were used to view the 7,000Å and the 4,000Å groups respectively.

Both the photomultipliers were of the side-window type and their cathode sensitivites are seen on consideration of fig. 2.1c to have been appropriate to the wavelenth regions concerned.

The signals from the photomultipliers were amplified by an electrometer amplifier and fed to a pen recorder. Since calibration of the complete system, optics, spectograph, photomultipliers, and recording electronics, was to be effected, no absolute values of amplification factors were needed, and, for the further details of the electronics involved, the reader is again referred to the thesis of Steers (ref. 11).

An optical scanner was built so that the intensity of lines emitted by the discharge could be scanned across any diameter between, as well as above and below, the work coils of the generator. The scanner was designed so that, when it was rotated through 180° vertically to view a tungsten ribbon lamp, the spectograph accepted the

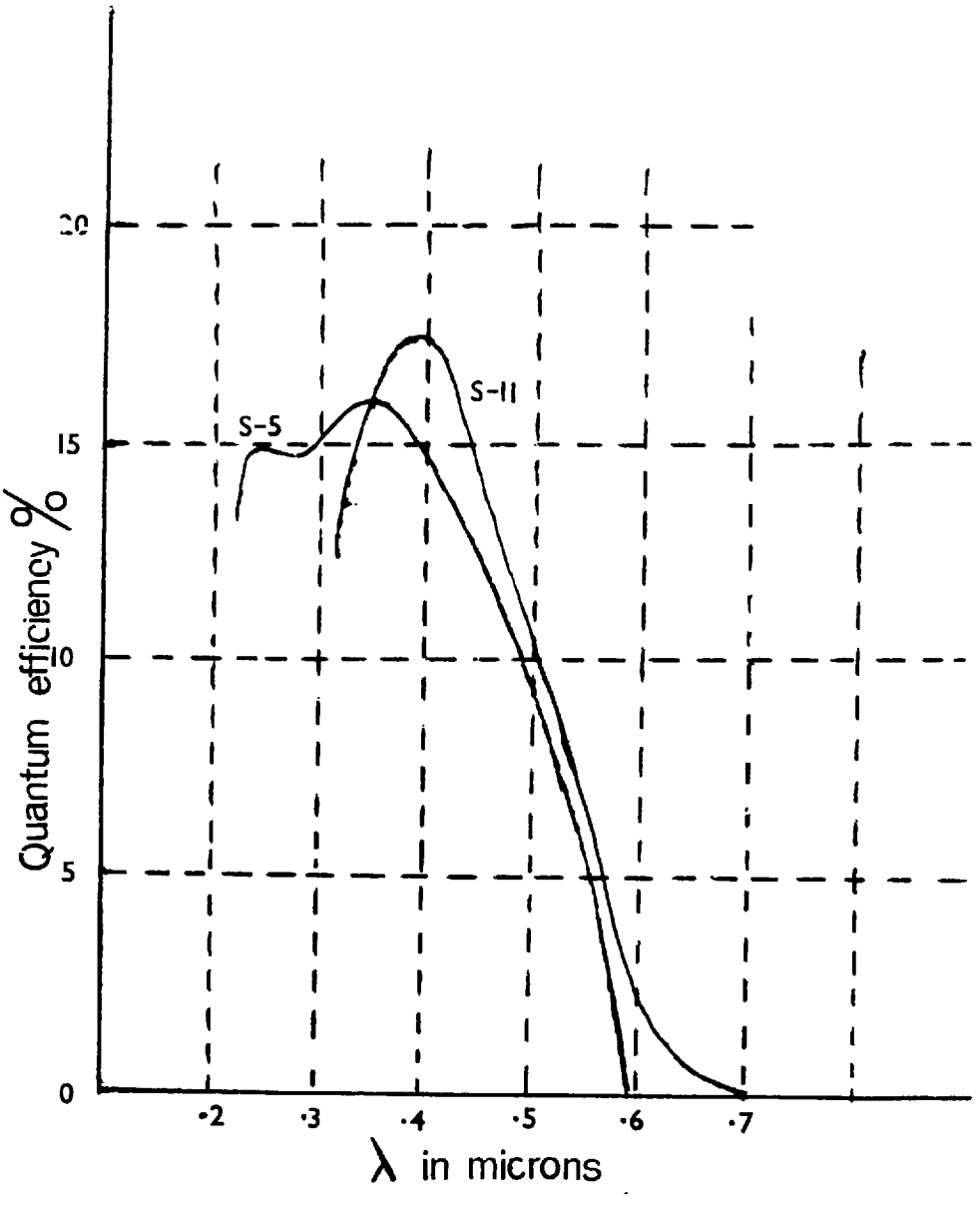

Fig 2.1 Cathode sensitivity of the photomultipliers.

same solid angle of intensity from a tungsten strip lamp as it did from the discharge, while keeping the mirrors and lenses of the optical system in the same positions, (fig. 2.2 and photo 3).

Prior to measuring the integrated intensity of each of the lines of the two groups chosen, each line was scanned through its wavelength range in the centre of the discharge, using 7μ slits on the photomultipliers, to ascertain the amount of light emitted in the line wings that would not be measured through using finite slits on the photomultipliers. Both groups of lines were found to have maximum half-widths of the order of 0.1Å. Consequently slit widths of 200μ were used for the intensity measurements. This corresponded to approximately 1Å for the red lines and $\frac{1}{2}$Å for the blue lines. The correction to be applied for the line wings amounted to about 10% for the blue lines and 2% for the red lines. Later, when the electron number density in the discharge had been measured, these corrections were determined using calculated values of Doppler and Stark widths. These corrections differed at most by 1% from the measured corrections, i.e. 10% of the correction. This was the correction to be applied to measurements made in the centre of the discharge. At the edges of the discharge, the corrections, because of lower electron density and temperature, were negligible.

The tungsten strip lamp used for the calibration was run off a 12 volt accumulator. Two variable resistances in parallel provided the fine and coarse current control for the lamp. The ammeter used to measure the current through the lamp was calibrated by the Standards laboratory of the Electrical Engineering Department of Imperial College. The calibration of current through the ribbon versus the temperature of the ribbon had been effected by the National Physical Laboratory.

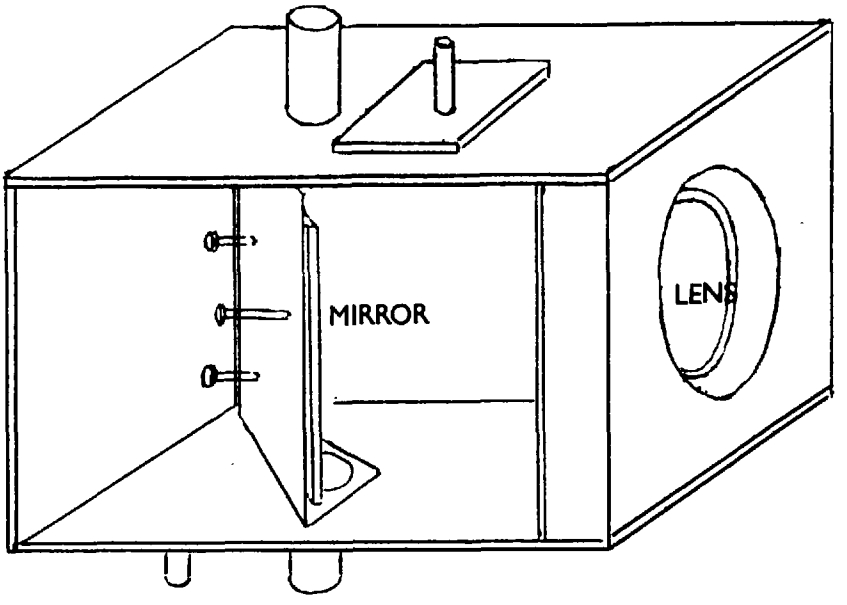

Scanner

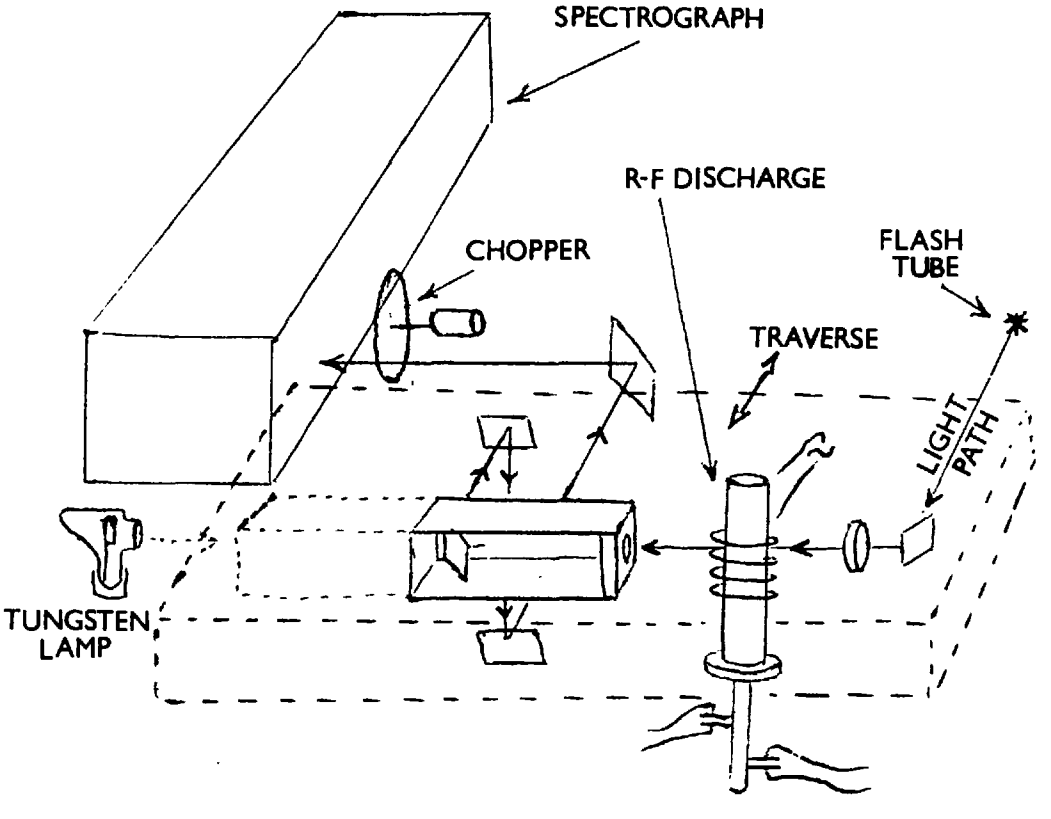

FIG 2.2. Optical path.

Results

Since the agreement between the value of transition probabilities determined by different experiments was at best only within 25%, spectral lines were chosen whose transition probabilities had been measured by more than one person. The actual value used was the average, weighted according to the errors quoted for the measurements. Nine lines from the $3p^5 4s - 3p^5 5p$ transition array and five lines from the $3p^5 4s - 3p^5 4p$ array were thus chosen.

The spatially integrated intensity of each of the lines was measured in 25 positions across the discharge. To obtain reasonable accuracy of measurement from the chart recorder, since the intensity of the lines varied by a factor of 40 from the chosen edge of the discharge to the centre, the input to the chart recorder was reduced for the centre of the discharge measurement by a potentiometer divider, thus allowing use of the maximum gain of the electrometer amplifier for the edge measurements. In this manner, each set of fourteen line intensities could be displayed on the chart, such that the most intense line of the group was almost full scale on the chart for each position across the discharge.

Since these integrated intensities had to be converted to a radial distribution by means of an Abel inversion equation (cf appendix 5), the manner in which each of the lines measured varied across an observed diameter of the discharge had to be known. Consequently one of the lines (the 4,300Å line) was carefully measured across the discharge, without any change of potentiometer setting or amplifier gain and this measurement used to correct the chart measurements for the changes of gain. At the end of a set of measurements across the discharge, the optical, detecting

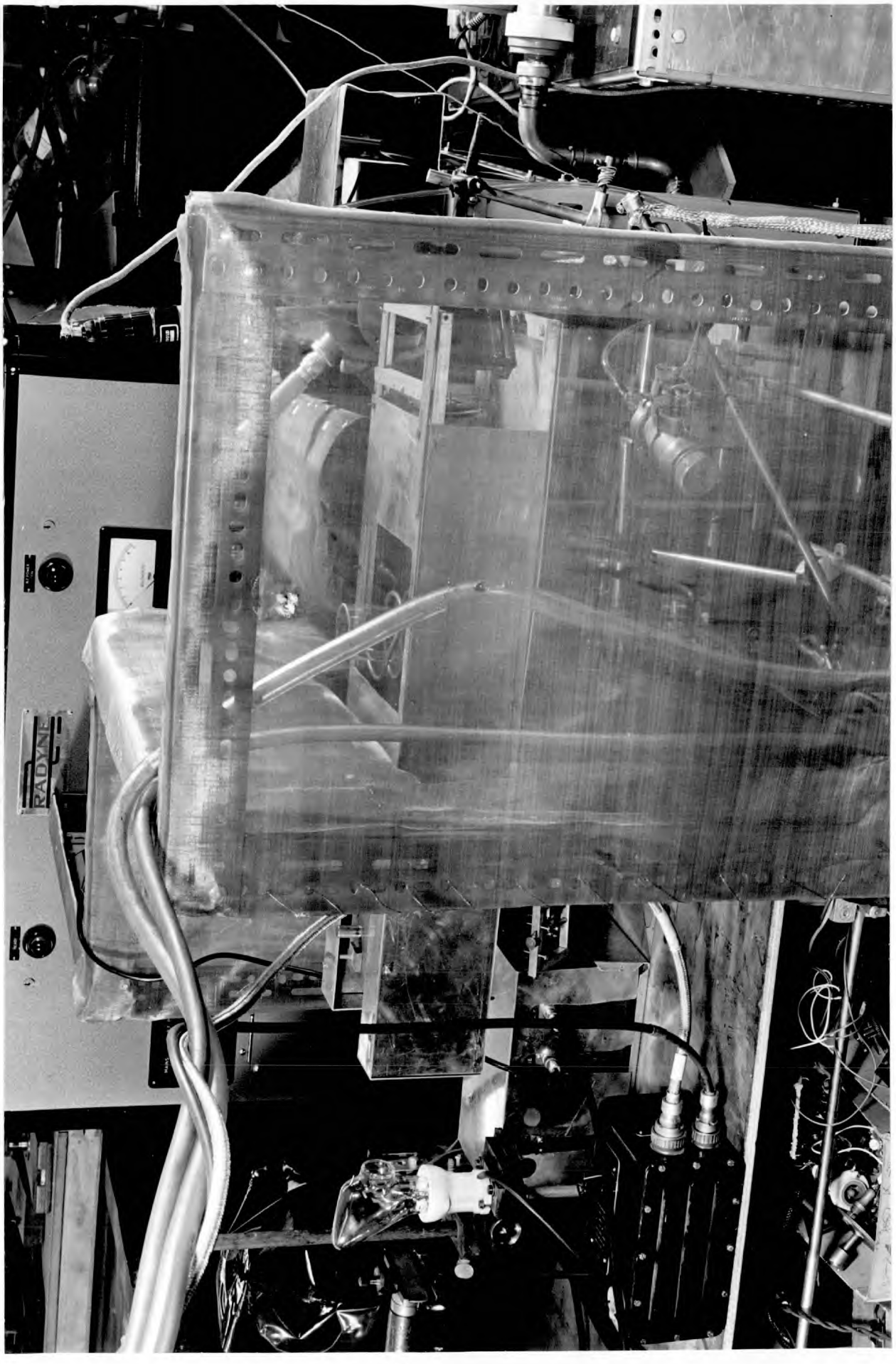

3

and recording systems were calibrated with the tungsten lamp, the intensity of which was recorded at wavelengths corresponding to measured lines.

The line intensities were measured from the continuum level, since they were measured by scanning the photomultipliers from the continuum on one side of the line, through the line, to the continuum the other side. Thus no correction had to be made for the continuum intensity.

The line intensities were then put onto a relative scale using the tungsten lamp calibration. The observed line distribution curves across the discharge were folded about the centre of the half-width of the intensity profile, and a smooth curve drawn through the average of the two curves. The asymmetry of the profiles, determined by the "maximum difference ratio" (see fig. 2.3) amounted to 5% at the most. (This asymmetry is accounted for by the absorption and refraction due to striations of the quartz tube (cf. Chapter 6). These smoothed curves were then "Abel inverted" and a graph of $\log I\lambda/gA$ versus E_s plotted for each of 12 radial positions. This was repeated between each of the six turns of the coils and above and below the extremities of the coil at positions of 1 cm. below and above the last and first coils. These temperatures, calculated from the graphs, are given in fig. 2.4 for each position. In the table in fig. 2.4, 1 means above the first coil, 1-2 between the first two coils, etc., and the temperature is given in 2 mm. steps out from the centre of the discharge. In fig. 2.5 the smoothed temperature profiles are given, and in fig. 2.6, the contours of equal temperature are shown.

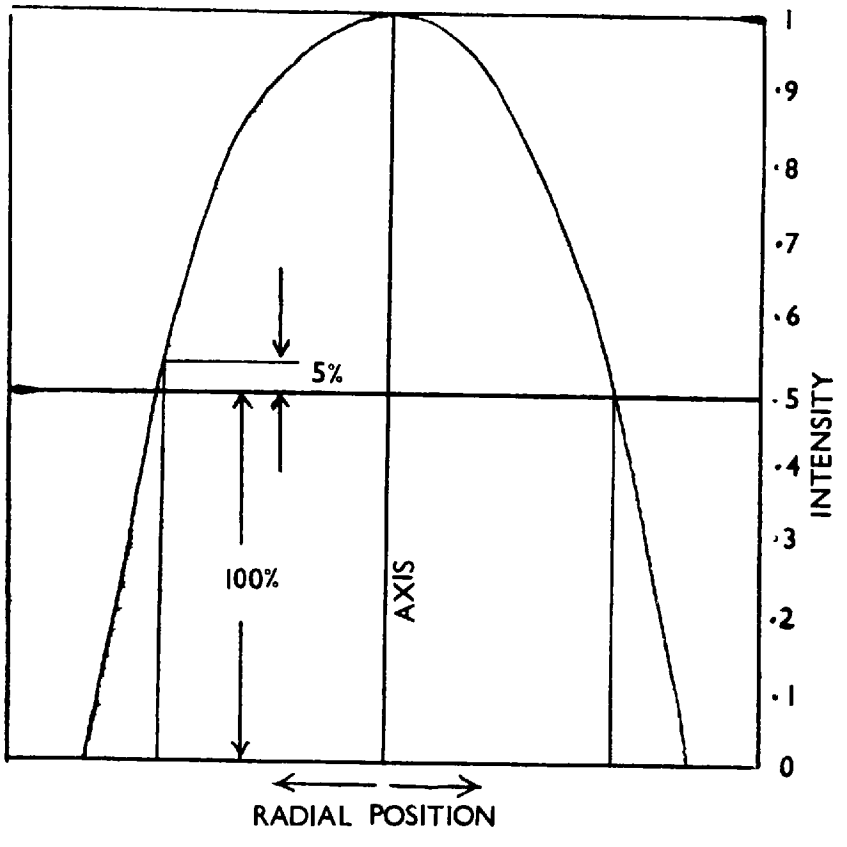

Fig. 2.3. Asymmetry of integrated line intensities.

Discussion of the temperature measurements

These measurements of the temperature of the discharge are in disagreement with the previous measurement by Reed (ref. 2) not only in peak temperature but also in the form of distribution (cf. fig. 1.1 and 1.2). Errors introduced by the inaccuracy of the transition probabilities and the measurement of the line intensities, their calibration and conversion to radial profiles, are not sufficient to account for the discrepancy of about 100% in peak temperature. However, the temperature measurements made here do agree with those of Dymshits and Koretskii (ref. 12). This relative line intensity method relies on the discharge being in local thermodynamic equilibrium, L.T.E., (for an explanation of the concept of L.T.E. see the next chapter), since the populations of the upper levels involved in the transitions are assumed to be related by a Boltzmann equation. This method gives an "excitation temperature" which could be different from the electron or ion temperature if the discharge is not in L.T.E.

To check on this temperature measurement, the line-to-continuum method was used to remeasure the temperature. This method does not depend on the assumption of L.T.E. to the extent of the relative line intensity method, (ref. 25). Consequently, if the difference in temperature between the results here and those of Reed are due to an incorrect assumption of L.T.E. in the discharge, this will become apparent by an inconsistency in the values of temperature obtained by different methods.

However, the method employed by Reed, the Fowler-Milne method, (ref. 4) relies on Saha's equation being applicable. (Saha's equation, which relates the electron and ion densities to the neutral atom density for a given temperature is discussed with L.T.E. in the next chapter). Also, it relies on the Boltzmann

Horizontal Position	Position Vertically						
	0	1	2	3	4	5	6
0	6,450	7,000	8,800	9,050	10,000	9,250	8,000
1	6,400	7,000	8,800	9,050	10,000	9,300	8,000
2	6,350	7,000	8,750	9,000	9,950	9,400	8,000
3	6,350	7,000	8,700	9,000	9,950	8,000	
4	6,300	7,050	8,750	9,050	10,000	9,650	8,000
5	6,300	7,050	8,750	9,050	10,000	9,700	7,950
6	6,250	7,150	8,800	9,050	10,050	9,750	7,900
7	6,250	7,250	8,800	9,100	10,100	9,700	7,850
8	6,200	7,450	8,850	9,150	10,150	9,600	7,750
9	6,100	7,000	9,000	9,250	10,200	9,400	7,650
10	5,950	7,700	9,100	[illegible]	10,150	9,150	7,450
11	5,700	7,750	9,150	[illegible]	10,000	8,750	7,000
12	5,100	7,700	9,150	9,500	9,700	8,150	5,750
13	4,250	7,650	9,050	9,500	9,250	7,000	–
14	3,000	7,500	8,750	9,450	8,700	4,800	–
15	–	7,280	8,500	9,250	7,750	–	–
16	–	6,800	7,700	8,700	6,100	–	–
17	–	6,250	6,750	6,900	4,600	–	–

FIG 2.4. Values of temperature

equation relating the upper level of the line involved to the ground state. Thus Reed's method also depends on L.T.E. and would be expected to give a similar result to those described here. The discrepancy becomes, therefore, all the more curious.

Line-to-continuum method

Provided the transition probability of a line emitted from the discharge is known, the ratio of the line intensity relative to a band of nearby continuum is a function of temperature only - in this case, electron temperature Te.

The intensity of the continuum emission, which is due to free-free and free-bound electron transitions, i.e. Bremsstrahlung and recombination radiation is given by (ref. 13)

$$E_\nu = 5.41 \times 18^{-46} \, Z^2 \frac{n_e n_i}{\sqrt{Te}} \qquad \text{watts/cm}^3\text{/st/sec.}$$

The theory on which the emission coefficient is calculated assumes that the recombination of electron and ions is into hydrogen-like states sufficiently dense to permit the sum over discrete states to be replaced by an integral, and that hydrogenic, screened Coulomb wave functions can be used to calculate the Gaunt factor.

Since the relative intensity method gives a temperature at which the second stage of ionisation is negligibly populated, then $n_e = n_i \gg n_{2i}$. The intensity of the line is given by

$$I(\nu) = n_s \, A_{sm} \frac{h\nu}{4\pi} \qquad \text{ergs/cm}^3\text{/st/sec.}$$

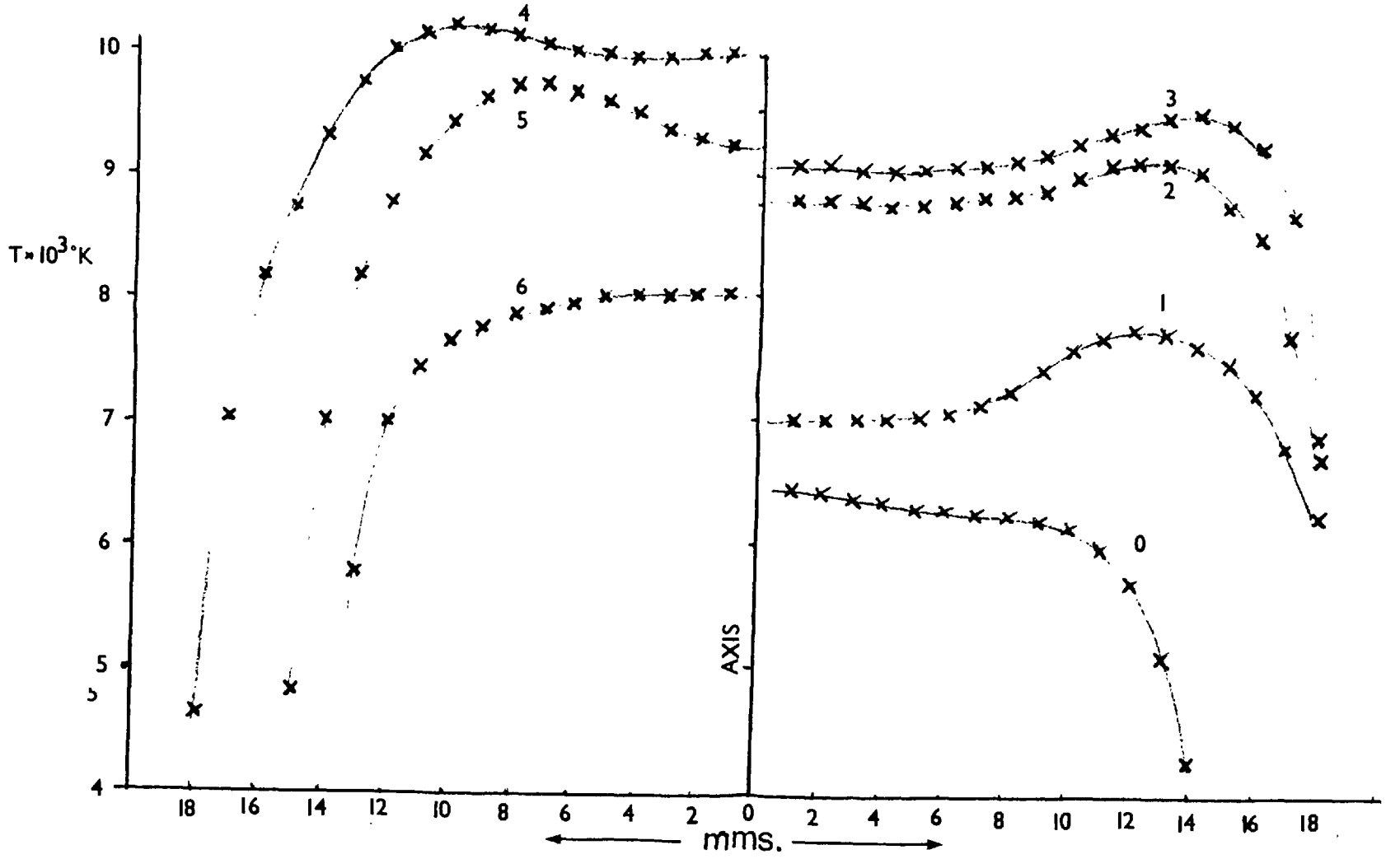

Fig 2.5 Temperature profiles

With Boltzmann's equation, $n_s = \frac{n_o g_s}{U_o(T)} \exp\left[\frac{-E_s}{kT}\right]$

and Saha's equation $\frac{n_e n_i}{n_o} = 2\left\{\frac{2\pi mkT_e}{h^2}\right\}^{3/2} \frac{Ui(T)}{U_o(T)} \exp\left[\frac{-Wi}{kT}\right]$

The line intensity can be written

$$I(\nu) = \frac{n_e^2}{T_e^{3/2}} \frac{g_s}{U_i(T)} A_{sm} \frac{h\nu}{4\pi} \frac{h^3}{2(2\pi mk)^{3/2}} \exp\left[\frac{W_i - E_s - \Delta W_i}{kTe}\right]$$

where W_i is the energy corresponding to the depression of the ionisation level, and $n_1 = n_e$ has been substituted.

The line chosen, the 4259Å line, has a measured transition probability ($\times 10^7$) of 0.25, (ref. 24) 0.33 (ref. 15) and 0.40 (ref.16), consequently the mean, $0.32 \times 10^7 sec^{-1}$ was chosen.

Substituting the values of all the known parameters into the above equation we get -

$$I(\nu) = 3.86 \times 10^{-30} \frac{n_e^2}{Te^{3/2}} \exp\left[\frac{W_i - E_s - \Delta W_i}{KTe}\right] \text{ watts/cm}^3\text{/st.}$$

Ui(T) is a slowly varying function in this regime of T, and is given by Olsen (ref. 4).

Now the emission coefficient of the continuum over a 1Å bandwidth at 4262Å is:-

$$E_\nu \Delta\nu = 8.9 \times 10^{-35} \frac{n_e^2}{\sqrt{Te}} \text{ watts/cm}^3\text{/st.}$$

Olsen (ref. 17), using a DC thermal arc in argon, which had well documented properties (ref. 4), found that a correction factor of 5x had to be applied to this expression for the continuum intensity. However, he later (ref. 14) amended this to a factor of 2.3x. He also found that the electron density and temperature dependence, as well as the frequency dependence, were correct in the visible region of the spectrum which he examined.

i.e. $E_\nu \Delta\nu = 2.05 \times 10^{-34} \frac{n_e^2}{\sqrt{Te}}$ watts/cm^3/st

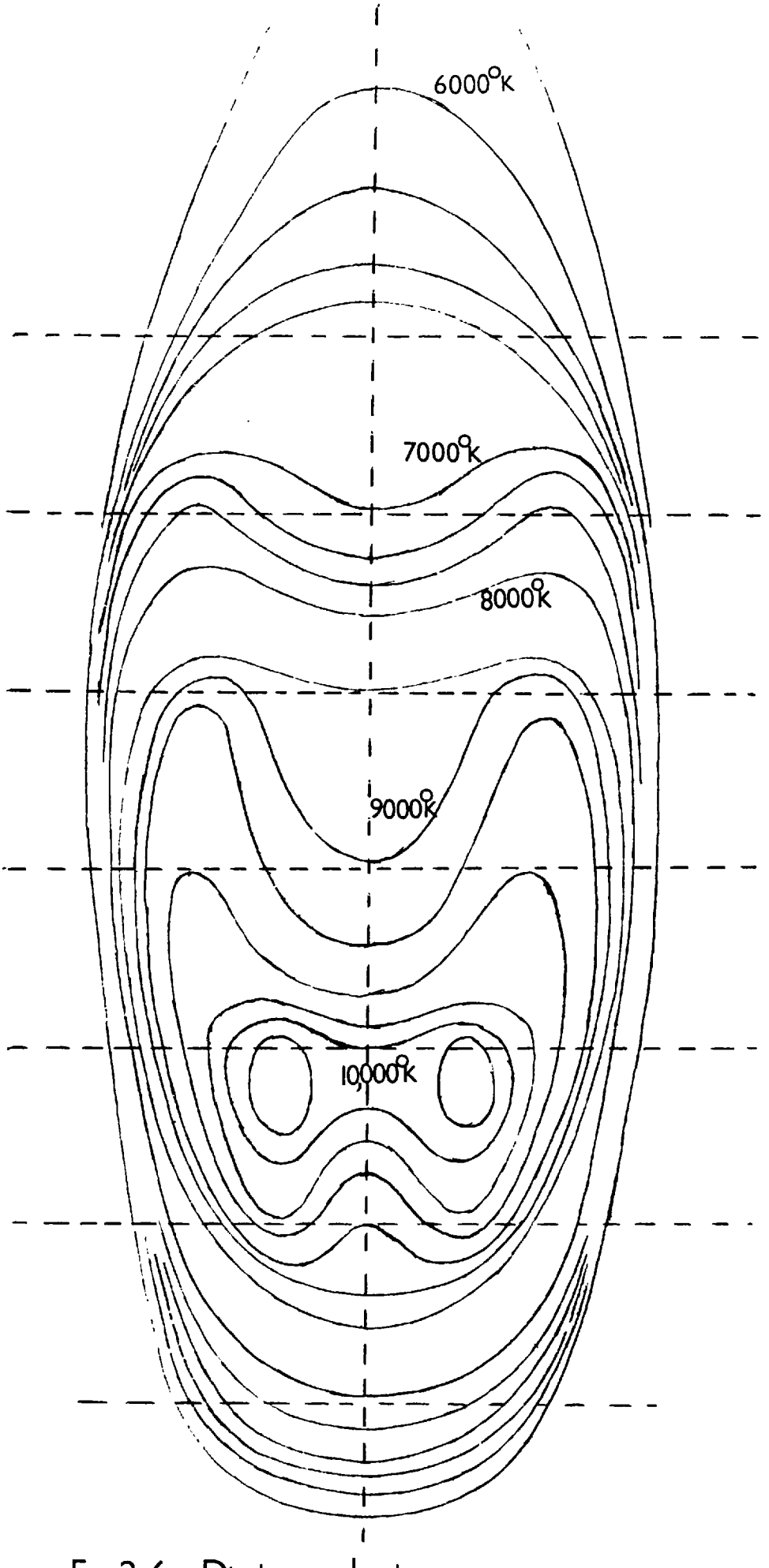

Fig. 2.6. Discharge Isotherms.

Since Olsen showed the frequency dependence to hold, one would expect the cut-off frequency, defined by the interval between the effective ionisation potential and the energy level above which the assumption of dense states is valid, corresponding to the $3d_6$ terms, to be $\nu_g = 4.6 \times 10^{14}$ sec^{-1}. Below this the levels are effectively discrete while above, smeared, and, taking into account the fact that ν_g is lowered by the depression of the ionisation potential ΔW_i, the above equation for the continuum intensity should be written

$$E_\nu \Delta\nu = 2.05 \times 10^{-34} \frac{n_e^2}{\sqrt{T_e}} \exp \frac{-h(\nu_1 - \nu_g + \Delta\nu_i)}{kT_e} \text{ watts/cm}^3\text{/st}$$

Now since $I(\nu) = 3.86 \times 10^{-30} \frac{n_e^2}{\sqrt{T_e}} \exp \left[\frac{W_i - E_s - \Delta W_i}{kT_e} \right]$ watts/cm^3/st

where $\Delta W_i = h\Delta\nu_i$

$$\frac{E_\nu \Delta\nu}{I(\nu)} = kT_e \exp \left[\frac{-(W_i - E_m - W_g)}{kT_e} \right]$$

where $h\nu = E_s - E_m$ and $h\nu_g = W_g$.

The constant K includes the correction to the continuum intensity and the transition probability of the line involved, both of which are subject to large errors. This ratio is plotted in fig. 2.7 as a function of T.

Experimental Details

The measurement of the line to continuum ratio was performed while the experiment described in chapter 3, the determination of electron density, was being set up. Consequently, a much simpler

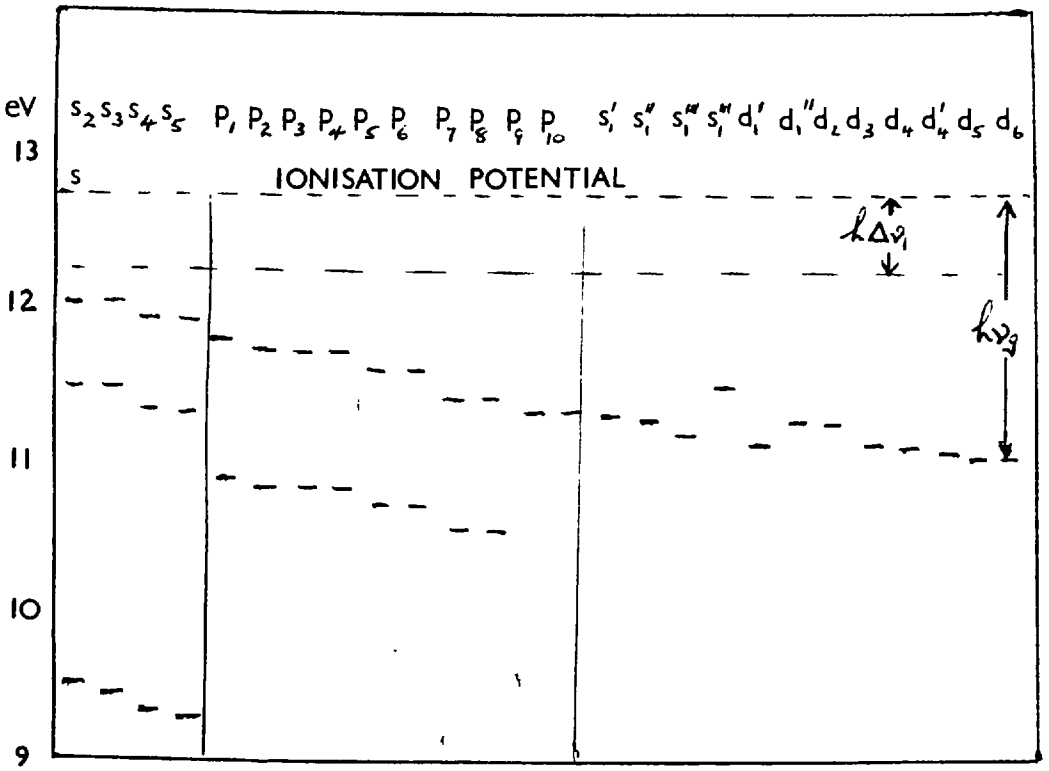

FIG 2.8. Argon energy levels.

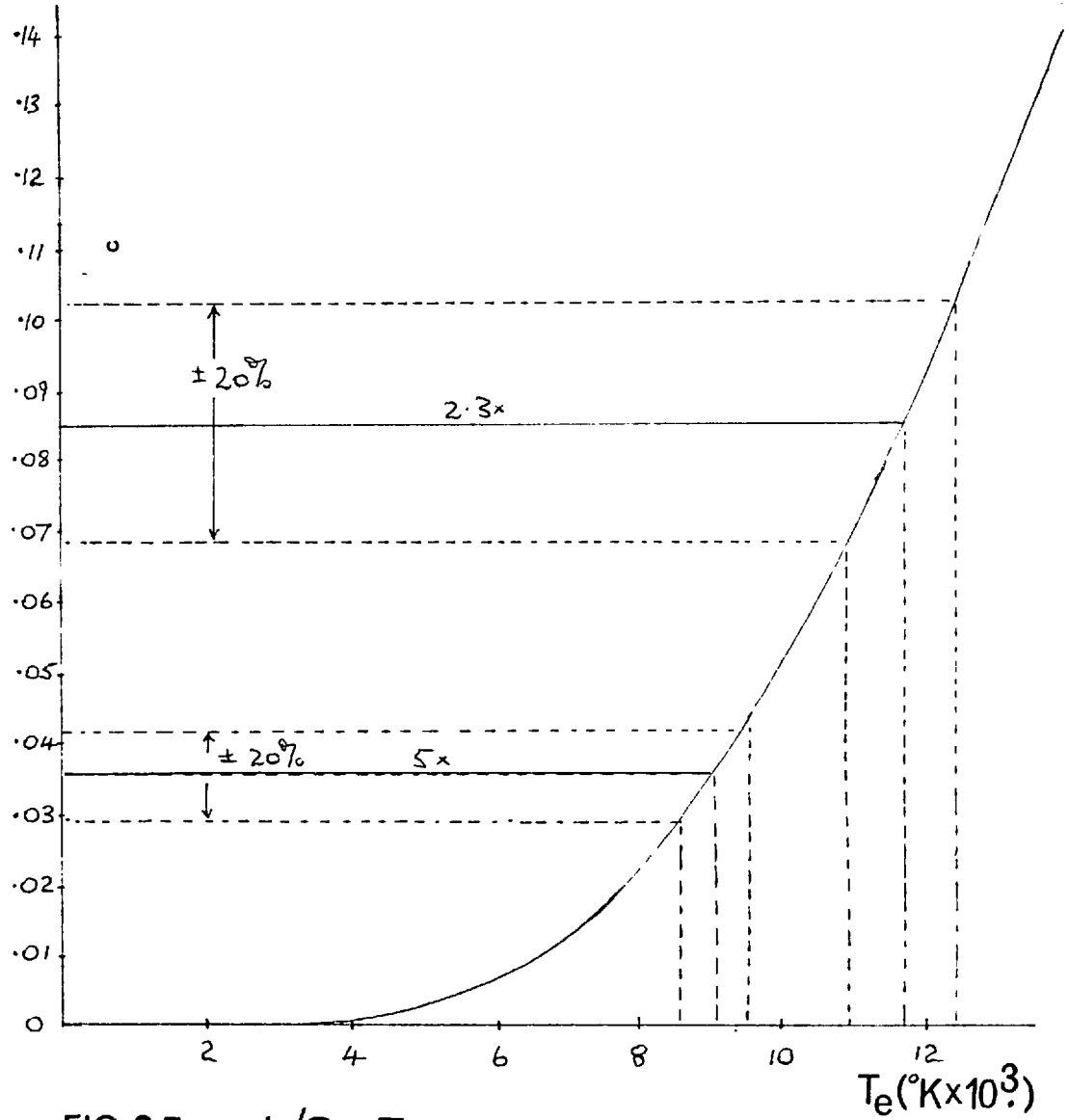

FIG 2.7 L/C v T

optical arrangement was used. Since this measurement was to be a check on the value of the temperature of the discharge obtained by the relative line intensity method compared with that measured by Reed (ref. 2), i.e. a determination of whether the discharge temperature was 10,000 or 17,000°K at its maximum, no scanning system was employed initially. Later the optical system used for the line intensity scans was used.

Initially the intensity of the 4259Å line was compared with that of a 1.1Å band of continuum centered at 4262Å, in the centre of the discharge only. The advantage of measuring the continuum adjacent to the line is the avoidance of any form of calibration for optical components and photomultiplier responses. The radiation at both wavelengths was chopped, measured by an RCA IP 28 photomultiplier on a constant deviation spectrograph and recorded on a Tektronix 555 oscilloscope with an AC-coupled L-type amplifier.

The slit widths of the spectrograph were carefully measured with a travelling microscope so that, with a knowledge of the dispersion provided by the suppliers of the instrument, the exact bandwidth of continuum radiation accepted would be known.

The 300 Hz ripple on both continuum and line was ignored since both were equally affected.

The ratio obtained was $0.085 \pm 20\%$. This corresponds, from fig. 2.7, to a temperature of $11{,}700 \pm 700$°K.

This value is higher than that previously measured but still much lower than Reed's value. However, no Abel inversion process has been carried out and this temperature is the result of a spatial integration through the discharge, and its accuracy as such must be doubted.

A more detailed experiment was then carried out, in which both the line intensity, in this case the 4300Å line, and the continuum intensity at 4302Å were scanned across the discharge, Abel inverted, and their ratio calculated. For agreement with the relative line intensity method, a factor of 5, as first proposed by Olsen, is needed to correct the continuum intensity. The 4300Å line has two measured transition probabilities, 0.032 (ref. 15) and 0.036 (ref. 16) x 10^7 Sec^{-1}. A value of 0.034 x 10^7 sec^{-1} was therefore chosen. In this experiment, using the optical set up of 2.1, the slith widths used corresponded to a band width of 1.25Å, and this time, the output signal from the photomultiplier was integrated with respect to time and displayed on the chart recorder.

Using the correction to the continuum intensity of 2.3 x the temperature obtained from this set of measurements was of the order of 11,800°K in the centre of the discharge with an off-axis peak of 12,000°K.

However, if the correction factor of 5 x is used, the first measurement, using the 4259Å line becomes 9300°K and the second radial profile measurement gives a central temperature of 9500°K and an off-axis peak of 9700°K, in reasonable agreement with the relative line intensity method.

Obviously, any experiment can be made to give the right answer by choosing an appropriate "correction factor"; what has to be decided here is, which is the proper correction.

Discussion of Correction factor for Continuum Intensity

To determine the correction factor Olsen (ref. 17) used a DC arc whose radial temperature profile had been determined using the Fowler-Milne method applied to the continuum, the argon I 7635Å and the argon II 4806Å line. However, the argon I line is expected, in the light of work discussed in the next chapter to show self-absorption under the conditions pertaining to the arc, while the argon II line has been proved (ref. 18) to have considerable self-absorption, so much so that the off-axis peak in the radial intensity profiles may have been caused, not by the temperature of line intensity maximum being reached but by the possibility of there being absorption in the centre of the discharge. However, this does not explain the continuum intensity having an off-axis peak in the same position as the argon I line.

Considerable doubt exists still (ref. 19) over the values of the depression of ionisation potential to be used in any given situation. For example, for a discharge of 9,000°K and 4×10^{15} electrons per cc., the Debye-Hückel theory gives 0.019eV , the Unsöld 0.111eV , Ecker-Weizel 0.122eV and Brunner 0.207eV (refs. 20, 21, 22, 23). Although this term cancels out in the calculation of $\varepsilon_\nu \Delta\nu / \Gamma_\nu$ performed above, it is used in the calculation of the electron and ion densities for the theoretical continuum intensity with which Olsen compared his experimental value.

In view of the fact that the 7635Å line exhibited self-absorption in his discharge, Olsen measured the temperature, using different spectral lines and obtained a new value of the continuum correction factor (ref. 24 and 14).

There are three possibilities by which this value of temperature obtained by the line-to-continuum method could be disputed. Either the correction is not 2.3x but 5x as originally proposed, not because of the remeasure of the temperature of the discharge used but because of an incorrect value of depression of ionisation potential, a wrong choice of ν_g, the cut-off frequency, or an incorrect plasma composition determination. Doubt has been cast on Olsen's remeasure of his discharge parameters by Popenoe and Shumaker (ref. 18), who show that self-absorption of the lines used by Olsen in his temperature determination was still present.

Taking these points singly, the choice of depression of ionisation potential can lead to errors in determining the electron and ion densities from the temperature of the discharge using Saha's equation. For Olsen's discharge the following depressions are given according to the various theories:-

Debye-Hückel	-	0.09 eV
Unsöld	-	0.44 eV
Ecker-Weizel	-	0.52 eV
Brunner	-	0.85 eV

When the extreme values are put into Saha's equation a variation of 50% in ion and electron density can be obtained, thus leading to a possible factor of two in the estimated theoretical continuum emission coefficient.

From fig. 2.8, a Grotrian diagram of argon I energy levels, it can be seen that the value of ν_g, above which there are dense hydrogenic states, can only be decreased from its value of $4.6 \times 10^{14} sec^{-1}$ corresponding to recombination into the lowest d state. A decrease of ν_g would give a higher temperature from the line-to-continuum ratio.

The last possibility seems the most likely since Olsen chose the Debye-Hückel depression of ionisation potential value and a choice of a value larger than this would give a greater computed value of electron and ion density and thus decrease the calculated continuum correction factor even further.

Thus the possibility of an incorrect temperature determination leading to a value of electron and ion density too great would be a possible cause of obtaining a correction factor of only half that which would be expected from the experiments described here. The criticism by Popenoe and Shumaker of Olsen's temperature determination (ref. 18) is such as to correct the factor in this way, i.e. the measured temperature and hence computed electron and ion densities are too high.

Until further measurements are made of the absolute continuum intensity from an argon discharge, no definite value (to better than a factor of two) can be ascribed to the correction factor.

300 Hz Temperature Measurement

In the preliminary experimentsdescribed in chapter 1, the line and continuum emission from the discharge were shown to vary at 300 Hz by approximately 20%.

This could be due to one of two processes, either the discharge was varying in size while the temperature stayed constant, causing the spatially integrated intensity to vary, or the discharge was of constant proportions but the temperature was varying and thus causing the emitted radiation to vary.

The rotating drum camera experiment described in the first chapter showed that the discharge was not varying in diameter, thus the second explanation must be the correct one. The following experiment proved that the temperature was fluctuating at 300 Hz.

Method and Results

A chopper disc, driven by a synchronous motor was placed in front of the entrance slit of the spectrograph. Slits were cut in the disc so that the spectrograph received a light pulse from the discharge of a duration $\pi/24$ every cycle. Since the synchronous motor was driven by the same power supply as the generator, the interval of light passed by the chopper always occurred at the same point on the 300 Hz wave. The disc could be rotated on the shaft of the motor so that light intensity from a different position within the cycle could be accepted. A pointer on the motor shaft, together with six equally spaced rulings round the disc, enabled the disc to be accurately set at six different positions within the cycle.

The spectral lines used for the relative line intensity method described in this chapter were those used for the previous determination.

Since the temperature was to be measured at six different points within the 300 Hz cycle, and since it would have to be measured several times because of the small variation anticipated, no attempt was made to convert any of the observed integrated line intensities to radial intensities. Also, in view of the fact that a measurement only of the variation and not the absolute scale of the temperature was required, the intensities were measured in the centre of the discharge only.

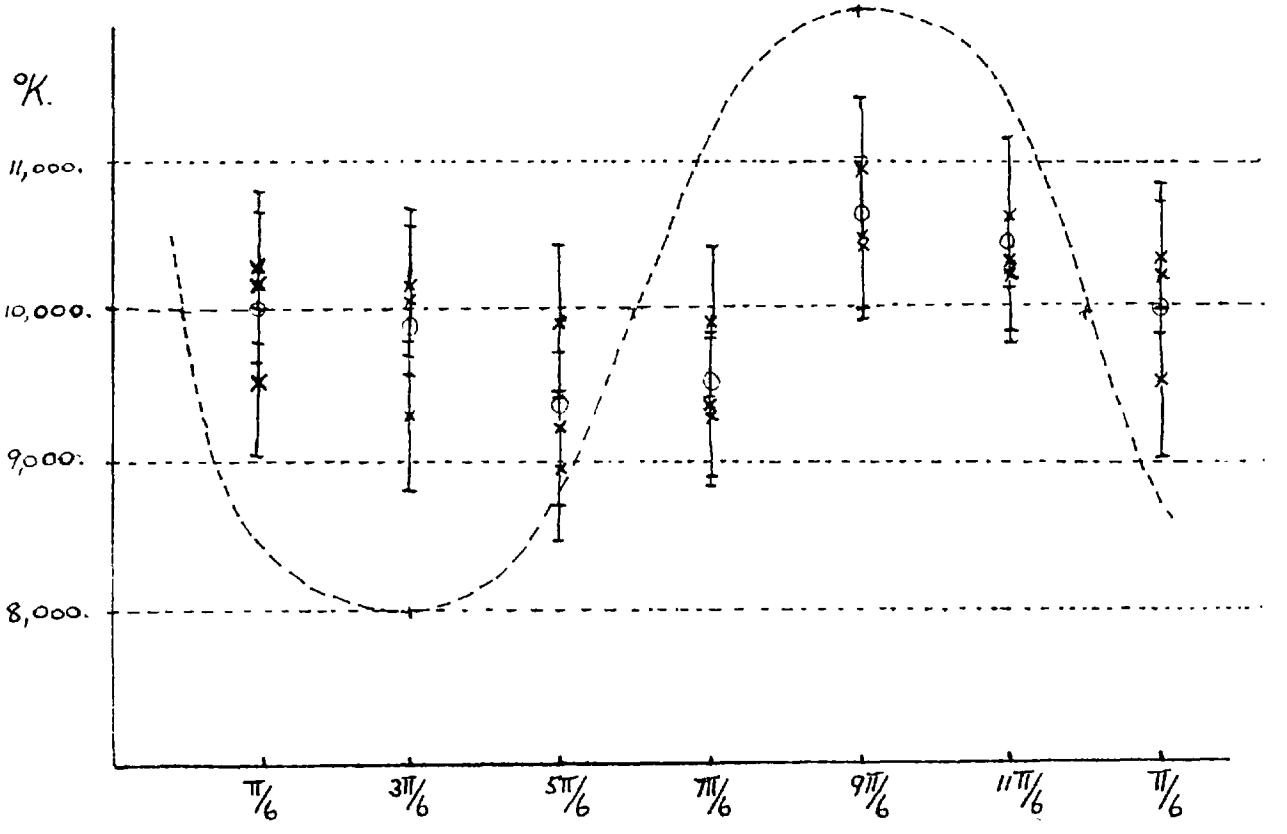

FIG 2.10 300Hz v T

The power input to the radio-frequency coil had been observed to have a 5% variation at 300 Hz so a monitor of the voltage determined the point within the cycle at which the measurements were made. One of the photomultipliers could be switched from the electrometer amplifier to a Tektronix 551 oscilloscope, whose other input was from a pick-up coil located near the R-F coil, so that the point within the power cycle at which measurements were being made could be easily determined.

Although the signals received by the photomultipliers were chopped at 300 Hz, the slow response time of the electrometer amplifier input (~1 sec.) averaged the signal. Since relative intensities only were required this was of no consequence.

The temperature (not true temperature, since the intensities have not been corrected for spatial integration) obtained are shown in fig. 2.9 and plotted along with the power cycle in fig. 2.10.

It is convincingly shown that the temperature of the discharge is varying with the power input, contrary to the results of Dymshits and Koretskii (ref. 12) who state that the peak temperature of the discharge is independent of the power input.

Position in 300 H_z Wave	T_1	T_2	T_3 ($^\circ$k)
$11\pi/6$	10,200	10,300	10,600
$9\pi/2$	10,900	10,400	10,400
$7\pi/6$	9,300	9,800	9,300
$5\pi/6$	8,800	9,900	9,200
$\pi/2$	9,300	10,200	10,100
$\pi/6$	9,500	10,300	10,200

FIG. 2.9. 300 H_z v T

Line (Å)	Upper Level	Electron Density (x 10^{15} cm^{-3})
4158	$5p^5$	4.2 ± 20%
4198	$5p^6$	3.5 ± 20%
4200	$5p^2$	3.4 ± 20%
4259	$5p^{10}$	4.1 ± 20%
4266	$5p^5$	3.2 ± 20%
4272	$5p^4$	4.0 ± 20%
4300	$5p^3$	3.0 ± 20%
4335	$5p^8$	4.0 ± 20%

FIG. 3.1. Values of n_e

CHAPTER 3

Measurement of Electron Density

Introduction

The discrepancy between the temperature obtained for the discharge by the methods described in the previous chapter and that measured by Reed (ref. 2) has still to be resolved. In all the methods used, local thermodynamic equilibrium has been assumed and a possible explanation for the discrepancy in results could be that the source is not in LTE and since the methods used depend to a different extent on LTE, the temperature determinations will not be self-consistent.

To determine the degree of LTE existing in the discharge and hence the validity of the temperature measurements which require its existence, the electron number density in the discharge was determined experimentally using an oscillating Fabry-Perot interferometer to determine the half-widths (i.e. width at half maximum intensity) of the argon I emission lines from which the instrument function and Doppler half-width could be subtracted to give the half-width due to Stark broadening. By using the published values of Stark-broadening parameters (ref. 25) the electron number density within the discharge could be obtained.

Also, if any of the lines used in the relative intensity temperature method suffered from self-absorption, this would be apparent by comparing lines emitted from the same upper level since their half-widths should be in proportion to the square of their wavelengths only.

Theory

The theory of the vibrating Fabry-Perot has been described in referenoes 71 and 72, and details of its operation can be found in reference 26. The theory of the Stark broadening of spectral lines by electron collisions has been adequately explained in ref. 25 and 43.

Method and Results

Since line widths were to be measured in the blue and the red region of the spectrum and the etalons of the Fabry-Perot with their high reflectivity and low transmission cause a serious loss of light intensity, separate photomultipliers were chosen for each region, an RCA IP-28 for the $3p^5 4s - 3p^5 4p$ lines in the blue and an RCA 6217 for the $3p^5 4s - 3p^5 5p$ lines in the red. The $3p^5 4s - 3p^5 5d$ lines (green region) were also investigated since they had very much larger Stark widths and provided a more accurate density determination.

Light from the discharge was focussed on the Fabry-Perot étalon and the central fringe of the interferenoe ring system focussed on to the entrace slit of a monochrometer which had the appropriate photomultiplier placed behind the exit slit. The output of the photomultiplier after amplificaation was recorded directly on a Tektronix 555 oscilloscope. The lens used to image the discharge could be scanned from side to side to enable the Fabry-Perot to accept light from different regions across a diameter of the discharge.

The observed line profile is a convolution of a Gaussian profile caused by Doppler broadening and a dispersion profile caused by Stark broadening. This resultant profile is known as a Voigt profile (ref. 74).

The 6965Å line was scanned and, by estimating the Doppler width from the relative intensity temperature determination, and the instrumental width by scanning a line of known width, the Stark half-width of the 6965Å line was determined (cf. ref. 73).

Taking the gas temperature as 9,000°K, and a corresponding Doppler $\frac{1}{2}$ 1/e width, i.e. half the width of the line profile at the position where the intensity has fallen to 1/e of its maximum of $g = 0.045$Å, and, using the CdI 6438Å line from a low pressure discharge lamp to estimate the instrumental width since the entire width of this line was due to the instrument (0.02Å) the Stark width was calculated (ref. 73) as $W = 0.018$Å.

Using the Stark broadening parameter for this line given by Griem (ref. 25), and 10,000°K for the temperature, an electron density of $N_e = 4.2 \times 10^{15} cm^{-3}$ was obtained.

Since the Stark broadening parameters have a very small dependence on temperature, no significant error is introduced by assuming 10,000°K for the discharge temperature.

The shape of the line profile was calculated from the above data and compared with the measured line profile. The calculated profile fitted the experimental profile very well (cf. ref. 26 for further details).

The above Stark width was very small and consequently subject to large errors, the $3p^5 4s - 3p^5 4p$ lines have smaller line widths due to Stark broadening than the $3p^5 4s - 3p^5 5p$ lines. The determination of electron density from these lines would be even more uncertain, so the $3p^5 4s - 3p^5 5p$ and 5d lines only were used for an electron density determination.

However, the widths of the $3p^5 4s - 3p^5 4p$ lines were measured to determine if there was any self-absorption occurring. This group of lines had larger transition probabilities and longer wavelengths than the $3p^5 4s - 3p^5 5p$ group and, since the probability of self-absorption is proportional to the transition probability and the third power of the wavelength this group would be the most sensitive to self-absorption. Comparing the widths of lines emitted from a common upper level, any self-absorption could be detected since the line widths should be in proportion to the square of their wavelengths only; any value of line width over and above this would indicate the presence of self-absorption.

By comparing the expected line profiles with the measured ones, the 7635Å line was found to have some self-absorption. Although the line was broadened to a greater extent than would have been expected, the increase was just within the limit of error of measurement and thus no value could be ascribed to the optical depth of this line. No other lines used in the relative intensity temperature measurement exhibited self-absorption and the 7635Å line was eliminated from all the previous temperature calculations.

By use of the $3p^5 4s - 3p^5 5p$ spectral lines, the values of electron density determined for the central region of the discharge are given in fig. 3.1.

All these values were obtained by integrating the line-profile through the inhomogeneous discharge column. The electron density determinations were only accurate to about $\pm$ 20% owing to the inherent inaccuracies in the Stark broadening parameters, and the errors involved in the profile measurements and their reduction and, since the temperature distribution was reasonably "flat-topped" no attempt was made to convert the values to a radial distribution.

An integrated radial distribution was obtained by measuring the profile of the 5495Å $3p^4 4s - 3p^5 5d$ spectral line across a diameter of the discharge. Since the 5d levels have much higher electron impact cross-sections than the 4p and 5p levels, the Stark width from this level is such that the Doppler width can be ignored in comparison. The value of electron density thus determined is shown in fig. 3.2. The inhomogeneity of the discharge seems unimportant considering the sharp fall off in the Stark width at the edges of the discharge.

The value of electron density pertaining to the centre of the discharge was, from the above measurements:-

$Ne = 4 \times 10^{15}$ electrons/cc ± 20%.

Discussion

The only assumption made in this method of determining electron density is that of a Maxwellian distribution of electron energies, a condition that is easily satisfied here. Therefore the results are expected to be reliable.

However, serious discrepancies with Griems' published values of Stark broadening parameters have been found both experimentally and theoretically (D.E. Roberts Ph.D. thesis) for Argon II and the validity of the Argon I parameters must be discussed.

Using Gericke's results for Ar I (ref. 15) Griem checked the Ar I parameters. However Gericke determined his discharge conditions from a temperature measurement using the absolute intensity of an Ar II line whose transition probability has recently been recalculated. Thus the Stark broadening parameters for Ar I need to be redetermined from the revised discharge conditions.

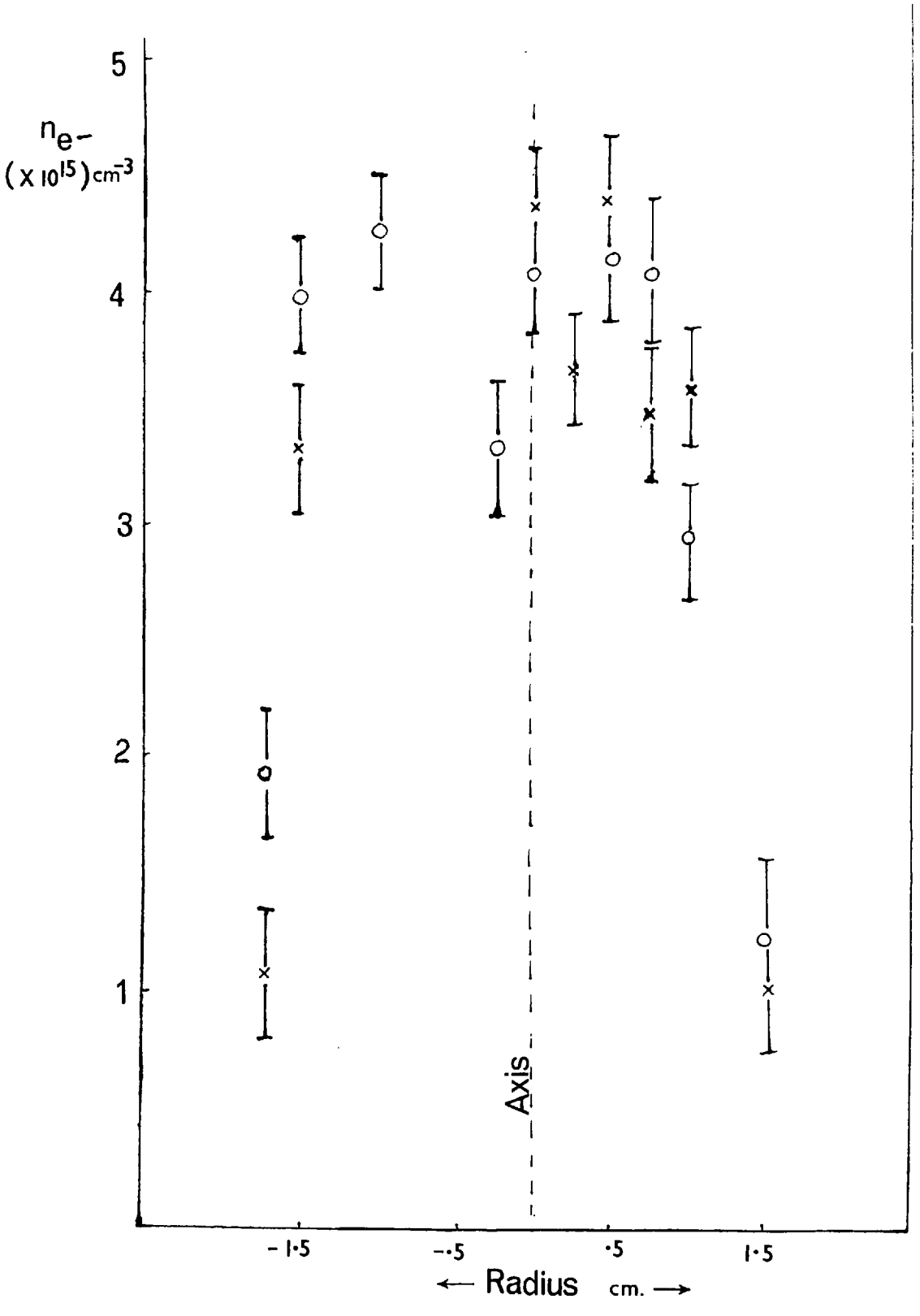

Fig 3·2 Electron number density v discharge radius.

For the Ar II line, Gericke used a transition probability of $6.77 \times 10^7 sec^{-1}$, Griem used a transition probability of $12.8 \times 10^7 sec^{-1}$, and a recent lifetime measurement gives $10.1 \times 10^7 sec^{-1}$.

As a result of the recalculation of Gericke's discharge conditions a correction factor of 1.16 was applied to the Ar I line broadening parameters. The results of the RF discharge measurements quoted here have been corrected for this.

In view of the considerable spread of these values for the Ar II transition probability, the true values of the Stark broadening parameters cannot yet be given to better than 20% for Ar I, imposing a similar error on the electron density determination.

Since the line widths due to Stark broadening, deduced from the total line widths after subtraction of Doppler and instrumental broadening, were rather small, it was possible that Van der Waals and natural broadening may have played some part in making up the line width. However, when calculated assuming pressure balance the Van der Waal broadening contribution is $W_{vw} \sim 10^{-3}$ Å and natural broadening $W_N \sim 10^{-3}$ Å.

In addition ion broadening would contribute approximately 4% of the final Stark profile, but in view of the possible 20% error involved above, these three contributions are insignificant and can therefore be ignored.

The value of electron density obtained from this experiment, i.e. $Ne = 4 \times 10^{15}$ electrons/cc., when substituted into Saha's equation together with pressure balance gives an electron temperature of 8,800°K. This is in excellent agreement withthe excitation temperature derived from the relative line intensity method and the electron temperature derived from the line to continuum ratio method (using the correction factor of 5x).

Equilibrium of the Discharge

Since we have now determined the excitation and electron temperature of the discharge as well as the electron number density, we can follow the method of Griem (ref. 25) to determine the validity of the local thermodynamic equilibrium (L.T.E.). This assumption was strongly invoked in the relative intensity temperature measurement, and to a lesser extent in the determination of electron temperature from the line to continuum ratio and from the electron density.

If L.T.E. pertains to the discharge, then electron density, electron temperature, ion temperature, excitation temperature, and populations of excited states, can all be related by thermodynamic equations, namely Saha's equation and Boltzmann's equation. These temperatures will be identical and, knowing any one of the above parameters, all others become calculable.

For this situation to exist, the condition that collisional rate processes dominate the radiative processes of decay and recombination must hold. Also, since the discharge is inhomogeneous and time dependent, (300 Hz temperature variation), it is necessary that the temperature variation with distance is such that an atom or ion cannot diffuse into a region of different electron temperature before equilibrating, and that the variation of temperature with time is such that there is no significant change of electron temperature during equilibration.

For a given excited level n to be in collisional equilibrium with respect to higher levels, its total transition probability for radiative decay must be smaller than its rate of

collisional excitation to the higher levels. This gives the following criterion (ref. 25):-

$$N_e \gg 7 \times 10^{18} \frac{Z^7}{n^{17/2}} \frac{(kT)^{\frac{1}{2}}}{(Z^2 Ei)} \quad cm^{-3}$$

where the symbols have their usual meaning,

i.e. $N_e \gg 3 \times 10^{15}/cm^{-3}$ for $n = 2$.

Consequently all excited levels in the discharge can be expected to be in L.T.E. with the free electrons (since $N_e = 4 \times 10^{15}$ here).

For the ground state, a separate validity criterion must be fulfilled which is more stringent. If the population of the first excited state is governed by a Boltzmann factor relating it to the ground state, then the system can be said to be in complete L.T.E., i.e. if the ground state is predominantly populated by collisional processes rather than radiative processes then it is in L.T.E. with respect to higher levels. From the radiative and collisional population rate equations the following requirement is derived:-

$$Ne \gg 9 \times 10^{17} \quad (E_z/E_n)^3 (kT/E_n)^{\frac{1}{2}} \quad cm^{-3}$$

where E_z is the energy level of the first excited state and E_i is the ionisation potential, i.e. $N_e \gg 7 \times 10^{16}$ cm^{-3}.

This is certainly not fulfilled and at first sight it would seem that the ground state cannot be in equilibrium with higher states. However, the radiative population rate of the ground state from the first excited states is reduced through self-absorption. Consequently this criterion on the electron density can be relaxed by a factor equal to the absorption coefficient of the resonance line radiation. This reduction factor is below 0.1 if the following relation is satisfied.

$$N_o d \gg \frac{4 \times 10^9}{f_{12} \lambda_{12}} \frac{(kT)^{\frac{1}{2}}}{(AEi)} \quad cm^{-2}$$

i.e. $8.8 \times 10^{17} \gg$ approx. 10^{14}

where N_o is the ground state density and d the physical size of the discharge.

This relation is well satisfied and the electron density necessary for ground state L.T.E. can be relaxed by an order of magnitude. There is also a further slight reduction in the criterion since it is probable that the second member of the resonance series is also being self-absorbed.

This gives the possibility that the ground state is within 10% of L.T.E., i.e. the collisional population rate is 10 x the radiative population rate.

However, a validity criterion given by Wilson (ref. 27) states that thermal equilibrium is only possible for an electron density such that

$$N_e \geqslant 2 \times 10^{16} \text{ cm}^{-3}$$

and this estimate allows for resonance line re-absorption. No account in these calculations is given of the effect of neutral atom-atom collisions. Although the atom-atom collisional de-excitation cross-section may be smaller than the electron-atom cross-section (no reliable values are available to compare, unfortunately), since the density of atoms is two orders of magnitude greater than that of the electrons one would expect them to play some part in the collisional depopulation scheme.

The agreement between the excitation temperature, that derived from the electron density in which a ground state density is assumed from pressure balance, and the line-to-continuum temperature measurement (with the 5 x correction factor) certainly lends support to the postulate of complete L.T.E.

Now there also exist temperature gradients in this discharge. If these are of such magnitude that a particle can easily diffuse into a region of very different temperature within its equilibration time, then deviations from L.T.E. can be expected. This effect is most likely to occur for the ground state neutral argon atoms. From velocity and mean free path considerations, an equilibration distance d_1 can be deduced over which the temperature must not vary significantly. The equilibration distance is of the order of a mm. for this discharge and nowhere, except at the extreme edges in the cool regions does the temperature vary to any extent over this distance. Since we are concerned only with the central, hot region of the discharge, this edge effect is of no consequence. In any case, the required rate of electron impact excitation from the ground state for L.T.E. is reduced at the edges of the discharge since ions and excited atoms from the hotter central region diffuse into these cooler regions.

Equilibration times must also be short compared to the rate of change of temperature (due to the 300 Hz ripple) within the discharge. Since the equilibration times in this discharge are of the order of 10^{-8} sec. or less, the effect of the 300 Hz temperature variation is negligible.

A comparison of this discharge source with others such as DC arcs and shock tubes, in the light of the above discussion, will be made in the next chapter.

Reed's Experiment

The method used by Reed consisted of measuring the total intensity of a line across the discharge, Abel inverting the spatial profile to obtain the true radial profile and equating the off-axis peaks with the intensity maxima of the emission of the spectral line used, i.e. the Fowler-Milne method (refs. 2 and 4).

This method depends on the fact that the intensity of a spectral line from a given ionisation stage (in this case the neutral atom) will increase with temperature, reach a maximum and then decrease at higher temperatures due to removal of atoms from that ionisation stage to a higher one. It is assumed that the population of the excited state forming the upper level of the transition concerned is in L.T.E. with the free electrons.

For the line used by Reed, the 7635Å 4p - 4s transition, the maximum intensity occurs at 15,000°K. When Reed made the Abel inversion of the spatial profile he obtained an off-axis peak in the line intensity. He identified this with the maximum intensity and assumed that the subsequent decrease in intensity from this maximum towards the axis of the discharge was due to the temperature exceeding this temperature of maximum intensity.

When this interpretation was applied to all the lines Abel inverted for the relative line intensity temperature determination, every line reproduced, to a few per cent accuracy, Reed's results. The 7635Å line itself gave the best agreement possibly because of its self-absorption - an additional contribution to the central dip in the Abel inverted profile.

However, the off-axis peaks in line intensity after Abel inversion are not due to the maximum intensity of the line being reached, and in the centre exceeded, as Reed assumed, but due to an

off-axis peak in the temperature. The central portion of the discharge is heated only by radiation and thermal diffusion and one would therefore expect its temperature to be below that in the skin-depth where the heating occurs.

Hence, the erroneously interpreted result of Reed for the temperature of this form of discharge should be ignored and not still quoted as "the expected temperature" (refs. 28, 29).

In conclusion it should be said that the Fowler-Milne method cannot be used in this type of discharge, but only when the distribution of two different ionisation stages of the same element can be examined and preferably where the temperature is a continuous smoothly varying function.

Conclusion

The characteristics of this R-F discharge are now known. It has a temperature profile approximating that of a shock-tube, i.e. the density (electron and atom) and temperature spatial variations are small. It has a low electron density compared to DC thermal arcs, and consequently there is a smaller broadening of highly excited states due to electron impacts. The R-F discharge appears to be very near to the ideal of L.T.E. There are no electrodes to "burn off" and consequently alter the operating characteristics during a series of measurements.

Therefore this R-F discharge seems emminently suitable for the measurement of argon I transition probabilities and the continuum correction factor. A survey of previous measurements of transition probabilities follows in the next chapter where the conclusion that

further work in this field is needed is reached. The subsequent chapters give details of these measurements.

P A R T 2

THE MEASUREMENT AND CALCULATION

OF NEUTRAL ARGON TRANSITION PROBABILITIES

CHAPTER 4

Survey of Experimental Measurementsof Transition Probabilities in Neutral Argon with Reference to the discharge sources used

Introduction

The determination of temperature in light sources such as plasma jets, arcs, and shock tubes can be simply performed by measuring the relative intensities of spectral lines from the neutral species, since the temperature is inversely proportional to the logarithm of the ratio of the total intensities, I, of lines arising from different energy levels En, provided local thermodynamic equilibrium (L.T.E.) exists between the levels involved in the transitions.

In discharge sources such as those mentioned above, L.T.E. does pertain to the excited levels in most cases and the temperature obtained will be not only an excitation temperature but also an equilibrium temperature, i.e. electron and ion temperature, in all probability. A graph of En versus log I/gA_{nm} where g is the statistical weight of E_n and A_{nm} is the transition probability from E_n to a lower level E_m, gives a straight line whose slope is inversely proportional to the temperature.

Lack of L.T.E. among the excited levels in the discharge would be apparent by a deviation of the graph (Boltzmann plot) from a straight line since the populations would no longer be controlled by a Boltzmann distribution.

Theoretical transition probabilities in neutral argon have been calculated for the two principal transitions,

$3p^5 5p$ - $3p^5 4s$

and $3p^5 4p$ - $3p^5 4s$

in LS, J_{1j} and intermediate coupling (ref. 30). Experimental measurements have also been made for these arrays (refs. 14, 15, 16, 18, 31, 32). Few measurements and no calculations have been made in transitions other than these.

Now these two groups of transitions have small energy spreads within themselves and, owing to difficulties in the experimental determinations of line intensities and the inherent inaccuracy of theoretical values, the two groups behave like two large, diffuse, points on the temperature determination graph, thus masking any deviations from L.T.E.

With transition probabilities available for higher energy levels, any deviations from linearity in the Boltzmann plot would become apparent and the accuracy of the temperature determination increased owing to the larger energy spread and greater number of lines involved.

It was therefore decided to measure transition probabilities in neutral argon from the following arrays:-

$(3p^5)$	4p - 4s	6s - 4p	4d - 4p
	5p - 4s	7s - 4p	5d - 4p
	6p - 4s		6d - 4p

The first two p - s transition arrays have already been measured, although not completely (out of 60 lines in these arrays, only 39 have been measured amongst 6 authors). It was therefore decided to remeasure these lines so that a complete self-consistent set of transition probabilities would be available for workers in the field.

Since doubt existed whether the ground state population of the R-F discharge was in L.T.E. (cf. previous chapter) and, since the Boltzmann plot method only requires relative values of log $I\lambda/gA$ it was decided to confine attention to relative transition probabilities only.

Also, examination of the equation for the intensity of a spectral line,

$$I(\nu) \propto A_{nm}\, e^{-Wn/kT}$$

shows that, for an error $\Delta E\%$ made in T, the corresponding error in A_{nm}, assuming no error in $I(\nu)$ will be approximately 17 $x\Delta E\%$ owing to the exponential factor; whereas when the error in the ratio,

$$\frac{I(\nu)_1}{I(\nu)_2} \propto \frac{A_1}{A_2} \exp\left[\frac{-W_1 + W_2}{kT}\right]$$

is examined, it is found that, by taking sufficiently small steps in energy difference, $W_1 - W_2$, the error involved can be made $\leqslant \Delta E\%$.

Thus, assuming a 2% error in knowledge of the temperature of the discharge, 34% error is immediately possible in an absolute transition probability determination whereas 2% or less is involved in a relative determination, assuming a discharge temperature of 10,000°K.

The feasibility and suitability of the R-F discharge source for determining neutral argon transition probabilities and the method to be used must now be discussed in the light of previous measurements.

Previous Measurements

The first recorded measurement of transition probabilities or line strengths in argon I for the $3p^5 4s - 3p^5 4p$ transitions are those of Schon (ref. 33) who, using the method of anomalous dispersion measured the ratio of transition probabilities of 5 lines in the infra-red. However, through not making a relative intensity measurement of the lines involved and using the f-sum rule (ref. 34), he was not able to quote absolute values. The method, called the Rozhdestvenskii hook method (ref. 35) used a Mach-Zehnder interferometer. For more complete detail and theory the reader is referred to various papers by Penkin (ref. 36) and Ostrovskii (ref. 37).

In 1956, Drawin (ref. 16) in the process of measuring the electron collision cross-section with hydrogen, helium and argon, using a gas vortex stabilised arc, determined ten transition probabilities in neutral argon. With the arc operating in argon containing a small percentage of hydrogen, he compared measured hydrogen line-profiles with those calculated by Holtzsmark. The temperature of the discharge was obtained by the application of Saha's equation. The arc used by Drawin operated at currents up to 200 amps. Observations were made "end-on" and the spectra recorded on photographic plates.

Gericke (ref. 15) using a solid-wall stabilised arc measured twenty argon I transition probabilities. The temperature in the "cascade-type" arc was determined using the absolute intensity of an argon II line whose transition probability had been determined by Olsen (ref. 4). Gericke's results were the first to include transition probabilities from levels other than 4p and 5p.

During the course of a programme designed to measure atom-electron collision cross-sections, Dickerman and Alpiner (ref. 39)

measured thirteen neutral argon lines from the 4p level. Neither Drawin nor Gericke had measured transition probabilities from this array owing to strong self-absorption ofthe lines in their discharges. The excitation source used by Dickerman and Alpiner was an arc similar to that of Olsen (ref. 4), operating at atmospheric pressure between a tungsten rod cathode and a copper plate anode. The Fowler-Milne method was used for determining the radial temperature. A correlation was made between the observed line profiles which showed self-absorption and the gf values obtained by Olsen (in a private communication later published, (ref. 40)); this showed that self-absorption was definitely proportional to the gf values and apparently thus confirmed their relative accuracy.

Measurements of 24 neutral argon lines were made by Razumovskaya (ref. 41); however, these differ by up to two orders of magnitude from previous measurements. Relative values of the oscillator strengths were obtained by determining the level populations by an absorption method and the relative values put onto an absolute scale using the Thomas-Kuhn sum rule. Measurements were made in a 6 MHz discharge at pressures of about 1 mm.; square section tubes were used to avoid "distortion caused by cylindrical tubes."

Olsen (ref. 24), using a high current arc at atmospheric pressure between a thoriated tungsten cathode and a cooled copper plate anode, measured 16 argon I and argon II transition probabilities. The Fowler-Milne method was used to determine the radial temperature profile by applying it to an argon I and an argon II line, and to the continuum. The discharge had already been shown to exhibit L.T.E. (ref. 4), and the particle densities and partition functions computed using the ionisation potential depression

previously estimated (ref. 17).

Doherty (ref. 31) used a conventional shock-tube to determine transition probabilities from the absolute line intensities of neutral argon which was mixed with neon in the shock tube.

The first measurement of argon oscillator strengths by the anomolous dispersion method since the work of Schon mentioned above was by Pery-Thorne and Chamberlain (ref. 32). Fourteen lines from the 4p - 4s level were measured and put onto an absolute scale by estimating an absolute value for one of the lines using the f-sum rule.

The wall-stabilised argon arc containing a trace of hydrogen was used by Popenoe and Shumaker (ref. 18) to measure argon transition probabilities. The line shape of $H\beta$ gave the electron number density which, with the assumption of local thermodynamic equilibrium gave, via the Boltzmann equation, the argon level populations. The transition probabilities of three argon lines, two neutral and one ionised were measured absolutely. From these three lines ten other argon line transition probabilities were obtained by a relative measurement without any hydrogen in the arc. The lines thus measured were from the 5p- 4s(5), 4d - 4p(2), 4p - 4s(1), 5s - 4p(2) and 6s - 4p(1) groups as well as two argon II lines. The numbers in parenthesis refer to the number of lines measured in that group.

The only theoretical calculation of transition probabilities in neutral argon in intermediate coupling was that of Garstang and Van Blerkom (ref. 30) who gave, for the 4p - 4s and 5p - 4s transitions, the transition probabilities in Ls, J_{ij} and intermediate coupling.

A summary of the groups of lines studied can be made as follows:-

Group I	$3p^5 4p - 3p^5 4s$
Group II	$3p^5 5p - 3p^5 4s$
Group III	$3p^5 nd - 3p^5 4p$
Group IV	$3p^5 ns - 3p^5 4p$

Drawin and Gericke measured lines from Group II only.

Pery-Thorne and Chamberlain measured lines only from Group I.

Olsen measured lines from both Groups I and II.

Popenoe and Shumaker measured 5 lines from Group II.
2 lines from Group III
1 line from Group I
3 lines from Group IV.

Doherty measured lines only from Group II.

Garstang and Van Blerkom calculated transition probabilities for Groups I and II.

Thus there is only one set of measurements which include all four groups of lines and then only eleven lines are given. These results are tabulated in figs. 7.18 - 7.25 where it can be seen that variations of up to a factor of 3 exist amongst the experimental values and variations of up to two orders of magnitude occur between the experimental values and calculated intermediate coupling values.

These values of transition probabilities will now be discussed with reference to the discharge sources used and the possible errors incurred.

Discussion of previous transition probability measurements

All Drawin's measurements were carried out in an arc containing a small percentage of hydrogen mixed with the argon. His diagnostic technique, based on the measurement of hydrogen line broadening, assumed that the mixture ratio of hydrogen to argon was the same in all positions in the arc and equal to the initial mixture, i.e. there was no "demixing" effect (refs. 25 and 42). The arc used by Drawin was constricted by the cold gas vortex and thus would have had a very large temperature gradient. Because of this gradient, a separation or demixing of the constituent gasses within the arc could occur, the ions and atoms of the gas with the lower ionisation potential (H_2) having a larger concentration gradient than those of the other gas (Ar). In the steady state of no net diffusion the ions and atoms of hydrogen would have a larger concentration in the hotter regions of the arc. Thus the temperature measured by the hydrogen line method gives the temperature pertaining to the hydrogen atoms and the use of an assumed constant gas ratio leads to serious errors wherever the assumption of pressure balance to obtain absolute values is invoked.

Richter (ref. 42) dividing the arc cylinder into radial zones, examined this separation for hydrogen mixed with argon as well as other gas mixtures. His results suggest that even with low current arcs, separation of the constituent gasses can occur, whilst with the solid wall-stabilised arc, a separation of over 20% was observed for a 10% hydrogen 90% argon mixture.

Pressure corrections in arcs due to the magnetic self-compression of the high current density and due to the continuous transport of momentum away from the central regions analogous to the radiometer effect, can be serious (ref. 25).

Electrode processes, which are extremely complex in high current arcs, and result in very strong local fields, can contribute to errors caused by magnetic self-compression, especially when the arc is viewed "end-on" as in Drawin's work.

The possibility of serious demixing was avoided by Gericke, who measured relative transition probabilities and thus avoided any assumption of pressure balance in the arc. However, to measure the temperature he used an argon II line whose transition probability he obtained (in a private communication) from Olsen. The value of this transition probability has since been shown to be in serious error (ref. 18, 43). The relative values were put onto an absolute scale by comparison with Bates and Damgaard calculations (ref. 44) and, although Gericke was the first person to measure transitions from arrays other than the 4p and 5p levels, his results must be viewed with suspicion. Also, although Gericke avoided the errors of separation, his arc, being of the solid-wall-stabilised type and carrying currents of up to 120 amps could still be affected by radial pressure variations.

The free-burning arc used by Olsen was operated at a current of 400 amps with anode and cathode separated by only 5 mms. The temperature was measured by using the Fowler-Milne method. The lines used were the argon II 4806Å, and the argon I 6965Å and 7635Å lines. He computed the self-absorption occurring for these lines and attempted to correct for it, but he assumed that the absorption coefficient reached a maximum at the same temperature (and hence position) as the line intensity. This is not so. He also estimated the self-absorption using approximate transition probabilities derived from the measured emission coefficients assuming no self-absorption, using the equation -

$$K_\lambda(T) = \frac{\lambda_o^4}{\Delta\lambda} A_{nm} C f(T)$$

where C is a constant for a given line derived from its integrated profile. $\Delta\lambda$, the line width, was assumed to be constant with temperature and electron density. Thus his estimated optical depth was incorrect.

Olsen's value of 0.2 for the optical depth of the 4806Å argon II line does not agree with calculations based on his measured conditions for the discharge (ref. 18). These calculations give values of 0.7 to 0.3 depending on the line width calculation, since considerable doubt has been thrown on the validity of Griem's Stark broadening parameters, (refs. 18, 26). These considerations have led to the belief that Olsen's off-axis peaks may in fact be due not to the temperature corresponding to maximum line intensity being reached but to self-absorption (ref. 18).

Doherty, using a conventional shock tube, which was comparatively free from the above pitfalls obtained a set of transition probabilities which agree reasonably well with those of Olsen. He also measured neon transition probabilities (actually oscillator strengths) but these have had doubt cast on them by the more recent work of McLean (ref. 45), whose T-tube experiments seem to indicate that Doherty's values for neon are incorrect by up to a factor of 3. Since Doherty's thesis is not available in this country and his work has not been published in a Journal, no comment or criticism of his results can be made.

The values given by Pery-Thorne and Chamberlain, whilst being the most complete set, were unfortunately, because of the method used,

confined to the 4p - 4s array. Possible errors incurred here by the use of the f-sum rule to put the relative oscillator strengths onto an absolute scale may not be as serious as deviations from pressure balance and demixing effects in the high current devices mentioned above.

The experiment of Popenoe and Shumaker, using a wall-stabilised arc, obviated demixing by measuring the hydrogen/argon ratio across the arc column. A thorough error treatment has been given by these authors in their paper and they concluded that their values were accurate to about 13%. Errors due to deviations from pressure balance due to magnetic self-compression effects and momentum transport effects were accounted for.

The only source of error not accounted for was the assumption in their plasma composition calculations, of the validity of the Debye correction to the ionisation potential. Deviations in the values of depression of ionisation potential could cause errors in the plasma composition calculations as mentioned in chapter 2. However, apart from this possibility, this work was the most careful and error conscious of all the published work; it is a pity that the number of lines treated was so few.

In all the methods of determining plasma composition from electron densities deduced from measured hydrogen line profiles, the variety of methods of calculating the depression of ionisation potential and their lack of agreement is a serious source of error. The theory of Stark broadening for hydrogen lines at best is subject to an uncertainty of 5%. Another source of error not mentioned above, but common to all arcs which have high temperature

gradients, is the deviation from local thermodynamic equilibrium due to the temperature of the arc varying significantly over a distance comparable to the equilibration distancesof an atom (ref. 25).

Conclusion

The radio-frequency plasma torch, while having a temperature profile approximating that of a shock tube, but having none of the disadvantages of intermittency, would seem to be an ideal tool for measuring transition probabilities. No significant errors can be caused by extreme temperature gradients since these only occur at the outer edges of the discharge where the contribution to the total intensity is negligible. The discharge is much larger than the wall and gas vortex stabilised vortex arcs making Abel inversion procedures simpler and more accurate. There is no large current flow nor any electrode processes which could cause pressure unbalance due to the radiometer effect and momentum transport effect. Doppler and Stark broadening at the temperature and electron density of the discharge are small, consequently total line intensities from highly excited states can be measured without serious difficulties. Provided a method of temperature determination is used which is independent of a transition probability, and not dependent significantly on an estimate of the ionisation potential depression, this R-F discharge should be ideal for measuring line intensities and hence transition probabilities. The temperature of the discharge is such that there will be no interference from argon II lines and the absence of electrodes means that there will be freedom from impurity spectral lines.

The atmospheric pressure radio-frequency discharge is therefore proposed as an extremely useful tool for extending existing transition probability measurements to higher energy level arrays and also repeating existing measurements for the purpose of comparison.

In the next chapter a survey is made of methods for measuring the temperature of the RF discharge accurately, so that transition probabilities can be measured.

CHAPTER 5

Survey of Methods for Measuring Discharge Temperatures Independent of any Transition Probability

Introduction

Since it is intended to measure transition probabilities by an absolute intensity determination, and since it has been shown in Chapter 3 that L.T.E. exists between the excited states in the discharge, a measurement of the temperature of the discharge must be made which is both accurate and independent of any atomic parameter such as transition probability or continuum intensity correction factor, and which depends on the existence of L.T.E. only between the excited states. These criteria reduce the methods for temperature determination in this discharge to three possibilities; a reversal technique, where the ratio of emission and absorption coefficients at a line centre with a background source yields the Planck function and hence the temperature; a method based on the determination of the electron number density which, with Saha's equation, will yield the temperature; and the Doppler profile method which is completely independent of the existence of L.T.E. These methods will be discussed in turn in this chapter.

The 'Reversal' method

This method has been stated to be inapplicable to inhomogeneous discharges (refs. 46, 25) and until recently has only been used for homogeneous systems such as shock tubes (ref. 47 and 75). However, in 1960 Freeman and Katz described

a method for the determination of the radial distribution of 'brightness' in a cylindrical luminous medium with self-absorption, (ref. 48), and in 1965, Elder, Jerrick and Birkeland developed a method for determining the radial profiles of the absorption and emission coefficients, and hence temperature in a cylindrically symmetric discharge which had self-absorption (ref. 49).

Since it has already been shown and proven in Chapter 2 that the 7635Å 4s - 4p spectral line exhibits self-absorption in the R-F discharge, this line would be suitable for an emission and absorption coefficient determination.

In a simple homogeneous discharge the basis of the method is as follows:-

First one measures the intensity emitted by a spectral line from the discharge $I_{\lambda p}$ which can be written $I_{\lambda p} = I_T \left[1 - \exp(-\tau_\lambda)\right]$ (1) where I_T is the Kirchoff-Planck function for the intensity of a black-body at temperature T, and τ_λ is the optical depth of the discharge at wavelength λ. A light source of known intensity $I_{\lambda c}$ is placed behind the discharge, and its attenuation through the discharge at the wavelength λ measured; the total intensity received in this case, $I_{\lambda t}$ is given by:-

$$I_{\lambda t} = I_{\lambda p} + I_{\lambda c} \exp(-\tau_\lambda)$$

$$\text{thus} \quad \exp(-\tau_\lambda) = \frac{I_{\lambda t} - I_{\lambda p}}{I_{\lambda c}} \qquad (2)$$

Since all the three quantities on the right hand side are measured, I_T can now be determined from equation (1) and thus the temperature found. Instead of using a background source, whose intensity must first be measured, a mirror can be placed behind the discharge and the intensity transmitted then becomes:-

$$I_{\lambda t} = I_{\lambda p} + I_{\lambda p} \exp(-\tau_\lambda)$$

so $$\exp(-\tau_\lambda) = \frac{I_{\lambda t}}{I_{\lambda p}} - 1$$

$$\therefore \quad I_{\lambda p} = I_T \left[1 - \frac{I_{\lambda t}}{I_{\lambda p}} - 1\right]$$

$$I_T = \frac{I^2_{\lambda p}}{\left[2I_{\lambda p} - I_{\lambda t}\right]}$$

In this case, only two measurements are made.

Another variation on this method is to vary the intensity of the background source until the signal received by the detector is equal to that of the background source, then $I_{\lambda o} = I_{\lambda t}$ and the temperature of the background source equals that of the discharge.

The following two methods are based on this 'reversal' technique. In the first method the absorption coefficient is determined and substituted into an equation for the "brightness" of the discharge, this yields the "brightness per unit depth" which gives the Kirchoff-Planck function and hence the temperature. The second method also requires the measurement of the absorption coefficient and the observed emissivity. The true emissivity is then determined using the absorption coefficient. The ratio of the true emissivity and the absorption coefficient yields the Kirchoff-Planck function for the spectral line involved.

Method A

The first method published (ref. 48) for the reversal technique of temperature determination in inhomogeneous discharges was as follows:-

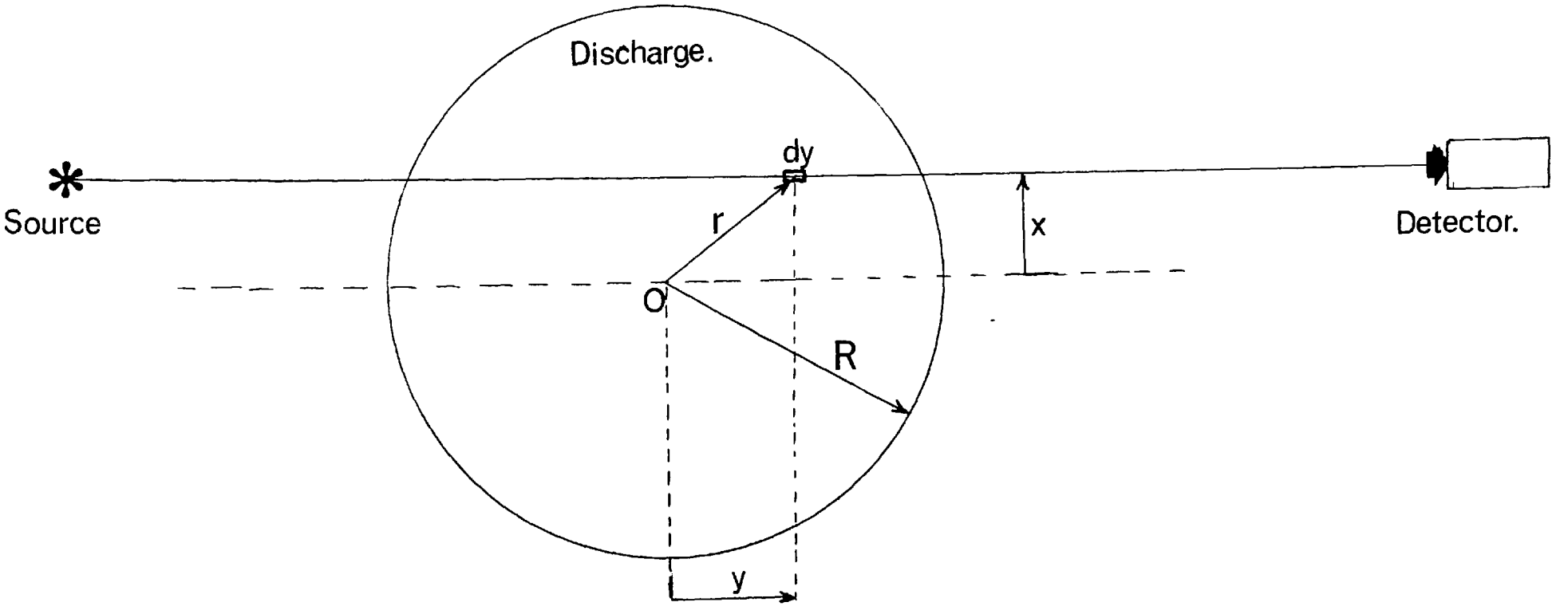

FIG. 5.1. Reversal technique arrangement.

In fig. 5.1, consider the detector receiving a signal J_{TOTx} due to the background source and the discharge, where in this case the background source is a mirror of reflectivity μ, reflecting the discharge emission back through the discharge. The contribution to J_{TOTx} from an element dy of the discharge at radius r is:-

$$J_r\,dy \quad \exp\left[-\int_y^{(R^2-x^2)^{\frac{1}{2}}} \alpha_p dy \right] \qquad \begin{aligned} r^2 &= x^2 + y^2 \\ p^2 &= x^2 + \eta^2 \end{aligned} \tag{3}$$

where α_p is the absorption coefficient and J_r is defined as the brightness per unit optical depth. The contribution from the mirror is given by:-

$$\mu J_x \exp\left[-\int_{(R^2 - x^2)^{1/2}}^{(R^2 - x^2)^{1/2}} \alpha_r \, dy \right] \tag{4}$$

where J_x is the observed brightness at x, i.e. the integration of equation (3) along a chord through the discharge.

$$\text{i.e.} \quad J_x = \int_{-(R^2 - x^2)^{1/2}}^{(R^2 - x^2)^{1/2}} dy\, J_r \left[\exp -\int_y^{R^2 - x^2} d\eta \alpha_p \right] \tag{5}$$

so

$$J_{ToTx} = J_x + \mu J_x \quad \exp\left[-\int_{-(R^2 - x^2)^{1/2}}^{(R^2 - x^2)^{1/2}} dy\, \alpha_r \right] \tag{6}$$

If we define $w_x = \frac{1}{\mu}\left[\frac{J_{ToTx}}{J_x} - 1\right] - 1$

Then equation (6) can be written

$$\log \frac{1}{1+w_x} = \int_{-(R^2 - x^2)^{1/2}}^{(R^2 - x^2)^{1/2}} dy\, \alpha_r \tag{7}$$

This equation can be written in the form of an Abel inversion equation,

$$\alpha_r = \frac{1}{\pi r} \frac{d}{dr} \int_r^R \mathrm{Log}_e\left[\frac{1}{1+w_x}\right] \frac{x\,dx}{(x^2 - r^2)^{1/2}} \tag{8}$$

Thus α_r, the absorptivity can be determined as a function of r, and, using the values obtained, the equation for J_x, equation (5), can be numerically solved.

The meaning of J_r can be seen by considering the equation of radiative transfer

$$-\frac{dI}{\alpha ds} = J + B$$

Integrating,

$$J_s = J_o \exp\left[-\int_o^s \alpha ds\right] + \int_o^s B(s^1) \exp\left[-\int_o^s \alpha\, ds\right] \alpha\, ds^1.$$

where J_o is the incident intensity from a background source and J_s is the intensity received by the detector.

Now this equation is identical to that for J_{TOTx} above if $B(r) \alpha r = J_r$ where B(r) is the Kirchoff-Planck function. This can be verified by integrating for a homogeneous system and letting $J_o = 0$. Hence J_r is the emission coefficient of the line if we define α_r to be its absorption coefficient.

Provided the reflectivity of the mirror is known, two measurements are required to give the discharge temperature, the absolute measurement of intensity J_x, and the relative intensity measurement $\mu J_x / (J_{TOTx} - J_x)$.
A disadvantage of this method is that equation (5) cannot be simply solved for J_r by an Abel inversion.

Method B

As before, two scans are taken, of the discharge emission at a spectral line centre and the attenuation of a background source (instead of a mirror) through the discharge at the line centre (ref. 29). If the intensity of the background source at a frequency corresponding to a line centre is J_f, the intensity of the line itself $J_\nu(x)$ and the intensity of both $J_{T\nu}(x)$ then

the transmission of the discharge $w_\nu(x)$ to the background source is given by

$$w_\nu(x) = \frac{J_{T\nu}(x) - J_\nu(x)}{J_f} \tag{9}$$

The transmission can also be written as

$$w_\nu(x) = \exp\left[-2\int_x^R \frac{k_\nu(r)\rho(r)r\,dr}{(r^2 - x^2)^{1/2}} \right] \tag{10}$$

where $K_\nu(r)\rho(r)$ is the volume absorption coefficient.

This equation can be rearranged into the form of an Abel inversion equation,

$$\text{i.e. } k_\nu(r)\rho(r) = -\frac{1}{\pi r}\frac{d}{dr}\int_r^R \log\left[\frac{1}{w_\nu(x)}\right]\frac{x}{(x^2 - r^2)^{1/2}}dx \tag{11}$$

The intensity $J_\nu(x)$ of the spectral line from the discharge is given by

$$J_\nu(x) = \int_{xo}^{xyo} j_\nu(r)\rho(r)\left\{1 + \exp\left[-2\int_{xo}^{xy_1} k_\nu(r')\rho(r')dy' \right]\right\} \times \left\{\exp\left[\int_{xy_1}^{xyo} k_\nu(r')\rho(r')dy' \right]\right\}dy \tag{12}$$

where $j_\nu(r)\rho(r)$ is the volume emission coefficient.

By rearranging the limits of this integral, the equation (12) can be rewritten

$$\frac{J_\nu(x)}{\sqrt{w_\nu(x)}} = 2\int_x^R j_\nu(r)\rho(r)\left\{\text{Cosh } G_\nu(xr)\right\}\frac{r}{(r^2 - x^2)^{1/2}}dr$$

where $G_\nu(xr) = \int_x^r \frac{k_\nu(r')\rho(r')dr'}{(r'^2 - x^2)^{1/2}}$

Writing $j_\nu(r)\rho(r) = j_{\nu o}(r)\rho(r) + j_{\nu 1}(r)\rho(r) + \ldots$

where $2\int_x^R j_{\nu o}(r)\rho(r)\frac{r}{(r^2 - x^2)^{1/2}} = \frac{J_\nu(x)}{\sqrt{w_\nu(x)}}$

and $\int_x^R j_{\nu n}(r)\rho(r)\frac{r}{(r^2-x^2)^{1/2}}dr = -\int_x^R j_{\nu n-1}(r)\rho(r)\left\{1-\text{Cosh } G_\nu(xr)\right\}\frac{rdr}{(r^2-x^2)^{1/2}}$

Now $j_{\nu 0}(r)\rho(r)$ can be obtained by an Abel inversion of $\frac{J_\nu(x)}{\int w_\nu(x)}$

Once this is found, $J_{\nu 1}(r)\rho(r)$ can be obtained. The term Cosh $G_\nu(xr)$ can be expanded and for transmissions $\gg$ 20% only the first term of the expansion is necessary, the second term being negligible ($<$1%),

$$\text{i.e. } 1 - \text{Cosh } G_\nu(xr) \simeq \frac{G^2_\nu(xr)}{2}$$

Thus, in this method, the absorption coefficient, which has been obtained by an Abel inversion procedure from the observed transmission is not used in the first approximation to the emission coefficient. Consequently errors made in the process of Abel inversion do not accumulate. Now the expression for the absorption coefficient, equation (11), because of the finite resolution of the spectrograph used gives the transmission multiplied by the slit function of the spectrograph integrated over the spectral width. In Appendix 3, it is shown that for a small error in the determination of temperature we require a large optical depth since the error is inversely proportional to the optical depth. Now to easily resolve a line it must have a large half-width. However, optical depth is inversely proportional to line width so that an easily resolved line will have a small optical depth whereupon the above criterion is relaxed and there is no need to resolve the line. Thus the narrower the line, the greater the need to resolve it! For equation (11) to be valid

$$\frac{1}{\Delta\nu}\int_\nu \log\frac{1}{w_\nu(x)} \text{ must } = \log\left[\frac{1}{\Delta\nu}\int w_\nu(x)dv\right]^{-1}$$

These equations are approximately equal for transmissions $\gg$ 80%.

$\Delta\nu$ is the spectral slit width over which the transmission is integrated. The error caused by the finite spectral slit width is analysed in Appendix 3.

Number Density Method

If L.T.E. exists in the discharge so that Saha's equation may be used to relate the electron number density to the electron, ion or neutral species temperature, all of which are equal under the conditions of L.T.E., then a measurement of electron density will immediately determine exactly the conditions within the discharge. However, as shown in chapter 2, the electron density determinations in the radio-frequency discharge are inaccurate owing to the presence of Doppler broadening, which in the centre of the discharge is dominant. Also the narrowness of the line profile makes accurate measurement difficult. The Stark broadening parameters calculated by Griem (ref. 43) are accurate to only 20%, cf. Chapter 2, and this would lead immediately to a 20% inaccuracy in the electron density determination. To obtain that part of the line profile caused by Stark broadening would require a knowledge of the temperature so that the Doppler broadening contribution to the total profile could be subtracted. Consequently, a reiterative process of substituting an expected temperature to determine the Doppler profile, subtracting that profile from the observed profile, deducing the electron number density (also slightly temperature dependent) and then checking if this density gives the correct temperature through Saha's equation and then modifying the temperature, would have to be performed for each position.

This problem can be alleviated by choosing a spectral line from a high energy level whose Stark broadening is such as to completely dominate any Doppler broadening which can then be ignored. Unfortunately few Stark broadening parameters have been determined for highly excited neutral argon lines and these will still be subject to an error of the order of 20%, if not more (ref. 25).

However, Stark broadening parameters have been determined with an accuracy of 10% experimentally and theoretically, for the principal hydrogen lines in the visible region, the Balmer series, and for certain helium lines. In the case of $H\beta$, the broadening parameter has been determined to about 5%. Consequently, seeding the discharge with hydrogen, so that the half-width of the line chosen, say $H\beta$, can be easily measured is a possible method of obtaining the temperature. This method has been used for example, by Wiese and Shumaker (ref. 50) to determine the radial temperature profile of a high current arc operating in an oxygen atmosphere, and by Popenoe and Shumaker (ref. 18) in an argon arc.

Under the approximate conditions for the discharge already found, i.e. temperature 10^4°K and electron density 4×10^{15}/cc, the half width of $H\beta$ would be 6.0Å of which the Doppler profile contribution would be 0.032Å, quite negligible. The $H\beta$ line occurs at 4861Å and to be able to measure the line profile accurately, since each intensity point would have to be Abel inverted across the discharge diameter, a scan of the line profile of $\pm$ 20Å would be required. At 4876Å there is a strong argon I line which is a transition from a 7d level to a 4p level

Due to the high level of excitation this line will have a Stark width of several angstroms and hence could interfere in the determination of the base line of the $H\beta$ profile. However, the degree of interferenoe could be assessed by operating the discharge in argon alone, measuring the continuum and interfering line oontributions in the speotral region involved and assuming that the addition of hydrogen to the discharge did not affect the total electron density so that the interfering argon line and continuum background would not be altered.

At approximately 10,000°K, the Saha functions for argon and hydrogen are identical, so this last assumption would be valid, i.e.

$$\frac{n_{e\,H}^{2}}{n_{oH}} = KT^{3/2}\ \frac{U_{iH(T)}}{U_{oH(T)}}\ \exp\left[\frac{-W_{iH}}{kT}\right] \doteq \frac{n_{e\,A}^{2}}{n_{oA}}$$

where $K = \dfrac{2(2\pi mk)^{3/2}}{(h)^{3}}$

W_{iH} is corrected for ionisation level depression and the other symbols have their usual meaning.

Now the method consists of measuring the total electron density $n_{eT} = n_{eH} + n_{eA}$ which, with the above Saha equations, a knowledge of the ratio of hydrogen to argon, and the assumption of pressure balance gives the temperature (in this case electron temperature) of the disoharge.

i.e. $p = (Ln_{oH} + n_{oH} + 2n_{eA} + 2n_{eH})\ kT$

$$n_{eH} = \sqrt{n_{oH} K\ \frac{Ui_{H}(T)}{U_{oH}(T)}}\ T^{3/4}\ \exp\left[-\frac{W_{iH}}{2kT}\right]$$

$$n_{eA} = \sqrt{Ln_{oH} \frac{K\, U_{1A}(T)}{U_{oA}(T)}}\; T^{3/4} \quad \exp\left[\frac{-W_{iA}}{2kT}\right]$$

where $L = \frac{n_{oA}}{n_{oH}}$

and $n_{eH} + n_{eA} = ne_T$ which is measured.

We thus have five equations and five unknowns, one of which is T, hence we can solve for T.

On analysing the error made in the determination of T caused by incorrect measurements of L and n_{eT}, it is found that this method is very accurate in the temperature range of the discharge owing to the rapid variation of n_e with a small variation of T, cf. Appendix 2.

However, the error analysis does not give the whole story; pressure balance and an absolute pressure are assumed, while "demixing" (cf. Chapter 4) is ignored. Both effects can seriously alter the accuracy of this method.

Although this method is indeperdent of neutral species concentration and gives an electron concentration at a given position within the discharge, a value of L, the mixture ratio of hydrogen to argon, has to be assumed to solve the above equations for T.

Owing to the difference in ionisation potentials of hydrogen and argon (assuming that all the hydrogen is dissociated by the time it reaches the region of interest), local concentrations of one or other of the gasses can exist in the discharge and the resulting compositions may bear no relation to the original predischarge composition.

An estimate of the demixing could be made by measuring the total intensity of an argon line and a hydrogen line across the discharge and seeing how the neutral concentration of each species varied with position (since the intensity of a line with the assumption of Boltzmann's equation is proportional to the ground state concentration). Unfortunately, to be able to do this the temperature profile across the discharge would have to be known. Consequently this would have to be assumed and, on obtaining the temperature via the above equations, reiterated to determine a more accurate value of L.

Along with the problem of solving the above equations there is thus this demixing estimation problem, the continuum background and interfering line problem, and the tedious process of Abel inverting, point by point, a line profile.

Doppler Profile Method

Although the Doppler broadening of a spectral line is a function of the neutral gas temperature only and is independent of any assumption concerning the equilibrium of the discharge, the usefulness of this method is limited since every line emitted by the discharge is affected by Stark broadening (cf. Chapter 3) and this contribution, albeit to an accuracy of 20%, would have to be subtracted from the total line profile to give the broadening due to the Doppler effect.

Each point across the line profile would have to be inverted across the discharge to give a radial profile of the line profile and then the correction made for Stark broadening.

Spectral lines can be chosen which have negligible Doppler broadening compared to Stark broadening (by considering high excitation level spectral lines) but apart from the resonance lines which also suffer from severe self-absorption and broadening from this effect, no lines can be chosen which have a negligible Stark effect. It is therefore at these electron densities, not worth while considering the Doppler effect method of measuring the disoharge gas temperature.

Conclusion

The method of reversal for temperature determination, while having an overall accuracy comparable to the H_β line profile method, has none of the problems of demixing. Also, because of the high resolution needed for the reversal technique (the only disadvantage of this method) the background continuum which must be accounted for in the line profile method, is negligible and no correction need be made.

In the reversal method, the calculation of the emission coefficient from the observed intensity requires a long iterative procedure involving the calculated value of the absorption coefficient (obtained from the transmission) to correct for self-absorption. This necessitates magnetic disc storage on an IBM 7090 computer (Birkeland 1966 private communication). However in cases of small absorption, i.e. transmissions $\gg$ 80%, no iterative procedure is necessary and for transmissions $>$ 60% only one iteration is required, which affects the first approximation to the emission coefficient by a few per cent only. Consequently the

correction to the emission coefficient was simply calculated by curve fitting the calculated absorption and emission coefficients and solving analytically without any significant loss of accuracy but with considerable saving of computer time. Details of this method are given in Appendix 4.

Thus, for simplicity, accuracy and a dependence on L.T.E. between two excited levels only, the reversal method was chosen as the method for determining the radial temperature profile of the R-F discharge. The next chapter gives the experimental details of this temperature measurement and the measurement of 116 transition probabilities.

CHAPTER 6

Temperature Measurement by the Reversal Technique and Transition Probability Measurements

Introduction

As concluded in the previous chapter, with sufficient care taken over the determination of the absolute emission coefficient of the spectral line involved, the reversal method is the most advantageous to use under the conditions which apply to the radio-frequency discharge. From the error analysis in Appendix 3, it is concluded that no significant error will be introduced by the finite resolution of the dispersive system used provided that a spectral slit width of less than the line half-width is used. By measuring the absorption coefficient a sufficient number of times in each position across the discharge so that errors caused by cathode dark noise of the photomultipliers used and shot noise, are reduced to the order of a few per cent, the final temperature determination should be capable of an accuracy of a few per cent. The accuracy of the temperature determination is verified by repeating the experiment for another spectral line and comparing the two temperature profiles obtained.

Apparatus

Spectral Line Choice The 7635Å, $1s_5 - 2p_6$ (Paschen notation) transition had already been shown to exhibit self-absorption both experimentally and theoretically (cf. Chapter 2), and although a line of longer wavelength, e.g. 8115Å would have a larger self-absorption due to the wavelength and transition probability

dependence of the optical depth, (since both are greater than those of the 7635Å line), the former line was chosen for detection reasons which are discussed later. The lower level of this transition is metastable and, although in L.T.E. there is collision domination in the level population mechanisms, it could be that this level being populated by collisional de-excitation and radiation from higher levels, and depopulated only by collisions, might have a higher population than would be expected from a Boltzmann distribution, leading to a larger value of absorption coefficient and smaller value of temperature than would be correct.

To check if this was occurring, the experiment was repeated using another self-absorbing spectral line which did not have a metastable lower level, the 7514Å $1s_4 - 2p_5$ line. Owing to its smaller value of self-absorption, more measurements were made of the emission and absorption coefficients of this line to ensure that the accuracy of the temperature obtained was comparable to that obtained using the 7635Å line.

Dispersive System

The approximate conditions already found for the R-F discharge indicated that the 7635Å line profile was composed of a Stark broadening contribution of 0.0235Å half-half width and a Doppler broadening contribution of 0.0493Å half 1/e width. In addition to this there was broadening due to self-absorption (ref. 52). The values for the 7514Å line were similar. Thus both lines had a total half-width of approximately 0.12Å. As mentioned

previously, a resolution better than the half-width of the line was needed to avoid serious errors caused by averaging the self-absorption coefficient over the line profile. Consequently a resolution of the order of 300,000 was required, so that not only was the half-width easily resolved but the natural width imposed by the grating did not influence the line profile or width in any way. This resolution was achieved by a 5", 30,000 line/inch grating operating in the second order.

At the wavelengths involved here, the angle of incidence of the grating was such that its focal plane was at a distance from the grating less than half its radius of curvature, i.e. for a 10 ft. radius of curvature grating, the focus of the 7635Å line in the second order was 4 ft. from the grating. Since grating focussing and tilt mechanisms in most spectrographs do not operate up to such short distances from the exit plane, a 21 ft. 30,000 line/inch grating was chosen and put in the 10 ft. normal incidence Eagle spectrograph previously described (cf. Chapter 2). Incorrect focal plane curvature was of no consequence since focus was required over such a small spectral width (~ 0.1Å), that the width accepted by the exit slit was completely within the depth of focus of the system. With the plate holder at its maximum angle of 45°, and an exit slit of 200μ, the bandwidth emerging from the exit slit was 0.09Å.

Background Source

From the caloulations on optical depth (cf. Chapter 2) a transmission of about 60% was expected for the 7635Å line and about 80% for the 7514Å line. The higher the intensity of the background source used, the greater the response from the detection system and the smaller the shot noise error (Appendix 5). Therefore an intense source of light in the 7,500 - 7.700Å region was required. Two possible sources were considered, a DC thermal arc in argon emitting both the above spectral lines, and a condenser discharge source, emitting a continuum.

Source 1:-

The inert gas thermal arc has been studied by Olsen (ref. 4) who recorded temperatures ranging from 10,000 to 25,000°K, using the Fowler-Milne method previously described (cf. chapter 2). The range of electron number densities recorded was from 10^{16} per cc. to 2×10^{17} per cc. The source was shown to be in local thermodynamic equilibrium by the agreement between the temperature determined by the atomic spectral line intensity and that determined in the higher temperature regions using an ionic spectral line.

Taking a temperature of 15,000°K and a corresponding electron number density (calculated from Saha's equation) of 2×10^{17} per cc. the 7635Å line would have a Stark broadened half width of 2Å and a shift of 1.5Å. Under the conditions of the radio frequency discharge, the shift of the 7635Å line was only 0.03Å. Now the intensity of that part of the profile of the 7635Å line in the DC thermal arc corresponding to the comparatively unshifted line in the radio-frequency discharge. was equivalent to an unshifted line at 11,000°K only.

Consequently, at the R-F discharge line centre, the DC arc line would not be significantly more intense. In fact, since the DC discharge was only 1 cm. in diameter compared to 3 cms. for the R-F discharge, the optically integrated intensities would be comparable.

Source 2:-

It has been shown by Parkinson and Reeves (ref. 53) that a "Garton" type flash tube (ref. 54, 55) has a continuum intensity corresponding to a blackbody at 29,000°K. The intense pulse of continuum radiation is produced by the discharge of a 10 KV low inductance capacitor through a ceramic capillary. The flash tube is shown in fig. 6.1. The flash tube has an intensity which is reproducable to a few per cent, it is simple to operate, needs no inert gas flow and can be triggered by a simple thyratron circuit. The only disadvantage is that the source is not continuous like the DC thermal arc but has a rise time of about 1μ sec. to maximum intensity and a decay lasting 10 secs. Consequently care had to be taken over integration of the detector output signal. This signal did not suffer as much from shot noise as the thermal arc owing to its greater intensity but each measurement still had to be repeated to reduce any error caused by it. The DC thermal arc had the advantage that the shot noise could be integrated out.

However, because of the higher intensity output and ease of operation, the flash tube was chosen as the background source for this experiment.

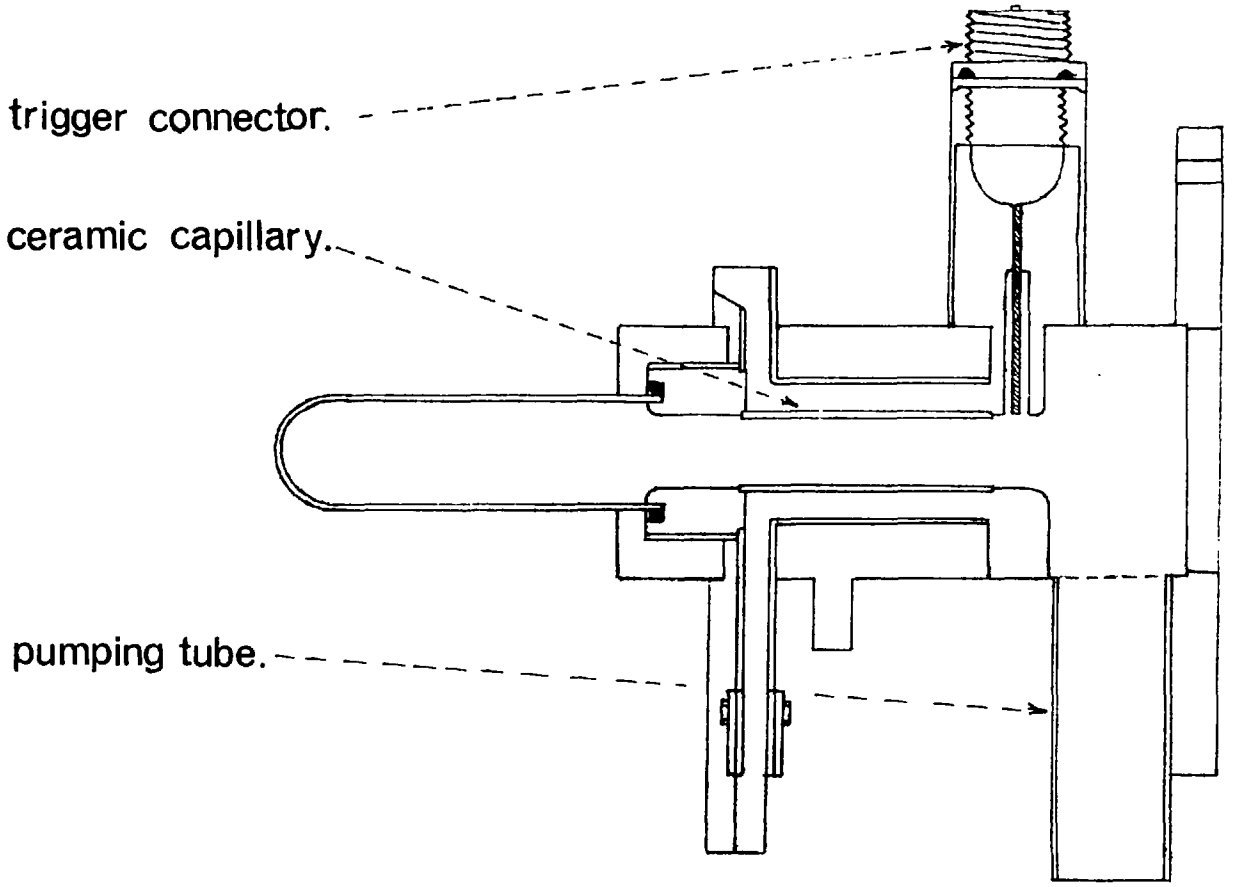

FIG. 6.1. 'Garton' type Flash-Tube.

Detectors

An RCA 7102 photomultiplier was chosen for detecting the signal since this had a AgOCs cathode surface which had the highest quantum efficiency of the photocathodes at the wavelengths concerned. The photomultiplier was cooled with liquid oxygen to reduce the cathode dark current. An extension glass-tube was sealed onto the photomultiplier.envelope and terminated by a window 6" in front of the photomultiplier cathode and liquid oxygen jacket, to prevent icing over of the cathode window. Before the end window was sealed on, silica gel was placed inside this tube to dry the air inside the tube. The end of the glass tube was clamped in a large brass collar to prevent any chilling of the extension window. The base pins and the gap between the base of the photomultiplier and its socket were sealed over with silicone rubber to prevent moisture condensing on to the terminals of the photomultiplier. The resistor chain of the photomultiplier was mounted in a separate compartment adjacent to the base of the photomultiplier, and warm air, from a commercial air blower, was pumped through this compartment to ensure that the resistors stayed at a constant temperature.

The whole assembly, as shown in fig. 6.2, was mounted on one of the photomultiplier carriages previously used (cf. Ref. 11) behind a 200μ slit.

An E.M.I. 9664B photomultiplier, accepting a bandwidth of 2.4Å was mounted adjacent to the RCA photomultiplier, to monitor the flash-tube intensity since the discharge continuum was transparent to the flash-tube continuum. Owing to the large spectral bandwidth accepted by this photomultiplier the signal was sufficiently noise free to obviate cooling the cathode.

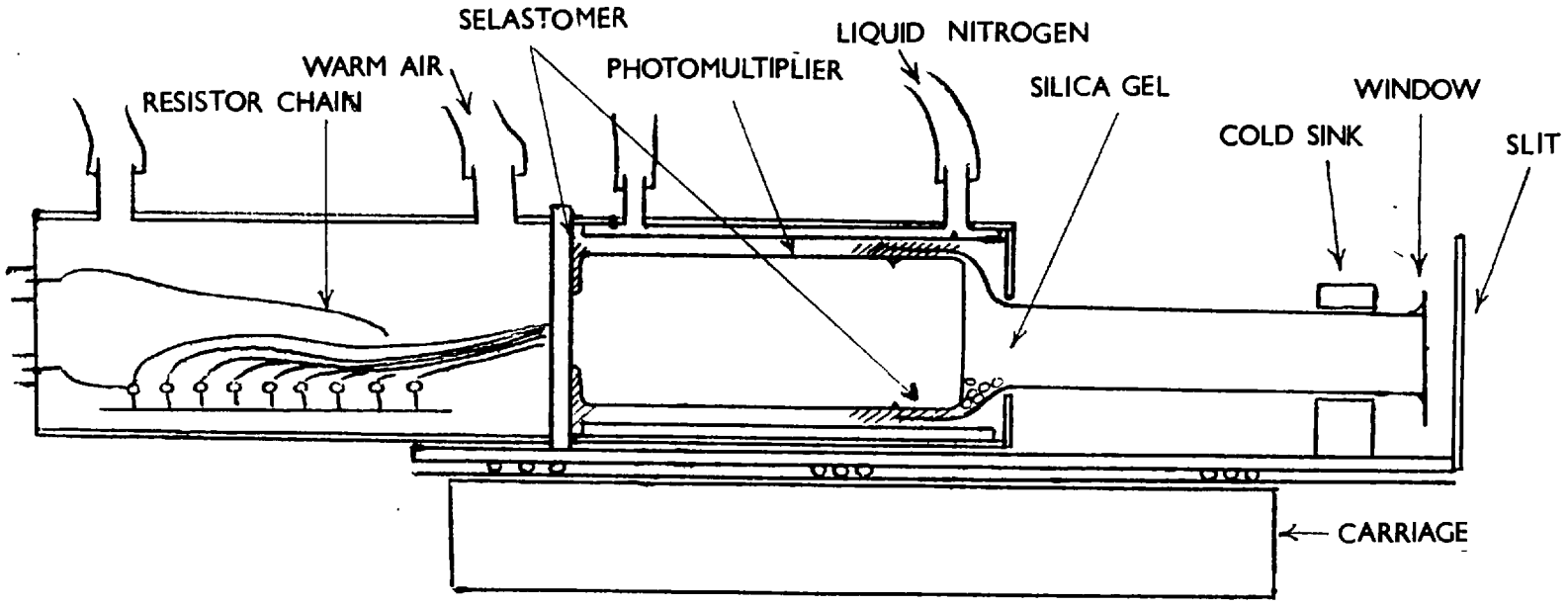

Fig. 6.2. Cooling system for photomultiplier.

Discharge Tube and Coil Arrangement

The discharge tube was mounted vertically so that the spatial scanning necessary could be easily performed horizontally. The coil used in previous experiments was unsatisfactory here, since an absolute measurement of intensity across the discharge was required; i.e. the dispersive system had to accept a constant volume of plasma regardless of the position of the scanner. The greater the height of the slab of plasma intensity accepted at any point, the less the shot noise and the smaller the error. An ordinary tapered coil as used previously was thus no use, the coil had to be wound with its planes horizontal and the drop from one turn to another had to occur at the side of the tube. To make this coil, a wooden cylinder was made and grooves 1 cm. apart cut round it. The cylinder was then cut twice down its length and one half, shifted one turn with respect to the other. The centre slab was reduced in width so that a gap existed at diametrically opposite points where the shift from one turn to the next could take place (fig. 6.3). The coil was then wound on this former, the centre slab slid out, and the wooden formers removed. The shape of the coil is as shown in fig. 6.3b. This coil was placed around the discharge tube so that its lower extremity was 1" above the centre quartz tube.

Optical and Scanning Arrangement

The optical path system was as shown in photo 3 and fig. 6.6; a one to one imaging system wasused so that a slit height on the spectrograph equal to the spacing between the R-F coils could be used.

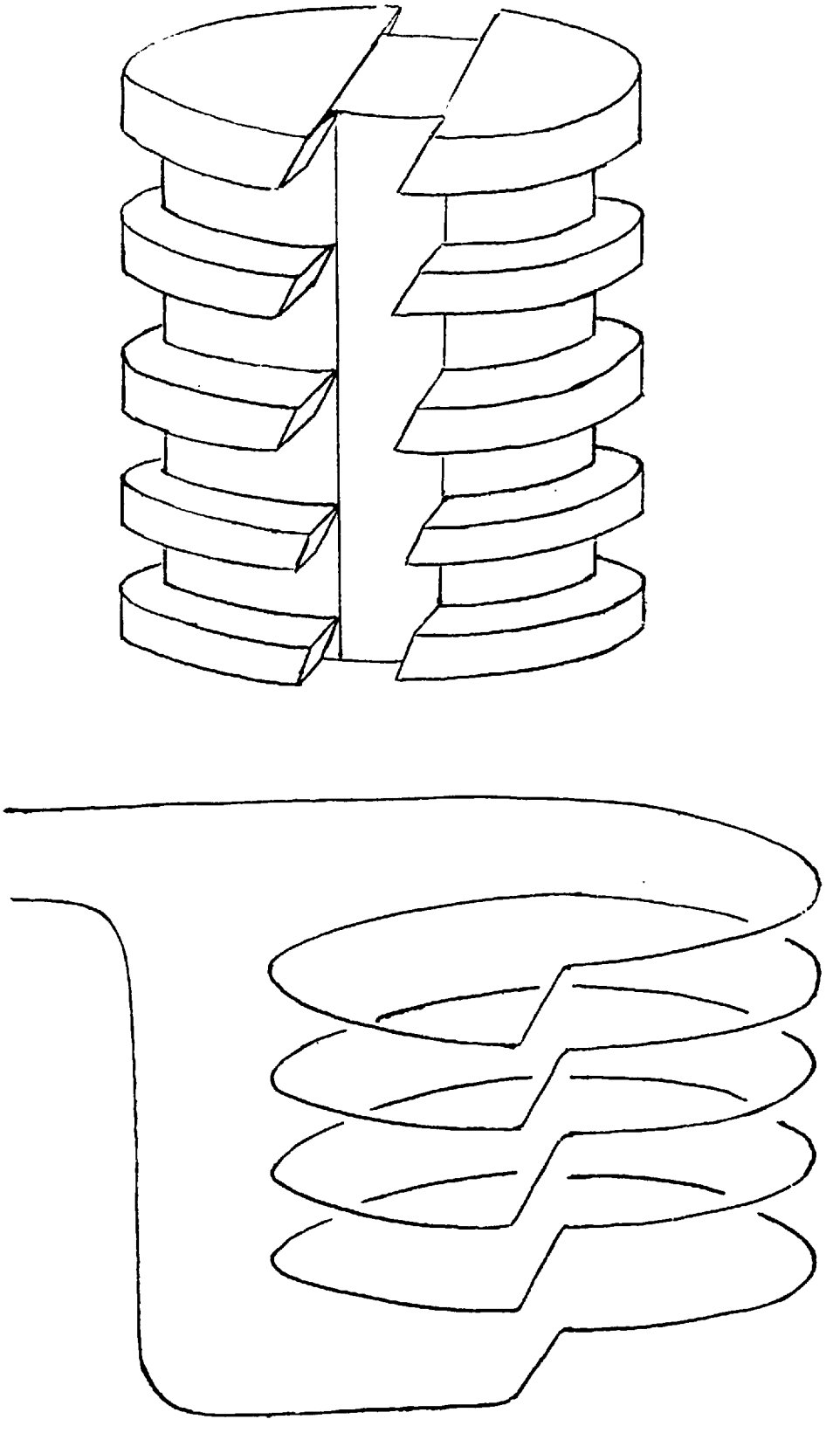

Fig. 6.3. Coil winder and coil.

A lens L of focal length 30 cms. was placed on the flash-tube side of the coil to reduce the lens effect of the quartz tube which caused the acceptance cone from the flash tube to scan across the flash tube capillary when the scanner was moved from one side of the quartz tube to the other. The mirrors and lenses which constituted the scanning part of the optical system were mounted on a frame which in turn was mounted at its centre of gravity on a microscope slide traverse, so that the position of the scanner could be accurately set.

Part of the scanning arrangement, mirror M_2 and Lens L could be rotated through 180° vertically so that the spectrograph and detector could receive the same solid angle of light from a calibrated tungsten black-body lamp as from the discharge. This way, the mirror involved in the calibration was kept at the same angle and the tungsten ribbon was effectively in the centre of the discharge, fig. 2.2. All the mirror mounts were made so that the mirrors could be adjusted in all directions to facilitate alignment.

The optical arrangement was aligned by placing a projector bulb in the spectrograph exit plane and, using visible light in the third order (~ 5090Å) emerging from the entrance slit of the spectrograph, lining up the mirrors and lenses so that the image of the spectrograph entrance slit appeared through the flash tube and was focussed in the centre of the discharge tube.

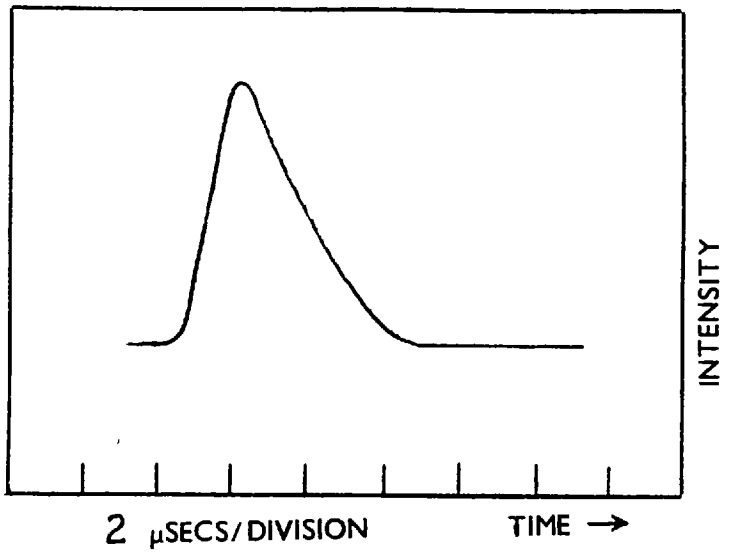

FLASH TUBE PULSE.

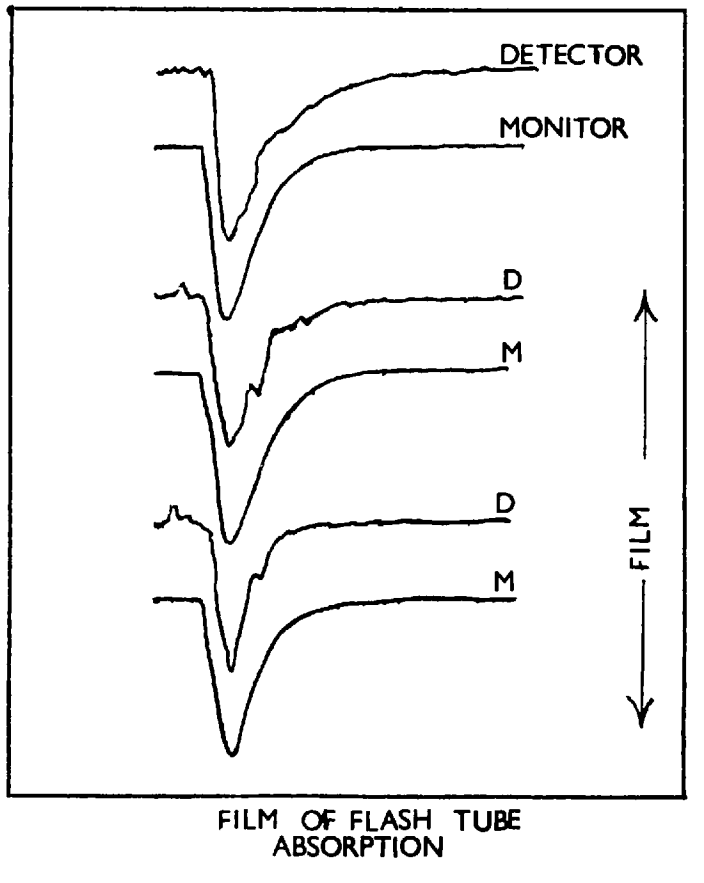

FILM OF FLASH TUBE ABSORPTION

FIG. 6.4. Flash tube intensity.

Electronics

Since the flash-tube emitted a continuum intensity which had a time dependence as shown in fig. 6.4 the signals taken from the detector photomultiplier and monitor photomultiplier were recorded on an oscilloscope.

The R-F discharge had already been shown (cf. Chapter 2) to have a 300 H_z ripple, both the line and the continuum intensities varying over the cycle. The measurements of absorption and emission therefore had to be made at the same point in the cycle. To effect this, a chopper blade, with slits accepting an interval corresponding to one twelfth of a cycle was placed in front of the entrance slit of the spectrograph. The chopper blade was driven by a synchronous motor operating from the same supply as the radio frequency generator so that the two would always be in phase. On one side of the chopper blade was positioned a pea-bulb and, on the other side an E.M.I. 1P21 photomultiplier whose output triggered the two beams and the gate output of the oscilloscope.

The gate output of the oscilloscope was fed to the grid of a thyratron which produced a 300 volt pulse, which in turn was fed to a coaxial transformer mounted on the flash tube and attached to a trigger pin which projected into the flash tube. The electronic block diagram and thyratron circuitry are shown in fig. 6.5.

The oscilloscope used was a Tektronix 551, with a type L amplifier for the detector photomultiplier and a type K amplifier for the monitor. Low capacitance coaxial cable was used to connect the detector to the amplifier, with a length of 8", to

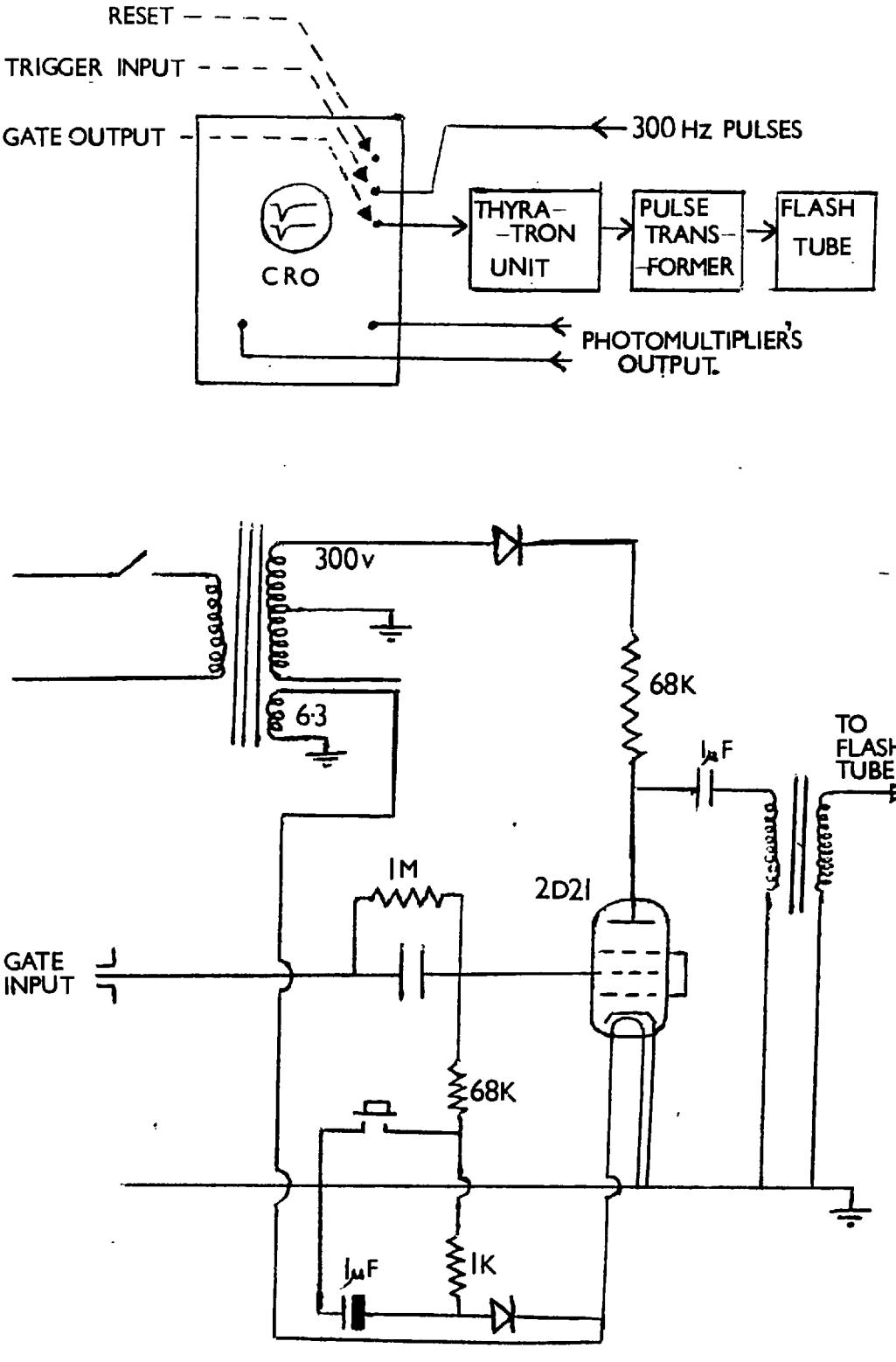

Fig. 6.5 Flash tube firing circuit.

minimise signal integration and allow a maximum resistance of 4.7 KΩ to be used as the photomultiplier load resistance. The flash tube condenser was charged by a 20 KV diode rectifier unit, through charging resistances. The rate of charging was such that the condenser could be charged to 8 KV and discharged through the flash tube every 10 seconds. Air was used as the filling gas for the flash tube which was kept at 50 microns pressure by means of a calibrated leak valve. Pumping was effected by a 2" diffusion pump and a single stage rotary pump.

Recording Method

Since the output signals were displayed on the oscilloscope screen and a scan of absorption across the discharge involved 25 traces of both the absorbed and unabsorbed flash-tube intensity, a 35 mm. camera was chosen to record the traces. A Shackman camera was used since this had a manual wind-on mechanism, and when mounted vertically so that the film wound vertically across the oscilloscope screen, three pairs of traces could be recorded on a 35 mm. length, since the traces were all the same shape and could therefore be stacked close together. This meant that three complete scans across the discharge plus calibration shots, making a total of about 170 traces, could be recorded on a 3 ft. length of film (fig. 6.4).

Calibrating Lamp

A 20 mm. x 2 mm. vertical ribbon tungsten lamp (W2KGV22i) was used to calibrate absolutely the emission of the 7635Å and 7514Å lines emitted by the discharge. This lamp was operated from a 12 volt accumulator and controlled by a variable coarse resistance in parallel with a variable fine resistance. The

accumulator was charged from the 220 volt DC supply using a tapped arm resistance chain. The detector signal from the calibration lamp was too small to record on the oscilloscope, and, in this case, the anode resistance was removed from the photomultiplier chain and an Ecko vibrating reed electrometer used to measure the current directly from the photomultiplier anode.

Experimental Details

A point midway between the maximum and minimum of the 300 Hz sine wave was chosen for the measurements since this would correlate with previous time-averaged temperature determinations. The chopper blade was accordingly rotated on the motor shaft until the correct position was obtained whereupon, with one of the chopper slits in line with the spectrograph entrance slit, the triggering photomultiplier and lamp were placed either side of another one of the chopper slits. Considerable screening of the R-F coil leads and flash-tube was necessary to eliminate radiative pick-up interfering with the signals on the oscilloscope. The extent of this screening can be seen in photograph 3. An explanation of the items in photograph 3 is given in fig. 6.6.

Although no difficulty triggering the flash-tube was experienced without the R-F power switched on, as soon as the R-F coil was energised the flash-tube would no longer discharge. This was caused by electrical interference charging the thyratron circuit input condenser to such an extent that the 20 volt pulse from the oscilloscope gate output could not bias the thyratron grid sufficiently positive to fire the thyratron. This difficulty was eliminated by putting a 1 MΩ resistance in parallel with the condenser to provide a leak for the interference yet a relatively high impedance compared with the capacitance to the 20 V gate output pulse.

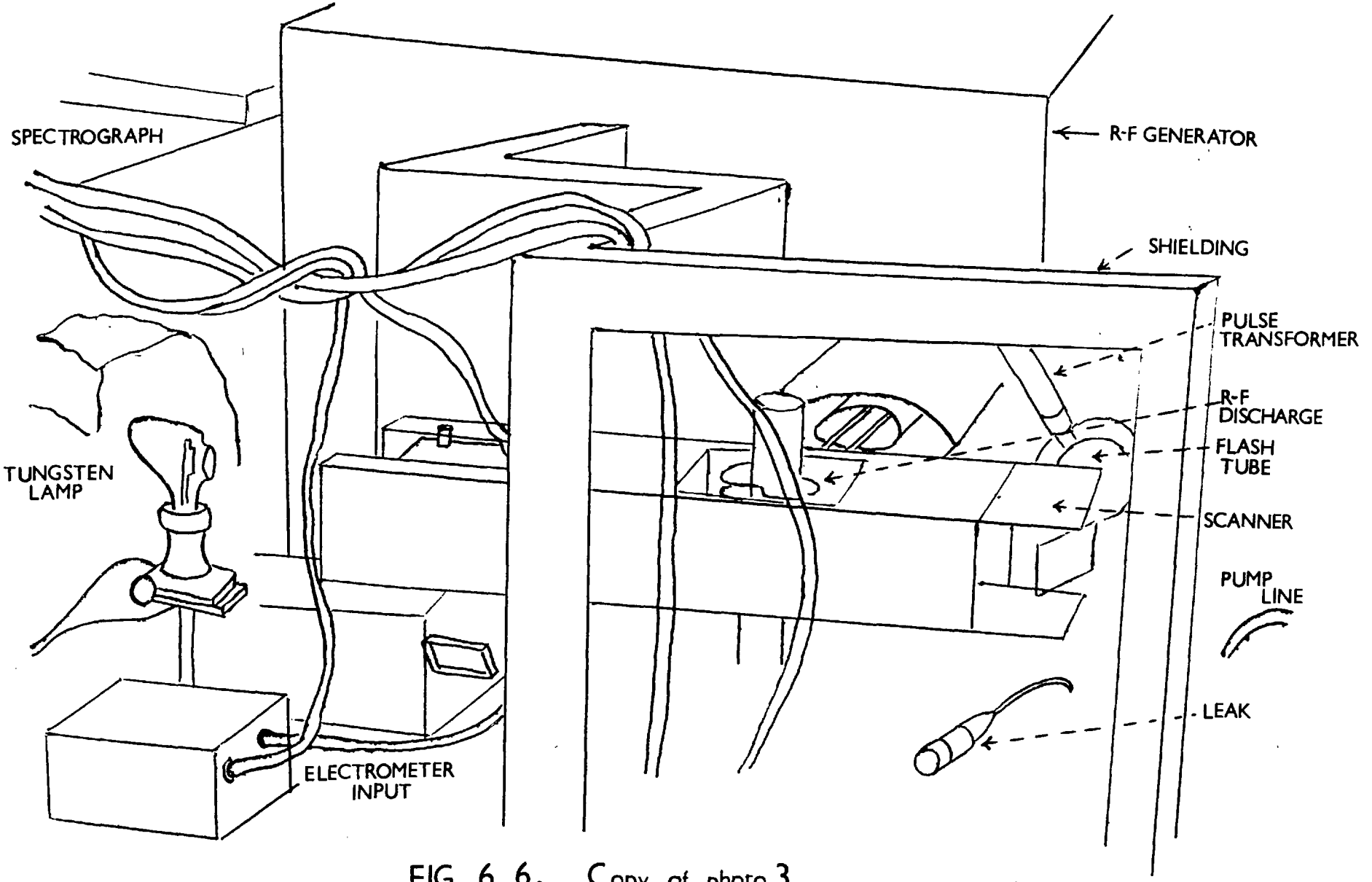

FIG. 6.6. Copy of photo 3

The Tektronix 551 oscilloscope was used in the AC coupled mode so that the transmission was measured from a base line which corresponded to the emission intensity. This obviated the need to subtract $J(x)$ from the transmission measurements and made absorption coefficient determinations simpler.

The transmission of the 7635Å line was measured 20 times in each of 25 positions across the discharge in 2 mm. steps. Since the transmission of the 7514Å line was greater than that of the 7635Å line it was measured a total of 16 times in 50 positions across the discharge, i.e. in 1 mm. steps. Prior to each set of measurements across the discharge, several traces of the flash-tube alone, from both the monitor and the detector photomultiplier were photographed to calibrate the monitor signal in terms of the detector signal.

The emission intensities were measured on a longer time base scan so that each trace showed 6 intensity pulses (from each of the chopper slits). The emission was measured three times (giving a total of 18 measurements) again in 2 mm. steps for the 7635Å line and 1 mm. steps for the 7514Å line. The detector photomultiplier load resistance for these measurements was changed to 120 KΩ since the emission intensity was recorded for approximately 300 μsecs. and thus integration was not as serious a problem. The total load resistance, i.e. the 120 KΩ and the oscilloscope input resistance of 1MΩ in parallel was measured on a resistance bridge.

The input resistance of the vibrating reed eleotrometer (10^8 $\pm$ 2%) was measured as follows:- ten 1M resistances were accurately measured and balanced on a potentiometer bridge against ten 10 MΩ resistances one at a time. The now calibrated ten

10 MΩ resistances were then balanced against the input resistance of the electrometer. This way, the electrometer input resistance was found to have a value of 101.5 MΩ .

The ammeter used to measure the current through the tungsten lamp was accurately calibrated in the Standards laboratory of the Electrical Engineering Department of this college.

The quartz discharge tube contained blemishes and striations due to the manufacturing process. The effect of these as well as the absorption of the tube were calibrated in a separate experiment. The quartz tube was marked where an axial light beam passed through it, then removed and set up in front of a constant deviation spectrograph, so that its position vertically and rotationally in front of this instrument was identical to its position in the main experiment with respect to the 10 ft. spectrograph. The quartz tube was mounted onto a screw traverse so that the tube could be scanned from side to side. The constant deviation spectrograph was fitted with a photomultiplier, an E.M.I. 9664B and its aperture reduced by means of stops so that it had an identical f number to the 10 ft. spectrograph. A heated platinum wire was then suspended down the centre of the tube under tension so that the wire would not distort on prolonged heating. The constant deviation spectrograph was set at 7635Å, the quartz tube moved from side to side in 1 mm. steps and the photomultiplier output recorded at each position on the electrometer. This was repeated at 7514Å and at sample wavelengths down to 3500Å. The quartz tube was then removed and the unattenuated signal measured. The correction factor for the quartz tube was calculated for each position across its diameter and this correction applied to the measured intensities of the

7635 and 7514Å lines. Within the limits of error on this experiment the correction for absorption of the quartz and the striations was independent of wavelength. The results for the temperature determination are given after the next section.

Transition probability measurements

Using the approximate intensity measurements for A I spectral lines, given by Dieke and Crosswhite (ref. 56), the strongest lines of the following arrays were chosen for measurement:-

4p - 4s	4d - 4p	6s - 4p
5p - 4s	5d - 4p	7s - 4p
6p - 4s	6d - 4p	

The RCA 7102 photomultiplier was replaced with an E.M.I. 9558 B which has the highest quantum yield in the region of the spectrum to be measured, i.e. 7500Å - 3500Å. The monitor photomultiplier was removed and the optical arrangement was kept identical to that in the above experiment. A 10 ft. radius of curvature, 15,000 line/inch grating replaced the grating used previously, and an exit slit of 0.40 mm. was used giving a spectral bandwidth of ~2Å.

The output signal was integrated and amplified by an electrometer amplifier circuit and displayed on a pen recorder (ref. 11). Since calibration of the complete optical and recording systems was effected in the same manner as the intensity measurements the effect of averaging the 300 Hz pulses from the chopper blade was cancelled out.

Now the intensity emitted by a spectral line is given by

$$I = \frac{h\nu}{4\pi} \frac{gn}{go} \; n_o \; A_{nm} \exp\left[-W_n/kT \right] \quad w/cm^3/st/sec \qquad 6.1$$

where the symbols have their usual meaning (cf. Chapter 2).

Radially across the discharge, only n_o and T will vary; n_o will vary in the same manner for all the spectral lines involved, but the exponential function will vary from line to line depending on the excitation energy W_n. For lines emitted from the same upper energy level, the intensity variation across the discharge will be identical, the only difference being an overall factor depending on the wavelength and the transition probability involved. Consequently, the most intense line (for accuracy at the edges of the discharge) of each group arising from a common upper level was chosen for Abel inversion; the other lines were simply measured at the centre point of the discharge.

With spectral lines emitted from the 4p - 4s and 5p - 4s groups, no correction is necessary for the finite slit width, i.e. no contribution to the total intensity comes from further than 1Å either side of the central wavelength. However with lines emitted from higher energy levels such as the 6p, 5d, 5d, 6s and 7s levels, the Stark broadening contribution is very much more and these spectral lines can have half-widths up to the order of 1Å, and, since the line has a dispersion profile, as much as 20% of the intensity can lie outside the exit slit width of 2Å.

Consequently, since all the broadening was due to the upper state only being perturbed (the lower state in these cases has negligible perturbations being the 4p and 4s levels), a measure of the contribution to the line intensity lying outside the slit width used can be made by scanning a representative line profile

from each of the upper levels in all the positions across the plasma. This was done using a 25 micron slit in front of the photomultiplier and scanning through the line profile to 10Å either side of the central wavelength so that the continuum level under the line profile could be accurately assessed. Profiles of the lines in each of 25 positions across the discharge were recorded on the pen-recorder and then traced on mm. graph-paper. Since the slit width to be used for measuring the total intensity was known the percentage to be added to the measured total intensity was easily calculated by comparing the area within the slit spectral bandwidth with that outside. The profiles of lines emitted from the 4p and 5p energy levels were also measured to check the assumption of there being no contribution from outside the integrating slit for these lines.

In cases where there was a line adjacent to the one being measured, a scan over a wavelength interval including both lines was made, again in the 25 positions across the discharge, so that the contributions to each line from the wing of the other could be measured.

The correction for the refraction and absorption of the quartz tube was added to these corrections.

Thus the experiment consisted of measuring the profiles of lines emitted from each upper energy level with the 25 micron entrance slit, in 25 positions across the discharge, estimating the corrections to be applied, then measuring their integrated intensities with the 0.4 mm. slit across the discharge. In this way, a complete knowledge of the variation of intensity across the discharge of any line from a given upper level was known.

The intensities of other lines from these energy levels were measured in the centre of the discharge only.

The contribution from the continuum to the integrated line intensities was estimated by measuring the continuum intensity either side of every line measured. The variation of continuum intensity across the discharge was also measured at various wavelengths.

The lines and the continuum which had been measured across the discharge were Abel inverted to give the radial emission coefficients. A dividing factor of Abel inverted, true intensity over total integrated intensity was thus found for each upper energy level, and the intensities of the lines measured just in the centre of the discharge converted to true intensities by this dividing factor. The dividing factor was also calculated for the continuum intensity and this contribution to the total intensity subtracted at each wavelength.

The optical, detecting and recording system was calibrated at each wavelength using the tungsten ribbon lamp as before. The intensity of each line in units of ergs/cm^2/steradian/sec., was then known and with the knowledge of the temperature in the centre of the discharge, the transition probability for each line was calculated since all the other parameters in the intensity equation (equation 6-1) were known.

Results of Temperature Measurement

The integrated absorption coefficients of the 7635Å and 7514Å lines were measured from the 35 mm. film traces and since

the choice of curves to pass through the measured points was open to error, two curves in each case were drawn, one through the maximum and one through the minimum of the error spread. These curves were then Abel-inverted and, in the case of the 7635Å line, the correction factor $j_1(\nu)$ calculated using the polynominal coefficients of $j_o(\nu)$ in both cases, but with different polynominal coefficients of $K(\nu)_{7635}$ according to the curve chosen. The corrections were then applied to the calculated value of $jo(\nu)$ giving two corrected emission coefficient curves, which, with their appropriate absorption coefficient curves, gave the radial distribution of temperature. For the 7514Å line, no correction to the emission coefficient $jo(\nu)$ is necessary, but again two different curves for the integrated absorption coefficient were drawn and Abel inverted to give $k(\nu)_{7514}$.

The emission coefficients were put onto an absolute scale as follows:-

Since the 35mm. traces were enlarged to facilitate measurement there was an enlargement factor corresponding to the magnification of the oscilloscope graticule. For example one unit of intensity of the 7514Å line corresponded to 1/2.75 cms. of oscilloscope graticule; let this factor be called A. On calibration, the oscilloscope was giving a deflection of 0.175V/cm. on the 02V/cm. scale; let this factor (.175V), be B. This voltage corresponded to $\frac{B}{R}$ amps where R was the nett resistance seen by the photomultiplier, i.e. that due to the anode resistance in parallel with the oscilloscope input resistance.

At this wavelength E ergs/cm^2/steradian/sec emitted by the tungsten ribbon lamp corresponded to I amps seen by the electrometer (where I has been corrected for the input resistance of

7635Å				7514Å Line	
I_o	J_o (Smoothed)	J_1' ($\times 10^{-3}$)	$J_1'' j_1$ ($\times 10^{-3}$)	I_o	J_o (Smoothed)
50.4	.188	.026	1.65	26.3	.098
50.2	.188	.462	1.23	26.2	.100
49.7	.192	.258	1.28	26.0	.103
49.2	.196	.515	1.6	25.6	.105
48.4	.205	.75	1.71	25.0	.109
46.8	.214	.87	1.82	24.0	.113
44.4	.219	1.05	1.93	22.5	.115
40.8	.221	1.09	1.91	20.5	.113
35.7	.210	.917	1.81	18.7	.107
29.6	.187	.79	1.67	15.5	.095
22.3	.138	.514	1.45	12.5	.079
17.3	.11	.31	1.40	9.4	.062
12.9	.082	.037	1.47	6.8	.046
9.15	.056	.18	1.88	4.5	.030
6.88	.043	.64	2.48	3.1	.023
4.85	.030	1.31	3.27	1.8	.013
3.30	.025	3.17	4.46	1.0	.009
1.80	.015	1.87	4.59	0.4	.003
0.76	.0073	3.62	4.37	0.2	.002
0.21	.0024	2.72	2.17	0.1	.001
0.10	-	.385	-	-	-
0.05	-	-	-	-	-
0.00	-	-	-	-	-

FIG 6.7. Emission coeffidents

the electrometer). Consequently one unit of intensity as measured from the enlarged oscilloscope traces corresponded to:-

$$A \times \frac{B}{R} \times \frac{E}{I} \text{ ergs/steradian/cm}^2\text{/sec.}$$

In the tables of measured intensities, one unit for the 7514Å line corresponds to 4.5×10^6 ergs/st/cm^2/sec and one unit for the 7635Å line corresponds to 4.15×10^6 ergs/st/cm^2/sec.

Fig. 6.7 gives the measured intensities and the smoothed Abel inverted intensities of the two lines together with the two corrections, $j_1(\nu)$, for the 7635Å line. In fig. 6.8 the measured absorption of each line is given, two curves having been plotted for each line, together with the smoothed absorption coefficients obtained by Abel inversion. In fig. 6.9 the resulting radial temperature distributions calculated from these coefficients using the calibration of measured intensity given above and the resulting smoothed average temperatures are tabulated. The temperature profiles, obtained by averaging the temperature profiles for each line, are shown in fig. 6.10.

Discussion of Temperature Measurement

The results of the transition probability values obtained here will be given and discussed in the next chapter; only the temperature measurement will be discussed here.

Since the values of the radial temperature obtained from each set of measurements agree within the limits of error there can have been no overpopulation of the lower level of 7635Å line owing to its metastability. As it is, the 7635Å line led to a slightly higher value of temperature than the 7514Å line, whereas if its

7635Å Line				7514Å Line			
Absorption %		k_1	k_2	Absorption %		k_1	k_2
K_1	K_2	Smoothed		K_1	K_2	Smoothed	
37.4	37.4	.0127	.9138	19.3	19.3	.072	.0645
37.4	37.4	.0131	.0141	19.2	19.3	.073	.0660
37.2	37.1	.0135	.0145	19.1	19.2	.074	.0680
36.8	36.8	.0139	.0153	18.8	19.0	.075	.070
36.1	36.0	.0143	.0160	18.2	18.6	.0765	.072
35.0	34.2	.0147	.0162	17.5	18.0	.0775	.0725
33.4	31.8	.0148	.0162	16.6	17.2	.0775	.0725
30.7	28.4	.0147	.0157	15.4	16.2	.0755	.072
28.0	25.0	.0144	.0140	13.8	15.0	.0725	.0695
25.0	21.3	.0135	.0120	12.2	13.5	.0675	.066
21.2	17.0	.0120	.0100	10.0	11.6	.0600	.061
17.4	13.6	.0102	.0080	7.8	9.5	.0505	.054
13.0	10.3	.0083	.0062	6.0	7.5	.0400	.045
9.7	7.8	.0065	.0048	4.0	5.6	0.285	.034
6.8	5.5	.0045	.0033	2.6	4.0	.0190	.024
4.6	4.0	.0026	-	1.5	2.8	.011	.019
3.2	2.8	-	-	0.7	1.8	-	-
2.0	1.8	-	-	0.3	1.0	-	-
1.1	1.0	-	-	0.1	0.5	-	-
0.4	0.3	-	-	0.0	0.2	-	-
0.2	0.1	-	-	-	0.1	-	-
0.1	0.05	-	-	-	0.0	-	-
0.0	0.00	-	-	-	-	-	-

FIG 6.8. Absorption coefficients

lower level had been overpopulated with respect to its Boltzmann distribution value, we would have expected, through the resultant increase in absorption from that level, a lower value of temperature than that given by the 7514Å line. Thus collisional depopulation, as would be expected in an L.T.E. discharge, keeps the population of the metastable level at its Boltzmann value, contrary to the beliefs of Brewer and McGregor (refs. 5, 7).

The two independent temperature measurements lie well within the expected random errors calculated in appendix 1.

1. Errors that would systematically affect both sets of temperature determination could be caused by -

a) incorrect tungsten lamp calibration,

b) incorrect oscilloscope calibration,

c) incorrect measurement of the nett anode resistance of the photomultiplier or the electrometer input resistance,

d) incorrect determination of the effects of the quartz tube, i.e. refraction and absorption.

All of these effects together might seriously influence the temperature result but singly would not have any appreciable effect.

The advantage of this method of temperature measurement is its inherent accuracy and, as well as independence of transition probabilities, the fact that it is not necessary to make the absorption and emission measurements on the line peak - anywhere in the line profile will give the same result. Consequently, provided the photomultiplier is not moved between sets of measurements its position on the line profile is not critical. Thus any shift of the line profile which may occur through taking measurements through a region of increasing electron density is not serious. Because of a shift in wavelength, the emission may suddenly drop and give an apparently misleading emission coefficient; however, the absorption coefficient will be

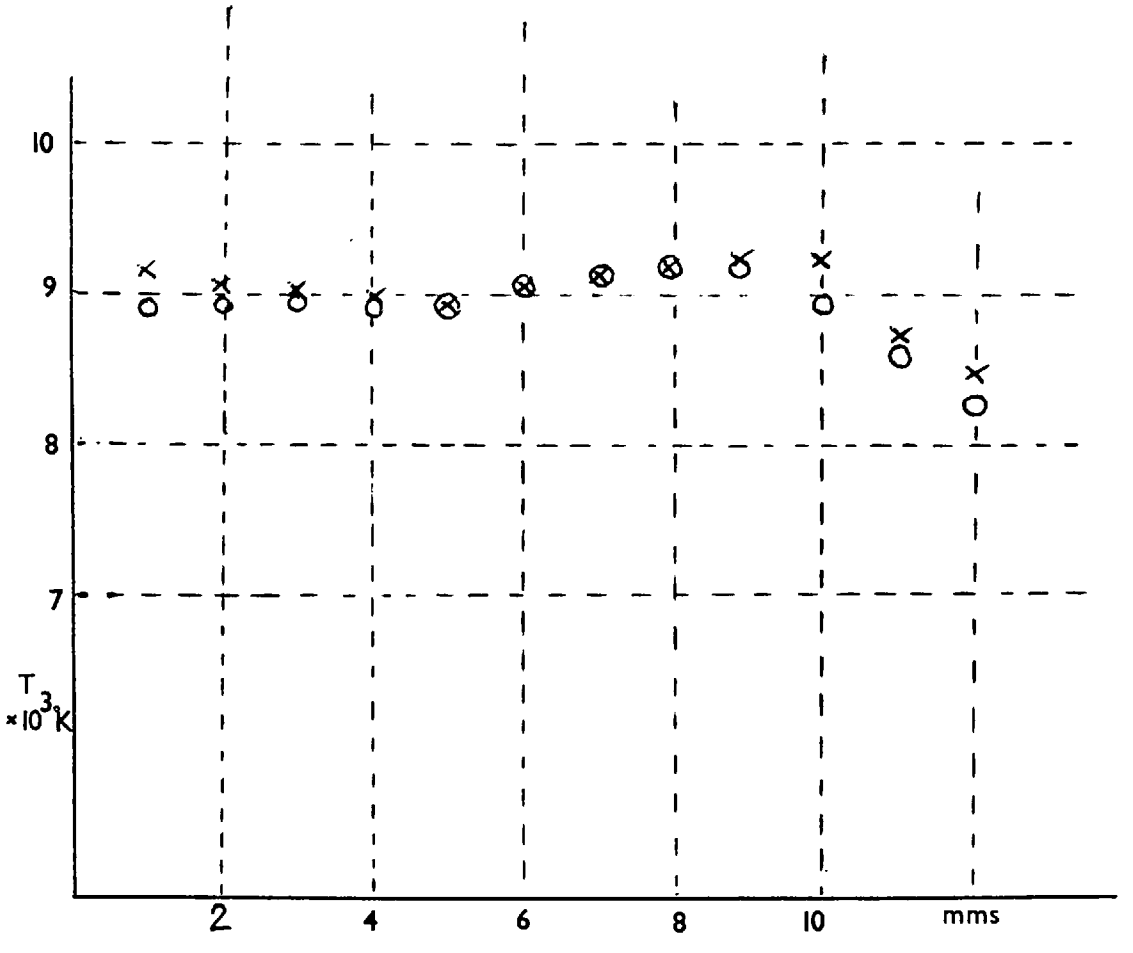

Fig 6.9 Temperature v Radial position.

similarly affected and, on taking their ratio, the effect will be cancelled out, and a true temperature obtained from the measurements.

Thus, this method of temperature measurement, although dismissed as inapplicable to inhomogeneous discharges (refs. 25, 46) is in fact quite applicable and, with careful design of apparatus, capable of providing very accurate temperature measurements when L.T.E. exists between the levels used for the measurements.

Absolute Continuum Intensity Measurement

In the course of measuring the absolute intensities of the spectral lines whose transition probabilities were being determined, the continuum intensity was also measured, since an estimate of the contribution to the total observed line intensity from the continuum under the line was required, so that it could be subtracted to give the true line intensity. Thus the continuum intensity was measured throughout the spectral region covered by the line intensity measurements, i.e. 7430Å - 3600Å, or 4×10^{14} sec^{-1} to 8.3×10^{14} sec^{-1}. The only previous measurements of the absolute continuum intensity of an argon discharge were those of Busz and Finkelnburg (ref. 62), over a range, $5 - 7 \times 10^{14}$ sec^{-1} and those of Olsen (ref. 17), over a range $2 - 10 \times 10^{14}$ sec^{-1}.

The discrepancy between Olsen's two published values of the continuum intensity correction has already been discussed in Chapter 2 and agreement with his first value, i.e. a factor 5 difference between the Unsold theory (ref. 21) and experiment, reached. For an agreement between the line to continuum measurement of temperature and the accurate reversal method of determination of temperature, a factor of about 5.5 would be needed to correct the continuum intensity. Consequently, in order to resolve the discrepancy of Olsen's first published value of 5, his second of 2.5, and the expected value of about 5, the continuum intensity measurements made here were put on to an

Normalised Radial Position	7635Å		7514Å			
	T_1	T_2	T_1	T_2	T AVE	T Smoothed
.04	9320	9000	8690	9070	9020	8970
.08	9200	8930	8730	9070	8980	8975
.12	9150	8900	8790	9100	8985	8980
.16	9130	8780	8810	9040	8940	8990
.20	9170	8780	8860	9070	8970	9010
.24	9230	8880	8940	9170	9055	9050
.28	9300	8970	8990	9240	9125	9120
.32	9340	9100	9050	9360	9210	9200
.36	9250	9300	8990	9290	9210	9185
.40	9080	9480	8840	8940	9085	9070
.44	8400	9030	8600	8590	8680	8780
.48	8270	8990	8490	8160	8480	8420

FIG 6.10. Values of temperature

absolute scale in terms of watts/cm^{3}st/sec, by interpolating the black-body calibration measurements which were made at wavelenths corresponding to the measured emission lines. Sixty measurements of continuum intensity were put onto an absolute scale.

Now the theory predicts a continuum which is frequency independent up to a cut off frequency ν_g, which, as stated in Chapter 2 was 4.6×10^{14} sec^{-1} for Argon I. Above this frequency the continuum varies as exp $-h\nu/kT$; thus a plot of the logarithm of the intensity versus frequency should give a straight line.

The cut-off frequency is reduced by the ionisation potential reduction.

Thus the continuum emission

$$E_\nu = \frac{K' K Z^2 n_i n_e}{\sqrt{T_e}} \exp\left[\frac{-h(\nu - \nu_g + \Delta\nu)}{kT}\right]$$

where $K = 5.41 \times 10^{-46}$ and K' is the correction to be determined.

Now the depression of ionisation potential in the discharge varies according to the theory chosen. Ideally, the continuum intensity should be measured up to the cut-off so that $\nu_g - \Delta\nu$ is immediately determined, however, owing to observational difficulties in this region ($\sim$7500Å) the measurements made have a large uncertainty and the exact cut-off frequency cannot be determined accurately. The values of depression of ionisation potential for the temperature and electron density in the centre of the discharge varies according to the theory used.

Deby-Hückel	gives	0.019eV
Unsöld	gives	0.111eV
Ecker-Weizel	gives	0.122eV
Brunner	gives	0.207eV

It has been suggested by Olsen (ref. 19) that Brunner has counted the microfield effect twice in his analysis; correcting for this gives a value of 0.111eV. However, Olsen's results tend to lend support to the uncorrected theory!

Thus we have a variation of 0.05 to 0.6×10^{14} sec^{-1} in the choice of the depression of ionisation potential.

Theoretical curves are given for a cut-off frequency of 4.6×10^{14} sec^{-1} depressed by 0.3 and 0.6×10^{14} sec^{-1} and are

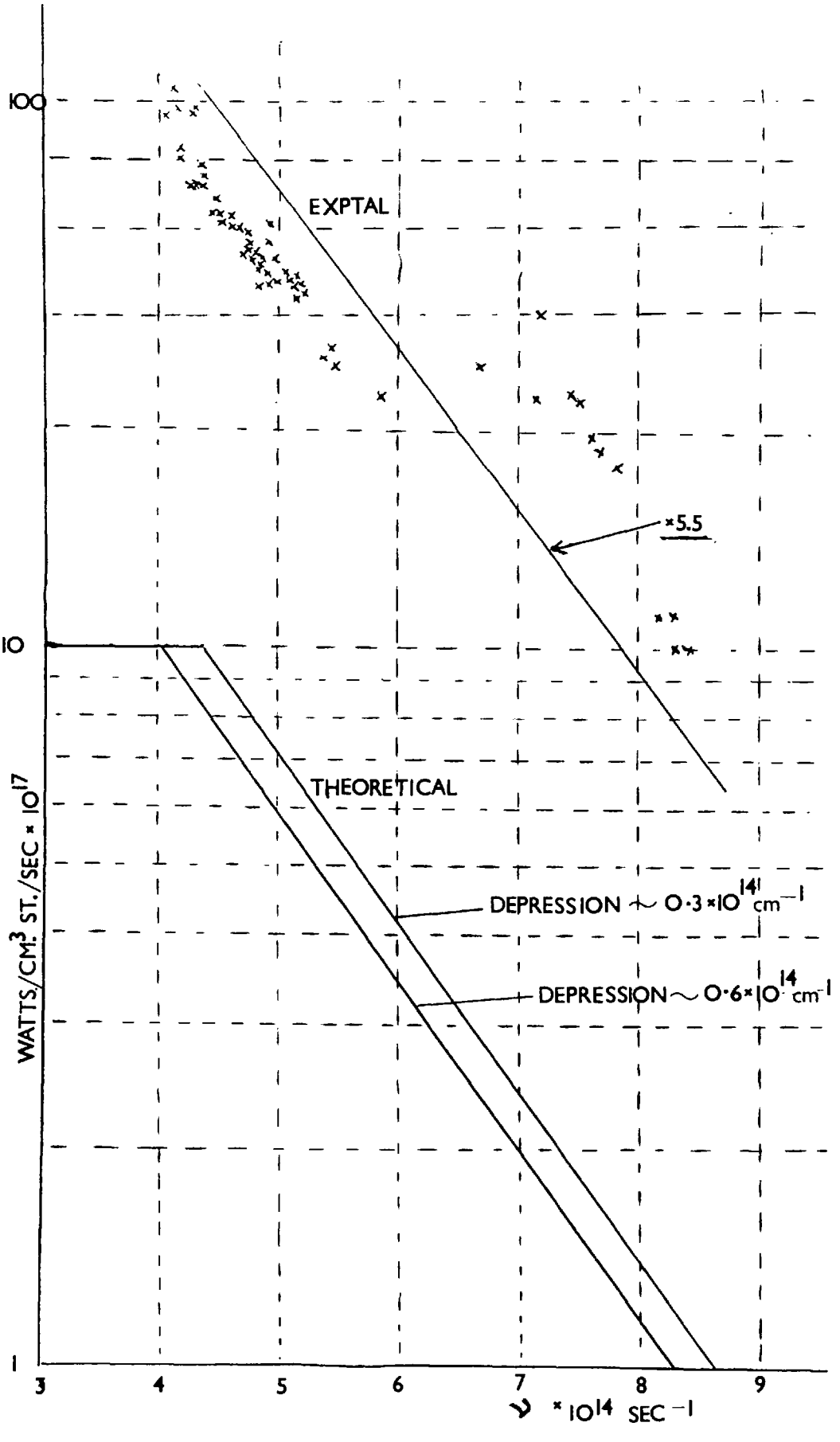

FIG 6.11 Continuum intensity v ν

compared with the experimental values in fig. 6.11. Owing to the small graph given by Olsen in his paper (ref. 17) with no actual values tabulated, it is not possible to compare these measurements accurately with his; however, the overall agreement is good.

If a depression of 0.21eV is used, the correction factor determined here appears to be 5.7 x whereas, if a value of 0.11eV is used the factor is 4.5x.

Since no levelling-off of the experimental results was observed above 4×10^{14} sec^{-1} it seemed possible that the ionisation potential depression was of the order of 0.2eV and the correction to the theoretical continuum 5.7x.

The values of n_e, n_i, and T_e used in the theoretical calculation, were those previously determined for the centre of the discharge. The values of n_e and consequently n_i in this temperature regime were subject to a 20% error due to theoretical uncertainties in the Stark broadening parameters used for their determination, as well as an error incurred through not Abel-inverting the electron density distribution.

Thus the theoretical continuum emission curves were expected to have an uncertainty of about 30% and consequently the correction factor determined here should be quoted as 5.7 ± 1.9.

However, the situation was not this serious since the temperature and density agreement through Saha's equation was extremely good (cf. Chapter 3) and the error through not making an Abel-inversion of the electron density, owing to the flat-topped profile of the distribution was not expected to be very significant - again the agreement between a radial temperature determination and that determined from an electron density obtained from integrated information would seem to indicate this.

Consequently a value of about 15% accuracy can be stated for the correction factor, i.e. 5.7 ± 1.0.

CHAPTER 7

Calculation of Theoretical Transition Probabilities

Introduction

No comparison of the transition probabilities measured in previous chapters with other experimental values is possible, since virtually none of them has been measured before. To effect a comparison, the transition probabilities were calculated for all the arrays measured. Since the rare gas atoms have been shown to have serious departures from LS coupling and although J_{1j} coupling is a better approximation, it is still not entirely satisfactory, therefore the calculations were carried out in intermediate coupling as well (ref. 58a).

In this chapter a description is given of the process of calculating transition probabilities in the three forms of coupling. The theoretical results obtained are then compared with the experimental ones.

A calculation of Argon I transition probabilities had already been made (ref. 30) for the 4p - 4s and 5p - 4s arrays, however since the values for all the experimentally measured arrays were repeated, these calculations were also repeated as a check on the method and the computer programme used. In fact 8 significant discrepancies were found with the previous values of theoretical J_{1j} coupling transition probabilities.

Method of Calculation

In order to calculate transition probabilities in intermediate coupling, the line strength matrices in LS coupling and the transformation matrix from LS coupling to intermediate coupling must be known (ref. 59).

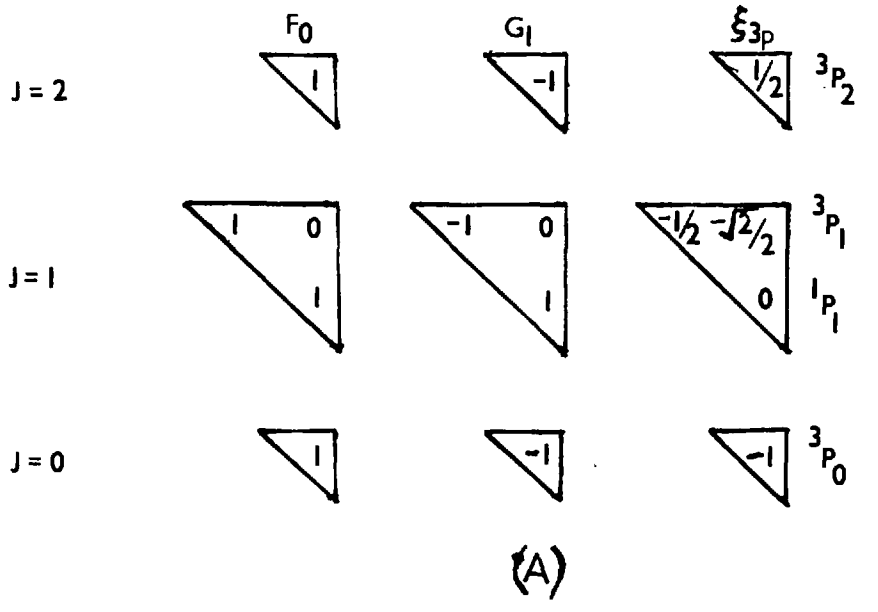

(A)

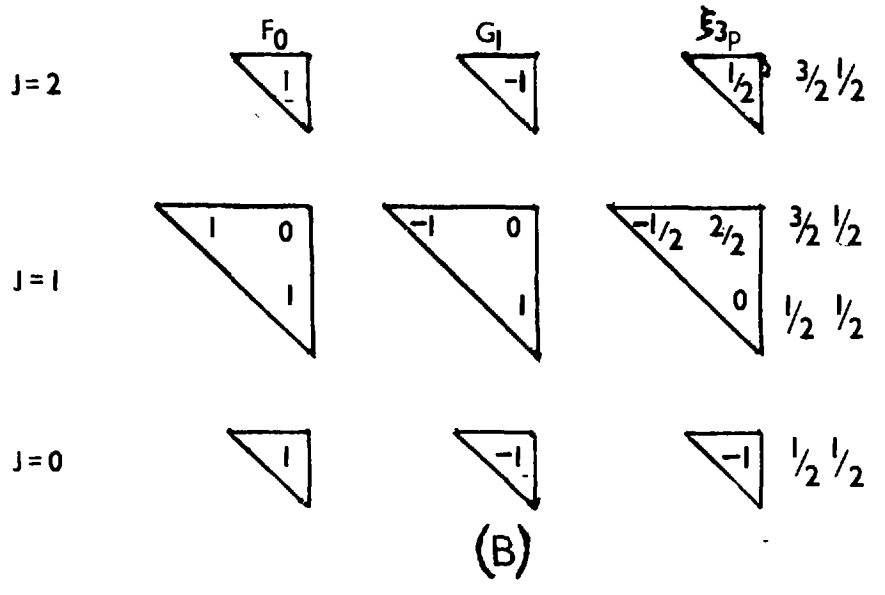

(B)

Figs. 7.1 & 7.2 Slater and spin-orbit values for $3p^5ns$ in LS and J_j coupling. (A) & (B).

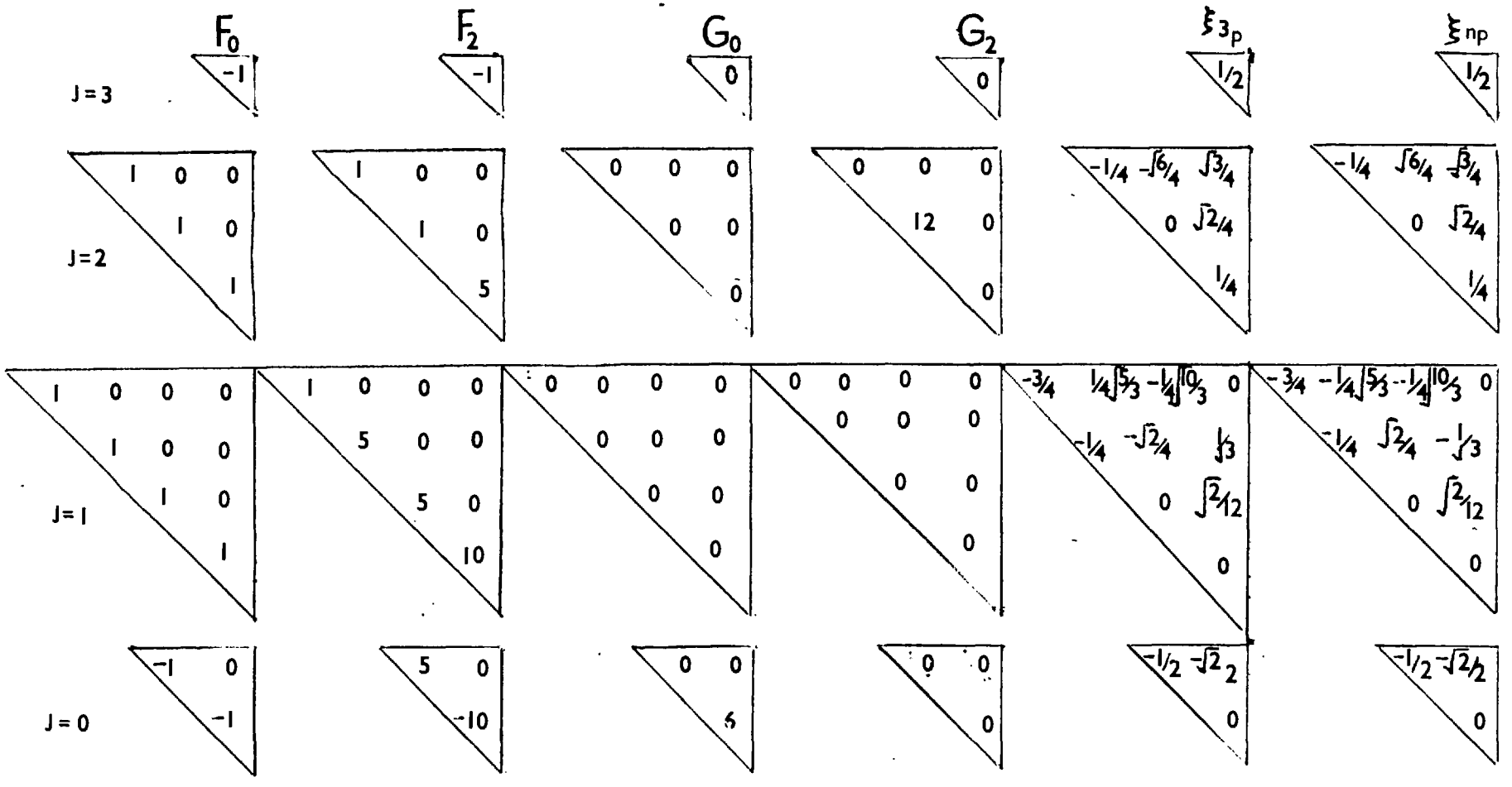

Fig 7.3 $3p^5np$ in LS coupling.

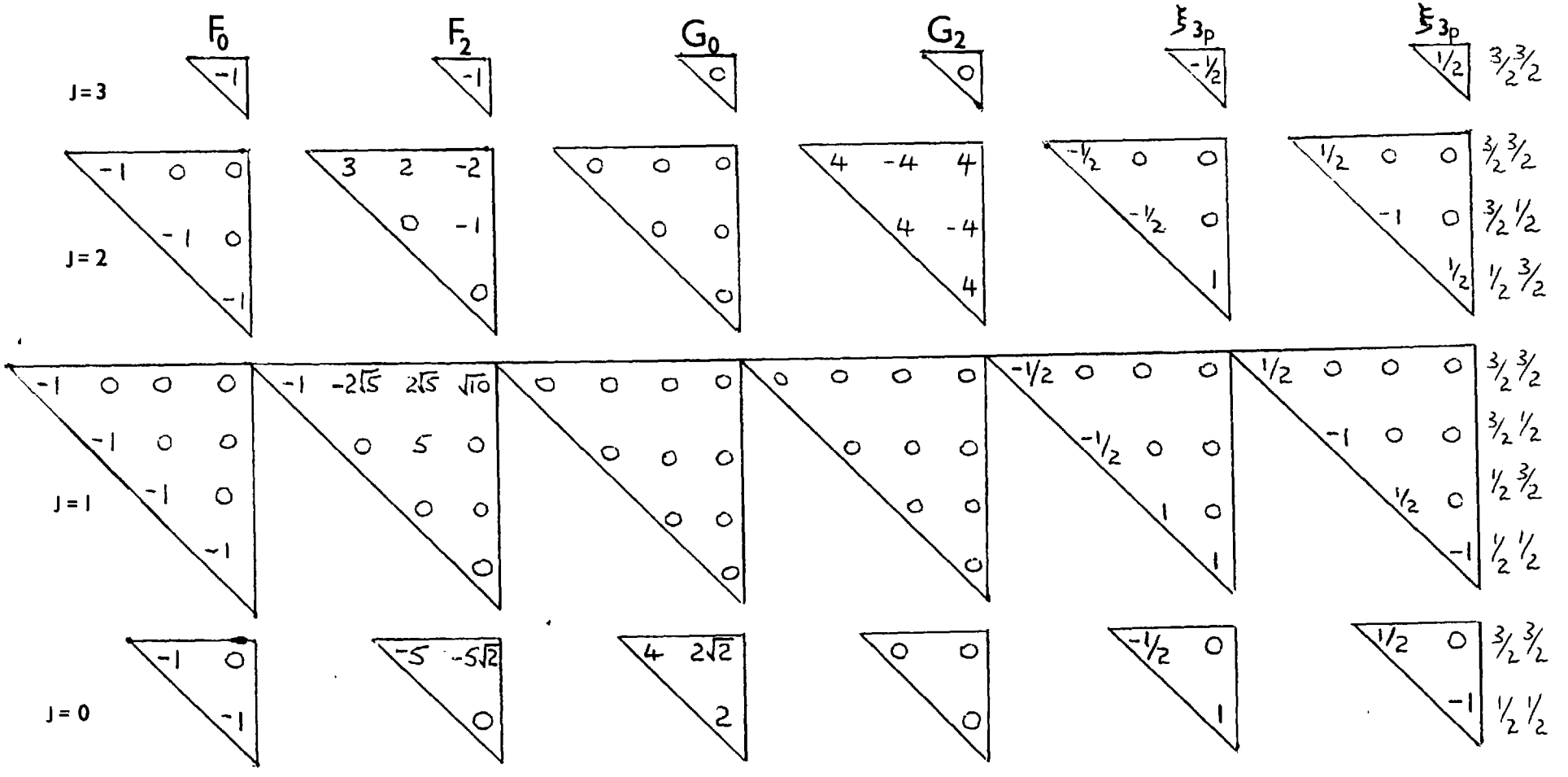

Fig. 7.4. p - states, J_{ij} coupling.

If ϕ_i and ϕ_f are the initial and final configuration LS wave functions represented by column matrices, and the transformation to intermediate coupling is written

$$\psi_i = A\phi_i, \quad \psi_f = B\phi_f$$

then the line strength matrix in intermediate coupling is related to that in L.S. coupling by:-

$$(S^{\frac{1}{2}})_{ic} = B(S^{\frac{1}{2}})_{LS}\tilde{A}$$

where $\tilde{A}$ is the transpose of A.

Now A is found by making $AH\tilde{A}$ diagonal, where H is the energy matrix of the initial configuration in LS coupling, and similarly B for the final configuration.

Now to construct the energy matrix H for the initial and final states involved in the transition array, the electrostatic and spin-orbit parameters need to be known.

These were obtained from Condon and Shortley (ref. 58) in terms of Slater and spin-orbit parameters, for LS coupling (ref. 58b) and J_{1j} coupling (ref. 58c).

To obtain the correct values of these parameters and therefore determine H and hence $\tilde{A}$, a least squares fitting of the calculated energy levels (i.e. eigenvalues) to the observed energy levels (ref. 10) was carried out where the calculated energy levels were determined from the complete energy matrix H, (including the Slater and spin-orbit parameters) with the parameters treated as variables and sample values substituted. The least squares fitting reiterations, carried out by an I.B.M. 7090, were terminated when a certain change in parameter (or tolerance) was reached.

The Slater and spin-orbit parameters for the $3p^5n$ s, p, d terms are given in their computer input form in the LS coupling scheme in figs. 7.1, 7.2, 7.3.

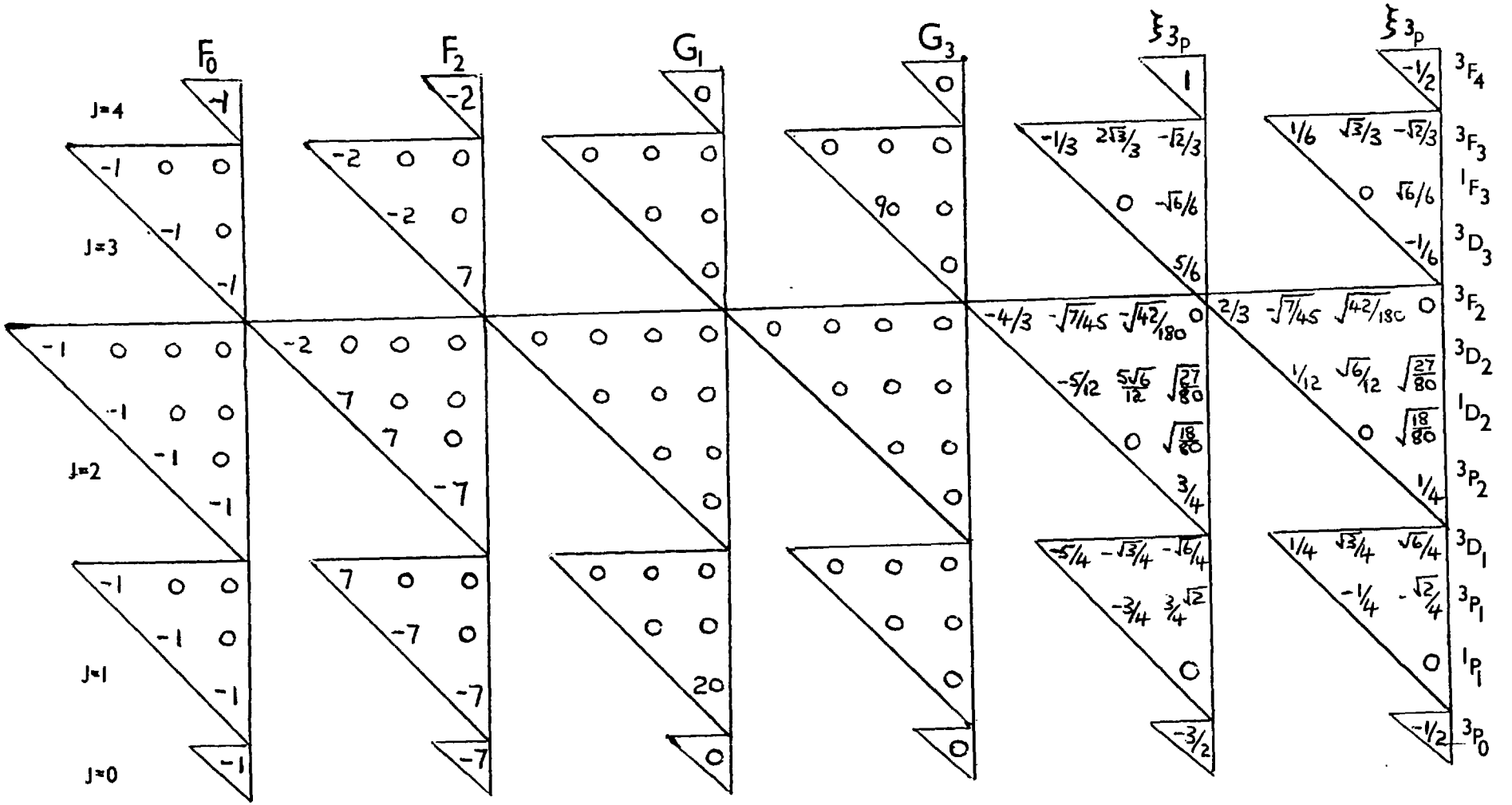

Fig. 7.5. d-states, LS coupling

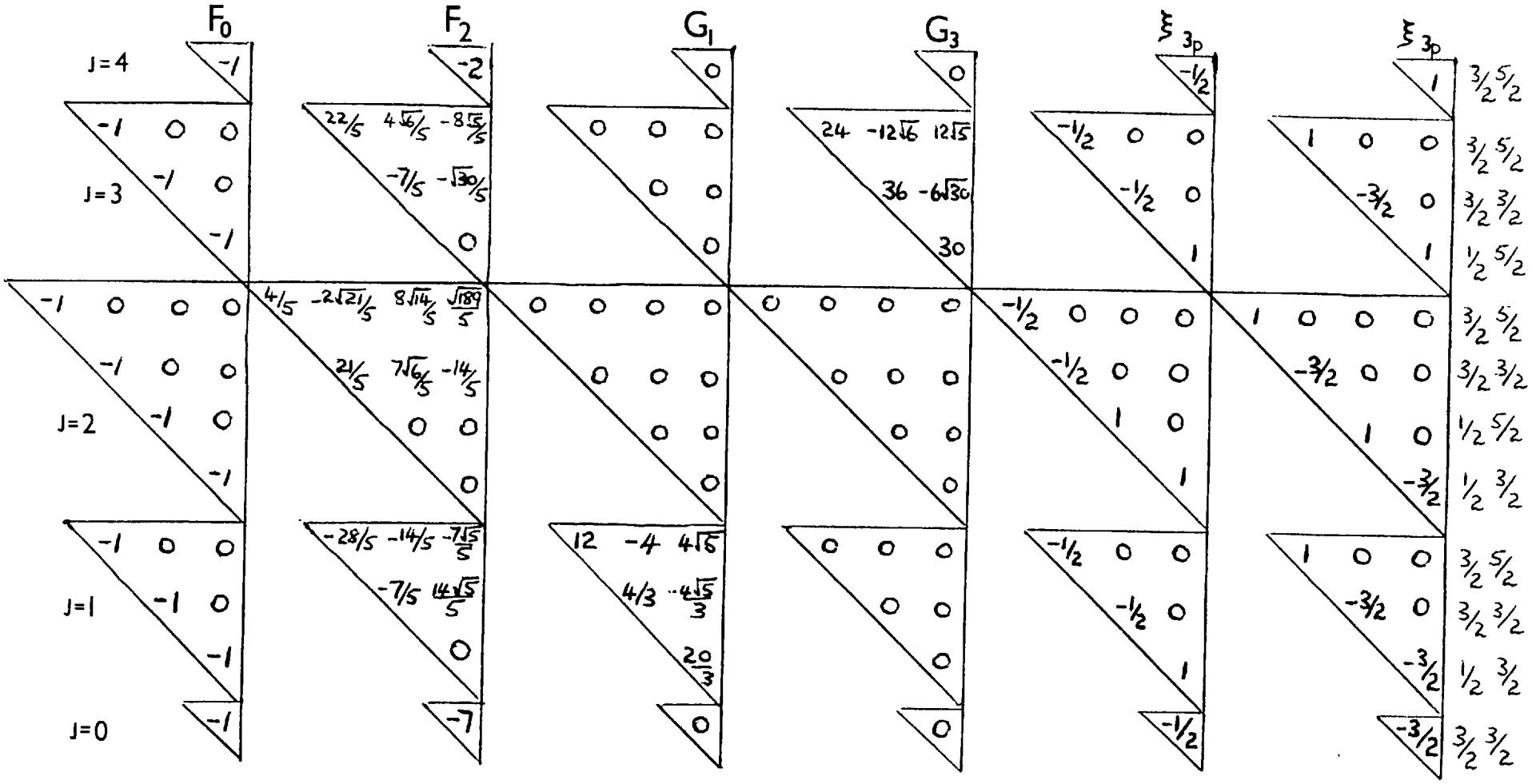

Fig. 7.6. d-states, J_{lj} coupling

The resulting eigenvectors of the energy matrix determine the mixing of the states involved and form the transformation matrix A from the initial line strength matrix to the intermediate coupling line-strength matrix.

The eigenvectors obtained from the LS coupling representation showed substantial mixing between the states involved, and thus one would expect the eigenvectors to be sensitive to the adopted parameters. As a check on the line strength matrices (calculated later) and on these parameter values, the process was also carried from the J_{1j} coupling representation; the Slater and spin-orbit input parameters are given in figs. 7.4, 7.2, 7.6. If there had been an incorrect choice of phase of a value of electrostatic or spin-orbit coupling, this would have shown by different parameters being obtained from each of the coupling schemes.

The mixing of the states, given by the square of the eigenvectors is shown for the 4p, 5p and 6p levels in LS and J_{1j} coupling in fig. 7.7. The inability of the LS coupling scheme to describe the levels unambiguously is clearly shown, J_{1j} coupling though not perfect is a far better approximation.

The levels, according to the mixing involved, were assigned their LS and J_{1j} notations as shown in fig. 7.8.

Mixing of states with the same total angular momentum in the same transition array has been considered. No interaction between levels of the same J value but different configuration has been considered here, since taking into account all the possible perturbations of a given energy level is an extremely difficult and lengthy task.

LEVEL	$^3D_2$	$^1p_2$	$^3p_2$	3/2 3/2	3/2 1/2	1/2 3/2
107289	25%	30%	45%	5%	6%	89%
106238	9%	37%	54%	90%	3%	7%
105617	66%	32%	2%	4%	92%	4%
118469	43%	35%	22%	0.1%	0.5%	99.4%
117184	3%	22%	75%	95%	5%	0%
116999	54%	42%	4%	5%	95%	0%
122635	47%	35%	18%	0%	0%	100%
121271	2%	23%	75%	97%	3%	0%
121192	52%	42%	6%	3%	97%	0%

FIG 7.7. Mixing of states

4p	5p	6p	Assignment
105463	116943	121165	$^3D_3$
105617	118469	122635	$^3D_2$
106087	118407	122601	$^3D_1$
107289	116999	121192	$^1D_2$
106238	117184	121271	$^3P_2$
107496	118459	122610	$^3P_1$
107054	117563	122791	$^3P_0$
107132	117151	121257	$^1P_1$
104260	116660	121069	$^3S_1$
108723	118871	121470	$^1S_0$

4s	6s	7s	Assignment
93144	119683	122440	$^3P_2$
93751	121161	123882	$^3P_1$
94553	121067	123873	$^3P_0$
95399	119760	122479	$^1P_1$

4d	5d	6d	Assignment
119023	122036	123653	$^3F_4$
119213	122160	123774	$^3F_3$
120601	123373	125067	$^3F_2$
120754	123557	125150	$^1F_3$
119566	122330	123833	$^3D_3$
120619	123506	125113	$^3D_2$
118907	122514	125286	$^3D_1$
118651	122087	123827	$^1D_2$
118512	121933	123809	$^3P_2$
	121794	123468	$^3P_1$
119848	123816	123509	$^3P_0$
		123822	$^1P_1$

FIG. 7.8. Cont.

JJ Level Assignment

4p	5p	6p	Assignment
105463	116943	121165	3a
107289	118469	122635	2c
106238	117184	121271	2a
105617	116999	121192	2b
107496	118459	122610	1c
107132	118407	122601	1d
106087	117151	121257	1b
104162	116660	121069	1a
108723	118871	122791	0b
107054	117563	121470	0a

4s	5s	7s	Assignment
93144	119683	122440	2b
95399	121161	123882	1d
93711	119760	122479	1b
94553	121067	123873	0d

4d	5d	6d	Assignment
119023	122036	123653	4a
120654	123447	125150	3c
119566	122330	123833	3a
119213	122160	123774	3b
120619	123506	125113	2c
120601	123373	125067	2d
119445	122282	123827	2b
118907	122087	123809	2a
121012	123816	125286	1d
119848	122514	123822	1a
118651	121933	123468	1b
118512	121794	123509	0b

FIG. 7.8.

The Slater and spin-orbit parameters finally obtained from the reiterative least squares fitting procedure from the LS coupling representation agreed almost identically with those obtained from the J_{1j} coupling representation after all the errors due to incorrect phases etc. had been corrected. They are given in fig. 7.9.

From this procedure the calculated energy levels agreed with those observed (ref. 10) for the lower energy arrays to a very high accuracy, although the standard deviation of the worst fitting set, the $3p^5 6d$ is of the order of 20 cm^{-1}, i.e. 0.016%. The calculated and observed values are given in fig. 7.10.

The next problem was that of calculating the line strength matrices for the transitions in both coupling schemes. Although relative values are given in Condon and Shortley (ref. 58), these would have to be put on to an absolute scale and have their phases calculated; therefore the line strengths were calculated from the basic formulae given by Wybourne (ref. 60). These formulae are written in terms of s, where s is defined below, and in terms of Racah 6-j symbols (ref. 61). For transitions $1^N 1'$ $1^N 1''$, the transition probability is defined as:-

$$A(\alpha J; \alpha' J') = \frac{1}{2J+1} \frac{64\pi^4\sigma^3}{3h} \mathcal{L}(\alpha J; \alpha' J')$$

where, in LS coupling, the line strength $\mathcal{L}(\alpha J; \alpha' J')$ is given by

$$\mathcal{L}^{1/2}(\alpha J; \alpha' J') = \mathcal{L}^{1/2}(\alpha SLJ; \alpha' SL' J')$$
$$= (-1)^{J+L'+S+L_1+L+\ell''+g_s} [LL'][JJ'] \begin{Bmatrix} J & 1 & J' \\ L' & S & L \end{Bmatrix} \begin{Bmatrix} L & 1 & L' \\ \ell'' & L_1 & \ell' \end{Bmatrix} \ell_>^{1/2}$$

and in J_{ij} coupling

$$\mathcal{L}^{1/2}(\alpha J; \alpha' J') = \mathcal{L}^{1/2}(\alpha_1 J_1 jJ; \alpha_1 J_1 j' J')$$
$$= (-1)^{J+L_1+j'+J-\ell''+S+g_s} [JJ'][jj'] \begin{Bmatrix} J & 1 & J' \\ j' & J_1 & j \end{Bmatrix} \begin{Bmatrix} j & 1 & j' \\ 1'' & s & l' \end{Bmatrix} \ell_>^{1/2} s$$

where σ is the wavenumber of the transition.

PARA-METER	LEVEL								
	4s	6s	7s	4p	5p	6p	4d	5d	6d
Fc	94339.7	120221.1	122943.8	106035.5	117450.	121654.3	119572	122544	124172.6
F_2	-	-	-	177.5	48.1	19.4	81.5	36.3	29.3
G_c	-	-	-	693.4	217.9	97.3	-	-	-
G_1	725.1	67.3	26.0	-	-	-	68.9	44.3	14.9
G_2	-	-	-	41.6	13.3	6.4	-	-	-
G_3	-	-	-	-	-	-	6.1	3.2	1.8
3p	938.5	951.3	950.8	920.7	946.9	945.0	894.7	888.1	927.3
4p	-	-	-	24.4	-	-	-	-	-
5p	-	-	-	-	14.6	-	-	-	-
6p	-	-	-	-	-	9.8	-	-	-
4d	-	-	-	-	-	-	2.9	-	-
5d	-	-	-	-	-	-	-	9.9	-
6d	-	-	-	-	-	-	-	-	4.7

FIG 7.9. Parameter values

$3p^5 4s$			$3p^5 6s$			$3p^5 7s$		
Obs.	Calc.	Diff.	Obs.	Calc.	Diff.	Obs.	Calc.	Diff.
93144	93145	- 1	119683	119678	5	122440	122442	- 2
95399	95399	0	121161	121153	8	123882	123887	- 4
93751	93749	2	119760	119765	- 5	122479	122477	2
94553	94553	0	121097	121105	- 8	123873	123869	4

$3p^5 4p$			$3p^5 5p$			$3p^5 6p$		
Obs.	Calc.	Diff.	Obs.	Calc.	Diff.	Obs.	Calc.	Diff.
105463	105410	53	116943	116936	7	121165	121167	- 2
107289	107267	22	118469	118466	3	122635	122631	4
106238	106264	- 26	117184	117189	- 5	121271	121213	- 2
105617	105607	10	116999	116999	0	121192	121194	- 2
107496	107520	- 24	118459	118469	-10	122610	122616	- 6
107132	107122	10	118407	118394	13	122601	122592	9
106087	106091	- 4	117151	117155	- 4	121257	121255	2
104102	104128	- 26	116660	116666	- 6	121069	121070	- 1
108723	108719	4	118871	118878	- 7	122791	122798	- 7
107054	107073	20	117563	117554	8	121470	121464	6

$3p^4 4d$			$3p^5 5d$			$3p^5 6d$		
Obs.	Calc.	Diff.	Obs.	Calc.	Diff.	Obs.	Calc.	Diff.
119023	118959	64	122036	122037	- 1	[illegible]	123646	7
120754	120719	35	123557	123555	2	125150	125158	- 8
119566	119619	- 53	122330	122349	- 19	123833	123874	- 41
119213	119174	39	122160	122132	28	123774	123734	40
120619	120674	- 55	123506	123488	18	125113	125126	- 13
120601	120561	40	123373	123434	- 61	125067	125115	- 48
119445	119445	0	122282	122255	27	123827	123851	- 24
118907	118913	- 6	122087	122059	28	123807	123677	132
121012	121035	- 23	123816	123773	43	125286	125220	66
119848	119827	21	122514	122560	- 46	123822	123847	- 25
118651	118668	- 17	121933	121910	23	123468	123555	- 87
118512	118559	- 47	121794	121831	- 37	123509	123511	- 2

FIG 7.10. Energy level values

s is given by

$$s(n'l'; n''l'') = -e \int_0^\infty rR(n'l')R(n''l'')dr$$

where $R(n'l')$ and $R(n''l'')$ are the radial wave functions of the initial and final configurations.

$$g = \tfrac{1}{2}(l'' - l' + 1)$$

and the notation $[XY] = [(2X+1)(2Y+1)]^{\frac{1}{2}}$

$l_>$ is the larger value of l involved in the transition.

The value of s, which is required to put the calculated line strength onto an absolute scale was obtained using the Coulomb approximation (ref. 44) whereby the electron involved is assumed to move in the field produced by the others. This is the simplest method; another method requires the numerical determination of self-consistent field wave-functions with exchange and polarisability corrections added. From the paper of Bates and Damgaard (ref. 44) which gives the Coulomb approximation values, the values of s^2 were obtained for each parent transition; i.e. values of n , the effective quantum number for each set of energy levels of a given parent were averaged and the value used to calculate s^2. These are given in fig. 7.11.

Landé g factors were also calculated in intermediate coupling (ref. 58d) and are compared with those derived from LS and J_{lj} coupling, and observed values in tables 7.12, 7.13 and 7.14.

Using the matrices A and B now obtained, the line strength matrices in the form of $\mathcal{L}^{\frac{1}{2}}$ were then used to calculate the line strength matrices in intermediate coupling.

i.e. $(S^{\frac{1}{2}})_{IC} = B_{LS} (S^{\frac{1}{2}})_{LS} \widetilde{A}_{LS}$

and $(S^{\frac{1}{2}})_{IC} = B_{J_{lj}} (S^{\frac{1}{2}})_{J_{lj}} \widetilde{A}_{J_{lj}}$

Transition	s^2	Transition	s^2	Transition	s^2
$4p(\frac{1}{2}) - 4s(\frac{1}{2})$	9.0	$6s(\frac{1}{2}) - 4p(\frac{1}{2})$	0.45	$4d(\frac{1}{2}) - 4p(\frac{1}{2})$	0.045
$4p(\frac{3}{2}) - 4s(\frac{3}{2})$	9.0	$6s(\frac{3}{2}) - 4p(\frac{3}{2})$	0.52	$4d(\frac{3}{2}) - 4p(\frac{3}{2})$	0.063
$5p(\frac{1}{2}) - 4s(\frac{1}{2})$	0.90	$7s(\frac{1}{2}) - 4p(\frac{1}{2})$	0.083	$5d(\frac{1}{2}) - 4p(\frac{1}{2})$	0.049
$5p(\frac{3}{2}) - 4s(\frac{3}{2})$	0.95	$7s(\frac{3}{2}) - 4p(\frac{3}{2})$	0.12	$5d(\frac{3}{2}) - 4p(\frac{3}{2})$	0.034
$6p(\frac{1}{2}) - 4s(\frac{1}{2})$	0.013			$6d(\frac{1}{2}) - 4p(\frac{1}{2})$	0.027
$6p(\frac{3}{2}) - 4s(\frac{3}{2})$	0.015			$6d(\frac{3}{2}) - 4p(\frac{3}{2})$	0.022

FIG 7.11 Values of s^2

	$3p^5 4s$				$3p^5 6s$				$3p^5 7s$			
LEVEL	93144	95399	93751	94553	119683	121161	119760	121097	122440	123882	122479	123873
DESIG.	$1s_5$	$1s_2$	$1s_4$	$1s_3$	$3s_5$	$3s_2$	$3s_4$	$3s_3$	$4s_5$	$4s_2$	$4s_4$	$4s_3$
LS	1.500	1.000	1.500	0.000	1.500	1.000	1.500	0.000	1.500	1.000	1.500	0.000
J_{1j}	1.500	1.333	1.167	0.000	1.500	1.333	1.167	0.000	1.500	1.333	1.167	0.000
OBS	1.506	1.102	1.404	0.000	1.500	1.271	1.184	0.000	1.506	1.296	1.164	0.000
IC	1.500	1.1014	1.399	0.000	1.500	1.311	1.189	0.000	1.500	1.325	1.175	0.000

	$3p^5 4p$									
LEVEL	105463	107289	106238	105617	107496	107132	106087	104102	108723	107054
DESIG.	$2p_9$	$2p_3$	$2p_6$	$2p_8$	$2p_2$	$2p_4$	$2p_7$	$2p_{10}$	$2p_1$	$2p_5$
LS	1.333	1.000	1.500	1.167	1.500	1.000	0.500	2.000	0.000	0.000
J_{1j}	1.333	1.167	1.333	1.167	0.666	1.500	1.333	1.500	0.000	0.000
OBS	1.338	1.260	1.305	1.112	1.380	0.819	0.838	1.985	0.000	0.000
IC	1.333	1.265	1.282	1.119	1.362	0.877	0.786	1.975	0.000	0.000

FIG 7.12. Landé g factors

						$3p^5 5p$				
LEVEL	116943	118469	117184	116999	118459	118407	117151	116660	118871	117563
DESIG.	$3p_9$	$3p_3$	$3p_6$	$3p_8$	$3p_2$	$3p_4$	$3p_7$	$3p_{10}$	$3p_1$	$3p_5$
LS	1.333	1.167	1.500	1.000	1.500	0.500	1.000	2.000	0.000	0.000
J_{1j}	1.333	1.167	1.333	1.167	0.666	1.500	1.333	1.500	0.000	0.000
OBS		1.18	1.42	1.09	1.45	0.61	1.01	1.90	0.000	0.000
IC	1.333	1.180	1.378	1.109	1.456	0.645	1.007	1.892	0.000	0.000

						$3p^5 6p$				
LEVEL	121165	122635	121271	121192	122610	122601	121257	121069	122791	121470
DESIG.	$4p_9$	$4p_3$	$4p_6$	$4p_8$	$4p_4$	$4p_2$	$4p_7$	$4p_{10}$	$4p_1$	$4p_5$
LS	1.333	1.167	1.500	1.000	1.500	0.500	1.000	2.000	0.000	0.000
J_{1j}	1.333	1.167	1.333	1.167	0.666	1.500	1.333	1.500	0.000	0.000
OBS	-	-	-	-	-	-	-	-	-	-
IC	1.333	1.170	1.378	1.119	1.502	0.626	1.032	1.839	0.000	0.000

FIC 7.13 Cont.

						$3p^5 4d$						
LEVEL	119024	120754	119566	119213	120619	120601	119445	118907	121012	119848	118651	118512
DESIG.	$4d_4'$	$4s_1'''$	$4d_1'$	$4d_4$	$4s_1'''$	$4s_1''$	$4d_1''$	$4d_3$	$4s_1'$	$4d_2$	$4d_5$	$4d_6$
LS	1.250	1.000	1.333	1.083	1.167	0.667	1.000	1.500	0.500	1.000	1.500	0.000
J_{1j}	1.250	1.111	1.240	1.067	1.290	0.767	1.067	1.211	0.833	1.100	1.066	0.000
OBS	1.255	1.133		1.077	0.987	1.057	0.908	1.437	0.877	0.768	1.467	0.000
IC	1.250	1.141	1.194	1.081	1.169	0.866	0.869	1.429	0.783	0.758	1.459	0.000

						$3p^5 5d$						
LEVEL	122036	123557	122330	122160	123506	123373	122282	122087	123816	122514	121933	121794
DESIG.	$5d_4'$	$5s_1'''$	$5d_1'$	$5d_4$	$5s_1''''$	$5s_1''$	$5d_1''$	$5d_3$	$5s_1'$	$5d_2$	$5d_5$	$5d_6$
LS	1.250	1.000	1.333	1.083	1.167	0.667	1.000	1.500	1.000	0.500	1.500	0.000
J_{1j}	1.250	1.111	1.240	1.067	1.290	0.767	1.067	1.211	0.833	1.100	1.066	0.000
OBS	1.253	1.127	1.199	1.076	0.802	1.265	0.941	1.387	0.846	0.813	1.400	0.000
IC	1.250	1.119	1.209	1.087	1.232	0.794	0.934	1.374	0.831	0.756	1.413	0.000

FIG 7.14 . Landé g factors

$3p^5 6d$

LEVEL	123653	124140	123833	123774	125113	125067	123827	123809	125286	123822	123468	123509
DESIG.	$6d_4'$	$6s_1'''$	$6d_1'$	$6d_4$	$6s_1''''$	$6s_1''$	$6d_1''$	$6d_3$	$6s_1'$	$6d_2$	$6d_5$	$6d_6$
LS	1.250	1.000	1.333	1.083	1.167	0.667	1.000	1.500	0.500	1.000	1.500	0.000
J_{1j}	1.250	1.111	1.240	1.067	1.290	0.767	1.067	1.211	0.833	1.100	1.066	0.000
OBS	1.256	1.098	1.245	1.052	0.777	1.264	1.107	1.206	-	-	1.233	0.000
IC	1.250	1.122	1.228	1.066	1.204	0.626	0.950	1.354	0.770	0.810	1.420	0.000

FIG 7.14. Cont

The line strength matrices in intermediate coupling should be the same when calculated from both coupling schemes.

In fact, eight significant discrepancies in previously calculated J_{1j} transition probabilities, summarised by Garstang and Von Blerkom (ref. 30) were found, due possibly to incorrect line strength determinations.

Results of Theoretical Calculation

The calculated values of the transition probabilities in intermediate coupling derived from LS and J_{1j} coupling, were identical, indicating that correct transformation matrices and correct line strength matrices had been used.

Experimental measurements only exist for the 4p - 4s and 5p - 4s arrays from other authors so that the experimental values for other arrays, determined in the preceding chapter can only be compared to the theoretical ones calculated here.

In tables 7.15, 7.16 and 7.17, all the theoretical values are listed, the wavelengths being given in Å units in vacuo.

Apart from the discrepancies in the J_{1j} values mentioned above, the calculated 4p - 4s and 5p - 4s arrays agree with those previously calculated (ref. 30), the difference of a few per cent, insignificant in the calculations, being due to a different choice of s^2.

It will be noticed that some of the transition probabilities of the 4d - 4p arrays are smaller than those of the 5d - 4p array, due to the value of s^2 increasing for those levels of parentage $\frac{1}{2}$, together with tho inverse wavelength cubed

TRANSITION PROBABILITIES

J_{UPPER}	J_{LOWER}	(Å)	LS	IC	J_{1j}
3	2	8117.5	3.33	3.33	3.33
2	2	7069.6		0.55	
2	2	7637.1	3.08	2.48	2.02
2	2	8017.3	0.88	0.97	1.74
2	1	8410.4	3.03	2.12	3.02
2	1	7366.6		0.86	
2	1	9225.9		0.57	
2	1	8008.3	0.89	0.49	1.71
2	1	9786.7		0.094	
2	1	8427.4	2.27	2.04	1.50
1	2	6967.7	2.24	0.73	
1	2	7149.0		0.14	
1	2	7726.2	0.11	0.53	
1	2	9125.8	1.33	1.67	1.98
1	1	8266.5		1.70	2.12
1	1	7275.4	1.19	0.19	
1	1	8523.0	2.92	1.25	0.97
1	1	7473.3		0.040	
1	1	9356.3		0.060	
1	1	8106.4	1.43	2.42	2.81
1	1	11490.3		0.017	
1	1	9660.9	0.67	0.46	0.33
1	0	7726.2	1.30	1.14	1.30
1	0	7949.8		1.91	2.39
1	0	8670.0	1.54	0.32	
1	0	10472.3	0.18	0.085	
0	1	7505.3	4.30	4.30	4.30
0	1	6679.1		0.0046	
0	1	8580.0		0.0019	
0	1	7517.1	4.24	4.23	4.22

FIG. 7.15. $4p$-$4s$ Transition probabilities

TRANSITION PROBABILITIES

J_{UPPER}	J_{LOWER}	(Å)	LS	IC	J_{ij}
3	2	4201.9	0.26	0.26	0.26
2	2	3948.7		0.0017	
2	2	4159.7	0.20	0.19	0.13
2	2	4192.0		0.076	0.13
2	1	4334.6		0.17	0.22
2	1	4045.6	0.022	0.058	
2	1	4590.3		0.17	
2	1	4267.5	0.061	0.052	0.12
2	1	4629.6	0.18	0.022	
2	1	4301.4		0.14	0.12
1	2	3950.2	0.13	0.0098	
1	2	3958.4	0.0086		
1	2	4165.5		0.040	0.044
1	2	4252.4	0.14	0.21	0.21
1	1	4336.5		0.10	0.15
1	1	4047.3	0.072	0.024	
1	1	4116.3		0.083	0.073
1	1	4055.8	0.012	0.015	
1	1	4197.3	0.19	0.027	
1	1	4273.5		0.17	0.20
1	1	4203.4		0.00028	
1	1	4365.1	0.077	0.039	0.039
1	0	4183.1	0.082	0.10	0.091
1	0	4192.2	0.13	0.14	0.16
1	0	4425.2		0.00095	
1	0	4523.5	0.022	0.0025	
0	1	4260.4	0.24	0.22	0.24
0	1	3980.9		0.022	
0	1	4511.8		0.014	
0	1	4199.6	0.20	0.24	0.26

FIG 7 15 $5p_2$-$4s$ Transition probabilities

TRANSITION PROBABILITIES

J_{UPPER}	J_{LOWER}	(Å)	LS	IC	J_{Lj}
3	2	3568.0	0.066	0.066	0.066
2	2	3390.9		0.020	
2	2	3555.3	0.051	0.046	0.033
2	2	3565.3		0.023	0.033
2	1	3671.6		0.0043	0.053
2	1	3462.1	0.055	0.015	
2	1	3865.2		0.0036	
2	1	3633.7	0.016	0.017	0.031
2	1	3877.0	0.046	0.0056	
2	1	3644.2		0.034	0.031
1	2	3393.7	0.033	0.0006	
1	2	3394.8	0.0022		
1	2	3557.1		0.0094	0.011
1	2	3581.0	0.038	0.056	0.055
1	1	3675.0		0.021	0.035
1	1	3465.1	0.019	0.0064	
1	1	3676.2		0.023	0.018
1	1	3466.2	0.030	0.0069	
1	1	3867.3	0.046	0.008	
1	1	3635.6		0.044	0.053
1	1	3895.6		0.0004	
1	1	3660.6	0.021	0.0082	0.010
1	0	3564.2	0.020	0.031	0.019
1	0	3565.3	0.033	0.027	0.039
1	0	3744.8			
1	0	3771.3	0.0055		
0	1	3650.7		0.047	0.054
0	1	3443.5	0.076	0.010	
0	1	3835.7	0.047	0.0065	
0	1	3607.6		0.056	0.065

FIG 7 15 6p-4s Transition probabilities

dependence of the transition probability. This implies that the 5d levels with parentage $\frac{1}{2}$ are being perturbed, causing their quantum defect to be larger rather than smaller than that for the 4d levels of parentage $\frac{1}{2}$. This perturbation of the levels is reflected in the Lande g values where, apart from the s''' and s'' levels, which again have parentage $\frac{1}{2}$, the agreement between intermediate coupling and observation is much better than that of the other coupling schemes.

In view of the fact that configuration interaction has been ignored and that the Coulomb approximation has been used to put the line strength onto an absolute scale, the accuracy of these theoretical values cannot be expected to be very good. Any estimate of an accuracy better than a factor of 2 either way, for the intermediate coupling values must be not only optimistic but rather unlikely. As for the J_{1j} and particularly the LS coupling values, the comparison with experimental values shows that up to several orders of magnitude discrepancy can be expected.

Results of The Experimental Measurement of Transition Probabilities

In figs. 7.18 to 7.25 the experimental values measured by the method described in the previous chapter are compared with the theoretical calculations and the measured values of other authors.

The number of Abel inversions of the lines from each upper state totalled 49. The number of lines measured in the centre of the discharge was 68, giving a total of 116 measured line intensities.

Transition Probabilities 6s-4p

J_{UPPER}	J_{LOWER}	(Å)	LS	IC	J_{1j}
2	3	7032.3	0.43	0.43	0.43
2	2	8068.4		0.022	
2	2	7437.7	0.19	0.16	0.12
2	2	7109.3	0.073	0.081	0.15
2	1	8205.5	0.048	0.016	
2	1	7967.5		0.0034	
2	1	7355.1	0.0045	0.021	0.14
2	1	6418.1	0.14	0.17	0.040
1	2	7208.8		0.36	0.40
1	2	6701.1	0.13	0.043	
1	2	6433.4	0.43	0.013	
1	2	8018.6	0.34	0.00042	
1	2	7395.4		0.13	0.22
1	2	7070.6		0.35	0.25
1	1	7318.0	0.058	0.13	0.077
1	1	7128.1		0.076	0.17
1	1	6633.9	0.13	0.014	
1	1	5862.0	0.15	0.045	
1	1	8153.9		0.0033	
1	1	7918.9	0.21	0.028	
1	1	7313.7		0.19	0.045
1	1	6386.5		0.059	0.33
1	0	8039.9		0.047	0.059
1	0	7088.7	0.086	0.018	
1	0	9060.4	0.047	0.0097	
1	0	7870.3		0.057	0.072
0	1	7352.4	0.23	0.20	0.46
0	1	7160.8		0.40	0.25
0	1	6662.2	0.51	0.11	
0	1	5884.1	0.15	0.073	

FIG. 7.16.

Transition Probabilities 7s-4p

J_{UPPER}	J_{LOWER}	(Å)	LS	IC	J_{1j}
2	3	5890.3	0.17	0.17	0.17
2	2	6600.2		0.0096	
2	2	6172.1	0.078	0.066	0.052
2	2	5944.2	0.029	0.034	0.059
2	1	6691.6	0.020	0.0070	
2	1	6532.5		0.0014	
2	1	6115.1	0.0018	0.0089	0.054
2	1	5453.2	0.052	0.066	0.016
1	2	6026.6		0.12	0.13
1	2	5667.6	0.039	0.012	
1	2	5475.0	0.13	0.0053	
1	2	6583.3	0.14		
1	2	6157.3		0.055	0.089
1	2	5930.5		0.14	0.098
1	1	6102.8	0.018	0.042	0.025
1	1	5970.1		0.024	0.054
1	1	5619.6	0.041	0.0056	
1	1	5055.6	0.044	0.014	
1	1	6674.2		0.0020	
1	1	6515.9	0.088	0.013	
1	1	6100.5		0.076	0.018
1	1	5441.8		0.022	0.13
1	0	6596.7		0.016	0.020
1	0	5942.5	0.027	0.0062	
1	0	7269.6	0.022	0.0050	
1	0	6483.0		0.024	0.030
0	1	6106.1	0.075	0.066	0.15
0	1	5973.4		0.13	0.081
0	1	5622.4	0.16	0.033	
0	1	5057.9	0.044	0.022	

FIG 7.16. Cont

These are divided amongst the transition arrays as follows:-

4p - 4s,	7,	6s - 4o	16,	4d - 4o	16,
5p - 4s	23,	7s - 4p	12,	5d - 4p	26,
6p - 4s	5,			6d - 4p	10,

In 4 regions of the spectrum, where two lines overlapped to a large extent, namely at 7353Å, 5942Å, 4191Å and 4045Å; the total gA value is given for the combination.

The absolute values for the transition probabilities are given here. Although the purpose of the experiment was to produce a large number of accurate relative values ($\sim 2\%$) the absolute values themselves seem, where comparison with other experimental values is possible, to be reasonably accurate although an error of the order of 40% would be expected.

Now the intensity of a spectral line

$$I(\nu) \text{ is proportional to } A_{nm} \exp\left[-W_n/kT\right]$$

differentiating,

$$dI(\nu) \propto dA \exp\left[\frac{-Wn}{kT}\right] - A_{nm}\frac{W_n}{kT}\frac{dT}{T}\exp\left[\frac{-W_n}{kT}\right]$$

dividing $$\frac{dI(\nu)}{I(\nu)} = \frac{dA_{nm}}{A_{nm}} - \frac{W_n}{kT}\frac{dT}{T}$$

Now in the temperature and energy level ranges investigated here,

$$\frac{Wn}{kT} \sim 17$$

consequently 2% error in T will produce 34% - 40% error in the calculation of the transition probability, neglecting any measuring and calibration error in I.

However, for relative measurements, the ratio of intensities of two lines is given by

$$R = \frac{I_1}{I_2} \text{ which is given by } \frac{A_1}{A_2}\frac{\exp\left[-W_1/kT\right]}{\exp\left[-W_2/kT\right]}$$

differentiating, dR is proportional to

$$\left\{d\left(\frac{A_1}{A_2}\right) \exp -\frac{(W_1-W_2)}{kT}\right\} - \frac{A_1}{A_2}\frac{(W_1-W_2)}{kT}\frac{dT}{T} \times \left[\exp -\frac{(W_1-W_2)}{kT}\right]$$

J_{UPPER}	J_{LOWER}	(Å)	LS	IC	J_{1j}
4	3	7374.6	0.19	0.19	0.19
3	3	6539.8		0.0027	
3	3	7090.7	0.034	0.043	
3	3	7272.7	0.022	0.032	0.027
3	2	7426.7	0.13	0.13	0.13
3	2	6889.0		0.0051	
3	2	6606.3		0.00022	
3	2	8154		0.0013	
3	2	7503.0	0.13	0.14	0.15
3	2	7169.0	0.0057	0.016	
3	2	8386.4			
3	2	7707.1		0.0022	0.0056
3	2	7355.1	0.17	0.16	0.16
2	3	6598.0	0.03	0.0011	
2	3	6605.9	0.00087	0.00033	
2	3	7152.1		0.0039	0.0097
2	3	7438.3	0.0043	0.0076	0.0037
2	2	7501.9		0.010	0.013
2	2	6953.6	0.031	0.017	
2	2	6665.8	0.032	0.0021	
2	2	7512.0		0.014	0.020
2	2	6962.3		0.0004	
2	2	6673.8	0.029	0.0021	
2	2	8226.4	0.034	0.00039	
2	2	7571.7		0.0023	0.012
2	2	7231.7		0.063	0.084
2	2	8607.3		0.012	

FIG. 7.17. 4d-4p Transition probabilities.

J_{UPPER}	J_{LOWER}	(Å)	LS	IC	J_{1j}
2	2	7893.3	0.049	0.052	0.055
2	2	7524.5	0.00074	0.011	
2	1	7620.2	0.070	0.094	0.11
2	1	7414.5		0.0035	
2	1	6881.4	0.0064	0.0022	
2	1	6054.4		0.0051	
2	1	7630.7		0.00087	0.0021
2	1	7424.5		0.12	0.11
2	1	6889.9	0.14	0.0057	
2	1	6061.0			
2	1	8368.9			
2	1	8121.5	0.11	0.00091	
2	1	7486.2		0.12	0.076
2	1	6517.6			0.015
2	1	8763.5	0.017	0.00017	
2	1	8492.6		0.0023	
2	1	7800.3	0.000045	0.0055	
2	1	6754.5	0.14	0.11	0.16
1	2	7287.0		0.0022	0.0039
1	2	6768.6	0.0037	0.0025	
1	2	6495.6	0.012	0.0057	
1	2	7962.4	0.0042	0.00021	
1	2	7347.5		0.00025	0.0096
1	2	7026.9		0.010	
1	2	8801.3		0.0038	
1	2	8056.1	0.025	0.022	0.013
1	2	7672.2	0.0035	0.0067	0.024
1	1	7398.6	0.043	0.038	0.019

FIG. 7.17. Cont.

J_{UPPER}	J_{LOWER}	(Å)	LS	IC	J_{lj}
1	1	7204.6		0.018	0.041
1	1	6700.2	0.035	0.0030	
1	1	5963.7		0.00079	
1	1	8095.9		0.00031	
1	1	7864.1	0.065	0.0098	
1	1	7266.9		0.076	
1	1	6350.8			0.13
1	1	8964.6	0.011	0.0059	
1	1	8681.3		0.0019	
1	1	7959.2	0.0011	0.0018	0.11
1	1	6873.3	0.13	0.15	0.0052
1	0	8137.4		0.048	0.056
1	0	7164.4	0.062	0.010	
1	0	8988.8	0.058	0.0085	
1	0	7816.2		0.066	0.080
1	0	10072.5		0.000065	
1	0	8622.9	0.016	0.0082	0.0066
0	1	9077.7	0.043	0.014	
0	1	8787.3		0.0030	
0	1	8048.3	0.0041	0.020	0.12
0	1	6939.6	0.13	0.16	0.038

FIG. 7.17. Cont.

J_{UPPER}	J_{LOWER}	(Å)	LS	IC	J_{1j}
4	3	6033.9	0.18	0.18	0.18
3	3	5526.7		0.00098	
3	3	5928.7	0.044	0.031	0.040
3	3	5989.1	0.022	0.034	0.026
3	2	6147.0	0.25	0.24	0.25
3	2	5774.0		0.018	
3	2	5574.1		0.0036	
3	2	6648.5		0.0036	
3	2	6214.3	0.13	0.12	0.14
3	2	5983.4	0.0054	0.019	
3	2	6724.5		0.0014	
3	2	6280.6		0.0021	0.0056
3	2	6044.9	0.17	0.15	0.16
2	3	5542.3	0.39	0.00048	
2	3	5583.5	0.0015		
2	3	5945.7		0.0033	0.0092
2	3	6015.4	0.0045	0.0093	0.0038
2	2	6166.4		0.022	0.025
2	2	5791.1	0.055	0.015	
2	2	5590.0	0.056	0.0029	
2	2	6217.4		0.028	0.037
2	2	5836.0		0.0026	
2	2	5631.9	0.053		
2	2	6669.8	0.035	0.0012	
2	2	6232.9		0.00093	0.011
2	2	60000.6		0.062	0.080
2	2	6757.7		0.010	

FIG 7.17. $5d - 4p$

J_{UPPER}	J_{LOWER}	(Å)	LS	IC	J_{1j}
2	2	6309.5	0.051	0.065	0.058
2	2	6071.6	0.00078	0.0026	
2	1	6246.1	0.14	0.19	0.22
2	1	6107.2		0.0066	
2	1	5740.9	0.012	0.0039	
2	1	5153.6		0.029	
2	1	6298.4		0.00075	0.0040
2	1	6157.3		0.20	0.21
2	1	5785.0	0.26	0.030	
2	1	5189.1			
2	1	6763.2			
2	1	6600.7	0.11	0.0085	
2	1	6174.7		0.10	0.074
2	1	5500.6			0.013
2	1	6853.5	0.012	0.0015	
2	1	6686.7		0.0018	
2	1	6250.0	0.000047	0.0046	
2	1	5560.2	0.13	0.10	0.15
1	2	5060.7	0.0052	0.0054	0.0075
1	2	5688.9		0.0030	
1	2	5494.8		0.00025	
1	2	6568.1			
1	2	6144.0	0.0054		0.0089
1	2	5918.2	0.018	0.0077	
1	2	6828.7		0.0041	
1	2	6371.5	0.028	0.025	0.014
1	2	6129.0	0.0037	0.0085	0.025

FIG. 7. 17. Cont.

J_{UPPER}	J_{LOWER}	(Å)	LS	IC	J_{1j}
1	1	6127.5		0.068	0.036
1	1	5993.8	0.081	0.039	0.077
1	1	5640.5		0.0026	
1	1	5072.5		0.0049	
1	1	6501.1		0.0075	
1	1	6087.5	0.050	0.069	
1	1	5431.2		0.0019	0.12
1	1	6756.3		0.0022	
1	1	6310.7	0.0011	0.0046	0.11
1	1	5608.2	0.13	0.15	0.0052
1	1	6658.7	0.064	0.00035	
1	1	6926.6	0.013	0.0093	
1	0	6625.6	0.079	0.10	0.11
1	0	5965.9		0.016	
1	0	7251.1		0.0066	
1	0	6468.3	0.092	0.069	0.077
1	0	7570.0			
1	0	6720.9	0.019	0.0049	0.0076
0	1	6994.0	0.051	0.016	
0	1	6820.4		0.0035	
0	1	6366.6	0.0044	0.022	0.13
0	1	5652.3	0.13	0.16	0.038

FIG. 7. 17. Cont.

J_{UPPER}	J_{LOWER}	(Å)	LS	IC	J_{1j}
4	3	5497.5	0.16	0.16	0.16
3	3	5079.5		0.00058	
3	3	5443.7	0.037	0.034	0.033
3	3	5461.2	0.018	0.021	0.022
3	2	5598.8	0.18	0.17	0.18
3	2	5287.6		0.0012	
3	2	5119.5		0.0046	
3	2	6044.5		0.0033	
3	2	5683.4	0.11	0.10	0.12
3	2	5489.7	0.0045	0.0052	
3	2	6066.1		0.0015	
3	2	5702.6			0.0049
3	2	5507.5	0.14	0.14	0.13
2	3	5089.1	0.27	0.00026	
2	3	5101.0	0.0010		
2	3	5445.4		0.0035	0.0077
2	3	5450.8	0.0039	0.0073	0.0033
2	2	5610.4		0.028	0.017
2	2	5298.0	0.039	0.0096	
2	2	5129.3	0.040	0.0020	
2	2	5624.9		0.0092	0.026
2	2	5311.0		0.00027	
2	2	5141.4	0.035		
2	2	6046.7	0.030	0.0016	
2	2	5685.4		0.0020	0.0097
2	2	5491.5		0.053	0.067
2	2	6053.3		0.0080	

FIG 7 17 $6d - 4p$

J_{UPPER}	J_{LOWER}	(Å)	LS	IC	J_{1j}
2	2	5691.2	0.045	0.058	0.052
2	2	5496.9	0.00067	0.0012	
2	1	5676.3	0.095	0.12	0.15
2	1	5561.4		0.0025	
2	1	5256.0	0.0080		
2	1	4759.4		0.022	
2	1	5691.2		0.0074	0.0028
2	1	5575.7		0.15	0.15
2	1	5268.7	0.18	0.027	
2	1	4769.9		0.0011	
2	1	6123.3			
2	1	5989.8	0.094	0.0086	
2	1	5637.0		0.086	0.061
2	1	5069.7			0.011
2	1	6130.1	0.012	0.0023	
2	1	5996.3		0.0018	
2	1	5642.7	0.000041	0.0073	
2	1	5074.3	0.11	0.083	0.13
1	2	5556.5		0.0039	0.005
1	2	5249.9	0.0044	0.0013	
1	2	5084.1	0.015	0.00087	
1	2	6048.5	0.0039	0.00068	
1	2	5687.0		0.00058	0.0073
1	2	5493.0		0.0085	
1	2	6180.9		0.0031	
1	2	5803.8	0.024	0.021	0.012
1	2	5601.9	0.0032	0.0051	0.021

FIG. 7.17. Cont.

J_{UPPER}	J_{LOWER}	(Å)	LS	IC	J_{1j}
1	1	5621.1	0.053	0.046	0.024
1	1	5508.4		0.021	0.051
1	1	5208.6	0.041	0.0088	
1	1	4720.5		0.0067	
1	1	6125.2			
1	1	5991.6	0.052	0.011	
1	1	5638.6		0.055	
1	1	5071.0		0.0012	0.092
1	1	6261.0	0.011	0.0093	
1	1	6121.4		0.00034	
1	1	5753.4	0.00097	0.00075	0.097
1	1	5163.7	0.11	0.12	0.0043
1	0	6037.6		0.060	0.078
1	0	5484.9	0.079	0.027	
1	0	6623.0	0.051	0.012	
1	0	5963.7		0.044	0.063
1	0	6782.0		0.00068	
1	0	6092.4	0.016	0.0093	0.0067
0	1	6244.9	0.046	0.015	
0	1	6106.1		0.0032	
0	1	5739.9	0.0039	0.019	0.12
0	1	5152.8	0.11	0.14	0.033

FIG. 7.17 Cont.

Now $\frac{W_1-W_2}{kT}$ is of the order of unity, consequently for an error of 2% in T, the error in the transition probabilities relative to each other should be in the region of 2 to 4%. A fuller discussion of the errors involved is given in Chapter 8, since the small errors of calibration and Abel inversion of the observed intensities will affect the accuracy of the relative values but not to any extent the absolute values.

Discussion of the experimental transition probabilities

4d - 4p array (fig. 7.18)

Sixteen transition probabilities have been measured from this array, four of which can be compared with other experimental determinations. For the 6871Å and 6752Å lines extremely good agreement exists with the values given by Popenoe and Shumaker (ref. 18). The 6059Å and 6052Å lines overlapped in their line wings and are subject to a larger possible error; it is perhaps significant that the total gA value for this pair is identical to the total gA value obtained by Gericke (ref. 15), although the

4p-4s Transition Probabilities ($x10^{-8}$ sec^{-1})

J_{UPPER}	(Å)	PDJ	O (ref.14)	Do (ref.31)	PT&C (ref.32)	P&S (ref. 8)	LS	IC	J_{1j}
2	7383	0.99	0.87	1.07	0.89			0.86	
1	7272	0.162	1.61				1.19	0.19	
1	7147	0.065			.3			0.14	
2	7067	0.35			.53			0.55	
1	6965	0.50	0.53		.87	.71	2.24	0.73	
0	6677	0.036						0.0046	

6p-4s Transition Probabilities ($x10^{-8}$ sec^{-1})

J_{UPPER}	(Å)	PDJ(1)	LS	IC	J_{1j}
0	3834	0.064	0.047	0.0065	
0	3649	0.035		0.047	0.054
0	3606	0.050		0.056	0.065
1	3635	0.012		0.044	0.053
3	3567	0.0044	0.066	0.066	0.066

FIG. 7.18. & 7.20. Transition probabilities

5p-4s Transition Probabilities ($x10^{-8}$ sec^{-1})

J_{UPPER}	(Å)	PDJ	C (ref.15)	DR (ref.16)	O (ref.14)	P&S (ref.18)	LS	IC	J_{1j}
1	4702	0.0087						0.0003	
2	4628	0.0025					0.18	0.022	
1	4522	0.0068					0.022	0.0025	
0	4510	0.087		0.102				0.014	
1	4335	0.024	0.036					0.1	0.15
2	4333	0.042	0.047					0.17	0.22
2	4300	0.026	0.033	0.036		0.041		0.14	0.12
1	4272	0.056	0.069	0.076	0.037	0.094		0.17	0.20
2	4266	0.019	0.026	0.028			0.061	0.052	0.12
0	4259	0.25	0.33	0.40	0.25	0.44	0.24	0.22	0.24
1	4251	0.013	0.0075				0.14	0.21	0.21
3	4200	0.049	0.077				0.26	0.26	0.26
0	4198	0.29	0.25				0.26	0.24	0.26
1	4181	0.047	0.041	0.042			0.082	0.10	0.081
1	4164	0.023	0.020	0.025				0.040	0.044
2	4158	0.086	0.12	0.17	0.066	0.16	0.20	0.19	0.13
1	4054	0.003					0.012	0.015	
1	3948	0.037					0.13	0.0098	
2	3947	0.023						0.0017	

FIG. 719. 5p - 4s Transition probabilities

individual values are about 15% different. The electron density in the arc used by Gericke was between 10^{16} per cc. and 10^{17} per cc. Since this would cause the pair of lines to overlap more seriously than in this experiment, the problem of distinguishing the individual line contributions may have led to errors on Gericke's part.

Only in two cases, the 7372Å and the 6951Å lines, are the intermediate coupling values in reasonable agreement with the experimental values. Good agreement would be expected with the 7372Å calculated value since, with a J upper of 4, there can be no serious configuration interaction effects from the close lying 6s levels. Good agreement would have been expected with the 7425Å ($s_{'''}$) line since, with LS, IC, and J_{1j} values equal, only configuration interaction effects can cause discrepancies from the experimental values, yet none of the 6s levels which could interact have a J value of 3. Similarly, the 6538Å (s''') line, which originates from the same upper level, has an IC value very different from the experimental. Although, in this array, there is little agreement between the experimental and theoretical values, the IC values are nearer on the whole, to the experimental values than either the LS or the J_{1j} values.

5d - 4p (fig. 7.19)

Three of the 26 measured values can be compared with other experimental values. The 6032Å value lies below, the 5650Å value lies above, and the 5606Å value is approximately the same as that of Gericke (15). It has been suggested by Popenoe and Shumaker (ref. 18) that Gericke's values should be increased by 35%. This would make the values for the 5650Å and 5606Å lines in better agreement with this experiment but increase that for the 6032Å

6s–4p Transition Probabilities ($\times 10^{-8}$ sec^{-1})

J_{UPPER}	(Å)	PDJ	P γS (ref.18)	LS	IC	J_{1j}
1	7392	0.071			0.13	0.22
0	7350	0.129		0.23	0.20	0.46
1	7316	0.095		0.058	0.13	0.077
1	7311	0.12			0.19	0.045
1	7206	0.27			0.36	0.40
0	7158	0.28		0.40	0.25	
1	7125	0.076			0.076	0.17
2	7107	0.046		0.073	0.081	0.15
1	7086	0.014		0.086	0.018	
2	7030	0.31	0.40	0.43	0.43	0.43
0	6660	0.133		0.51	0.11	
1	6431	0.011		0.43	0.013	
2	6416	0.19		0.14	0.17	0.04
1	6384	0.062			0.059	0.33
0	5882	0.12		0.15	0.073	
1	5860	0,030		0.15	0.045	

FIG 7.21. Transition probabilities

7s-4p Transition Probabilities ($x10^{-8}$ sec^{-1})

J_{UPPER}	(Å)	PDJ	LS	IC	J_{1j}
1	6090	0.057	0.016	0.0093	0.0067
3	6064	0.017		0.0015	
1	5802	0.060	0.024	0.021	0.012
3	5700	0.0073			0.0049
1	5600	0.052	0.0032	0.0051	0.021
2	5574	0.087		0.15	0.15
1	5506	0.087		0.021	0.051
2	15495	0.14	0.16	0.16	0.16
3	5459	0.014	0.018	0.021	0.022
1	5162	0.19	0.11	0.12	0.0043

6d-4p Transition Probabilities ($x10^{-8}$ sec^{-1})

J_{UPPER}	(Å)	PDJ	LS	IC	J_{1j}
2	6170	0.058	0.078	0.066	0.052
1	6098	0.048		0.076	0.018
1	6101	0.23	0.018	0.042	0.025
1	6025	0.14		0.12	0.13
0	5971	0.13		0.13	0.081
2	5888	0.14	0.17	0.17	0.17
1	5618	0.019	0.041	0.0056	
1	5473	0.033	0.13	0.0053	
2	5451	0.042	0.052	0.066	0.016
1	5439	0.020		0.022	0.13

FIG 7.22.& 7.25. Transition probabilities

to nearly twice the value measured here. In view of the fact that the 6032Å line value obtained here agrees very well with the LS, IC and J_{1j} value (cf. 7372°, 4d - 4p line, also from a J = 4 upper level), it would appear that again Gericke has possibly made errors in calculating adjacent line wing contributions since this line overlaps to a large extent the 6043Å line.

The 6212Å ($5d_1'$) line, one would expect, in view of its lack of configuration interaction and small interaction with the other J = 3 level (LS J_{1j} and IC values approximately equal) to agree well with experiment. Again this is not so. With the 6145Å (s_1''') line, also of J = 3 upper level, but different parentage one would expect again good experimental agreement. However, the 6043Å ($5d_4$) J = 3 line, and the 5987Å line which originates from the same upper level, do agree well with experiment. In almost half the cases, agreement is better with either J_{1j} or LS coupling than with intermediate coupling.

<u>6d - 4p</u> (fig. 7.20)

No other experimental values are available for comparison. Only for the 5495Å, ($6_{d\ 3}$) s = 2, is there good agreement with experiment. (The 6039Å, $5d_3$ line was in very good agreement with experiment also). Three lines with a J = 3 upper level were measured, all from the $6d_4$ level, only the 5459Å line (J = 3 to J = 3 transition) has an experimental value approaching the theoretical and then it is nearest to the LS value. On the whole, the agreement here is poor. The values of σ^2 are very much smaller for higher energy levels and therefore subject to a greater uncertainty and, since the line strengths are also much smaller, they must be subject to configuration interaction. Consequently the lack of agreement at high energy levels is not surprising.

4d-4p T.P. ($\times 10^{-8}$ sec^{-1})

J_{UPPER}	(Å)	PDJ	P & S (ref.18)	G (ref.15)	LS	IC	J_{Lj}
2	7484	0.035				0.12	0.076
3	7425	0.028			0.13	0.13	0.13
2	7412	0.046				0.0035	
4	7372	0.22			0.19	0.19	0.19
2	6960	0.036				0.0004	
2	6951	0.024			0.031	0.017	
0	6937	0.38			0.13	0.16	0.039
2	6879	0.023			0.0064	0.0022	
1	6871	0.43	0.40		0.13	0.15	0.0052
2	6752	0.32	0.29		0.14	0.11	0.16
2	6664	0.023			0.032	0.0021	
2	6604	0.053			0.0009	0.0003	
3	6538	0.017				0.0027	
2	6059	0.034		0.038			
2	6052	0.029		0.025		0.0051	
1	5912	0.090				0.0008	

FIG. 7.23. Transition probabilities

5d-4p TRANSITION PROBABILITIES (x 10^{-8} sec^{-1})

J_{UPPER}	(Å)	PDJ	(ref. G15)	LS	IC	J_{1j}
1	6827	0.047			0.0041	
2	6756	0.051			0.010	
1	6719	0.040		0.019	0.0049	0.0076
1	6466	0.021		0.092	0.069	0.077
1	6369	0.065		0.028	0.025	0.014
0	6364	0.066		0.0044	0.022	0.013
2	6307	0.050		0.051	0.065	0.058
2	6276	0.074			0.0008	0.004
2	6248	0.0060		0.00005	0.0046	
2	6215	0.060			0.028	0.037
3	6212	0.041		0.13	0.12	0.14
2	6173	0.060			0.10	0.074
2	6165	0.015			0.022	0.025
2	6155	0.024			0.20	0.21
3	6145	0.070		0.25	0.24	0.25
3	6043	0.12		0.17	0.15	0.16
4	6032	0.016	0.21	0.18	0.18	0.18
2	6013	0.015		0.0045	0.0093	0.0038
2	5999	0.027			0.062	0.080
3	5987	0.023		0.022	0.034	0.026
2	5834	0.052			0.0026	
2	5739	0.10		0.012	0.0039	
0	6560	0.27	0.19	0.13	0.16	0.0382
1	5606	0.17	0.15	0.13	0.15	0.0052
2	5588	0.017		0.056	0.0029	
2	5151	0.046			0.029	

FIG. 7.24. Transition probabilities 5d - 4p

6s - 4p (fig. 7.21)

One other experimental value for the 7030Å J = 2 to J = 3 line is available for comparison. The measured value lies 30% below that of Popenoe and Shumaker (ref. 18) whose value agrees well with the theoretical value. For this array there is reasonable agreement between experiment and intermediate coupling, only for four lines is agreement with one of the other coupling schemes better.

7s - 4p (fig. 7.22)

No experimental values are available for comparison. Again for the J = 2 to J = 3, 5888Å line, agreement is good between experiment and theory. For this array also, the experimental values agree reasonable well with the calculated IC values.

4p - 4s (fig. 7.23)

Apart from the 6677Å transition, agreement between the experimental values and the intermediate coupling values is very good. All the lines measured are either forbidden or have negligible J_{ij} values and only two have values in LS coupling; however, the lines have substantial experimental values, thus the importance of intermediate coupling is clearly demonstrated.

The good agreement between experimental and intermediate coupling values is due to the lack of configuration interaction and the large values of σ^2 and the line strengths.

Apart from the discrepancy of an order of magnitude with Olsen's value (ref. 24) for the 7272Å line (the IC value agrees with this experiment) the results agree within the limits of error with other experimental values. (Olsen's value for the 7272Å line was divided by 10 when used in the relative intensity temperature determination).

LINE PAIR gA VALUES

J_{UPPER}	(Å)	Transition	PDJ	Dr (ref.16)	LS	IC	J_{Lj}	Theoret. gA.
3	7353	4d-4p	0.785		(0.17	0.16	0.16)	1.2
2	7353	6s-4p			(0.005	0.021	0.14)	
2	5942	7s-4p	0.18		(0.029	0.034	0.059)	0.19
1	5940	72-4p			(0.027	0.0062	)	
1	4191	59-4s	0.197		(0.13	0.14	0.16)	0.80
2	4190	59-4s			(	0.076	0.13)	
1	4045	5p-4s	0.146	0.037	(0.072	0.024	)	0.36
2	4044	5p-4s			(0.022	0.058	)	

FIG. 7. 26. $_{g}A$ Values.

5p - 4s (fig. 7.24)

Because of the smaller value of σ^2, the smaller line strengths and configuration interaction beginning to occur, the calculated intermediate coupling values are not in as good agreement with experiment as the 4p - 4s array. The experimental values of Popenoe and Shumaker again seem to be at least 50% greater than those measured here. For the 4259Å line there is excellent agreement with both Olsen's and the theoretical (LS, IC, and J_{1j}) values, Popenoe and Shumaker's value being 70% greater. Good agreement is found with Gericke's values (which Popenoe and Shumaker state must be increased by 35% - because of a difference between the argon II transition probability value he used for his diagnostics and that measured by Popenoe and Shumaker). Although the values here appear to be on the low side compared to other experimenters, Olsen's values (unfortunately only three are available for comparison) are even smaller.

6p - 4s (fig. 7.25)

Only theoretical values are available for comparison again and the agreement with these is poor. This is understandable in view of the very small value of σ^2, (1/600 that for the 4p - 4s array) and the possible interaction with the 5F configuration. Again intermediate coupling is a better approximation than either LS or J_{1j} coupling but even so, it is a poor approximation.

Pairs (fig. 7.26)

The total intermediate coupling value of gA is compared with the measured gA and in the first two cases agreement is quite good. In the last case, if all the contribution to the

total gA comes from the 4044Å line then reasonable agreement is obtained with Drawin's (ref. 16) measured value. Since the gA value is used in relative intensity methods for temperature determinations, it is hoped that these lines need not be excluded from such methods but used, and measured as pairs.

Conclusion

The values of the experimentally determined transition probabilities, although not intended as accurate absolute values, agree extremely well where comparison is possible with existing values, and it is therefore expected that the values for which no comparison can be made are equally accurate (to within 30%) and will provide a useful and comprehensive range of values.

It is interesting to note the good agreement with Olsen's transition probabilities values, although there is disagreement with his value of 2.5x for the absolute continuum intensity correction factor (cf. Chapter 2 and Chapter 6). The temperature quoted by Olsen (ref. 4) for the arc used in the experiment in which he determined an absolute continuum intensity correction factor of 5 was later shown to be erroneously measured and a revised temperature quoted (ref. 18). Using this revised temperature he remeasured the absolute continuum intensity, obtaining a correction factor of 2.5, and measured the transition probabilities quoted here. However, the correction to the temperature, although having a marked effect on the transition probabilities, was quite small and certainly would not account for the difference in the quoted continuum correction factor. Thus it is possible to reconcile the agreement with his first continuum factor with the agreement with his transition probabilities derived from a revised temperature.

Only for low lying states are the values of intermediate coupling transition probabilities in good agreement with experiment. For highly excited transitions, a more detailed

theory which takes into account configuration interaction perturbations is needed. It is hoped that these calculated values, the first made for six out of the eight arrays, will spotlight the difficulties and encourage further work.

CHAPTER 8

Discussion of errors in the experimental transition probabilities.

Introduction

In order to assess the accuracy of the transition probabilities and their values compared with those published by other authors, an investigation must be made into the possible errors involved in the experiment and the effects on the final value .

Discussion of transition probability accuracy with respect to:-

Stability of the Discharge

A reproducibility test had already been performed on the r-f discharge and it was found that the light intensity was reproducible to two per cent while the temperature profile was reproducible within the errors of the relative line intensity method. The variation in emitted intensity could be due to a difference in size of the discharge from day to day due to a slightly different argon gas flow rate. Since all the measurements made on any particular spectral line, e.g. intensity profile across the discharge, total intensity, etc., were made without switching off the discharge, actual fluctuations in intensity during a measurement would not only be small, but averaged out owing to the integrating effect of the electronic recording system.

The power fed to the discharge was constant over as much as an hour's continuous operation. The R-F coil and oscillator valves soon reach a steady state temperature, about one minute after switching on the power, consequently after an initial slight drop in current fed to the discharge, the operating parameters of the generator became constant.

The pressure in the discharge was assumed to be one atmosphere; however, a slight overpressure is bound to be present to cause the gas to flow. . . . Since the tube had a diameter of two inches and there were no flow distortions (venturi or nozzles), near the discharge itself the over pressure would be negligible. The effect of magnetic self-compression due to the current flowing in the discharge was balanced in the steady state by an increase in the gas pressure. This effect and the momentum transfer effect which accompanies heat conduction and is also balanced by a pressure gradient, give over-pressures of about 10^{-2} dyne/cm^2 and 10^{-3} dyn/cm^2, i.e. negligible.

Thus the main contribution to errors from the discharge itself relate to its reproducibility and this at the outside could have given a two per cent error in the intensity measurements and hence transition probabilities.

8.3 Optical Arrangement

Possible errors caused by the assymetrical refraction and absorption of the discharge tube walls have already been accounted for. The scanning device was positioned to better than 0.1 mm. across the discharge and errors caused by observing different regions of the discharge through mispositioning would be smoothed out in the folding and Abel-inversion process.

Local differences in optical refractivity in the discharge due to free electrons, ground state atoms and at the peak of the observed lines could affect the intensity profiles and lead to errors in both the temperature measurement and the transition

probability measurements. However, using the equations given by Griem (ref. 25) these effects were all shown to be negligible, $n - 1 \sim 10^{-3}$, for all contributions to the refractive index.

No emission lines were measured which had any measurable optical depth. The 7635Å and 7514Å lines were both shown theoretically and experimentally to suffer from self-absorption in the discharge. The only other line which had any calculable self absorption was the 6965Å line and the calculated effect on this line was to reduce its measured emission intensity in the centre of the discharge by 4.5 per cent.

8.4 Detecting System

Since photomultiplier currents were kept to about 10^{-9} amps or less, no fatigue effects should have been present to have caused a non-linearity of response. As with the temperature measurements a pea-bulb was kept lighted in the spectrograph in between measurements so that the photocathode was under a constant low level of illumination. The reproducibility tests that were carried out determined the reproducibility not of the discharge alone but of the whole recording system as well, i.e. a few per cent from day to day.

8.5 Calibration

This is where the largest overall errors are likely to be

encountered. Although precautions were taken so that the complete optical, detecting and recording system accepted the same solid angle from the tungsten ribbon lamp as from the discharge, with all the mirrors at the same angle, the temperature of the ribbon itself was subject to a possible error of calibration. The emissivity curves of De Vos (ref. 63) themselves are subject to a 2% error and the ammeter used to determine the current through the lamp, although calibrated, could only be set to 1% or 0.05 amp - this would correspond to a difference of the order of 5°K which, at 2500°K, the operating temperature of the lamp, corresponded to a 3% difference in emissivity. Thus the combined uncertainties of calibration could be of the order of 4%. This would be directly reflected in the transition probability determination. The calibration error could also have affected the temperature determination as an error in the absolute emission intensity calibration.

This would lead to a 1.5% temperature error, which would reflect as a 1.5% inaccuracy of the relative transition probabilities and as much as 25% inaccuracy in the absolute values. However, this inaccuracy is already accounted for in the quoted inaccuracy of the temperature determination

8.6 Treatment of Data

The correction for the amount of light from a given spectral line lying outside the detector slit is itself a source of error. The maximum correction applied was of the order of 40% although three-quarters of the lines needed no correction (except that for

absorption by the quartz discharge tube). The line profiles were scanned by the detector using a narrow entrance slit and since the dispersion was known to about 1%, the amount of profile which lay outside the integrating slit was easily estimated. This was done by tracing the profile from the recorder chart onto mm. graph paper and measuring the ratio of area enclosed by the slit to that lying outside the slit. This process entailed a slight loss of accuracy but this, being only of the order of 1% at the most was negligible compared to the calibration error. The detector was set on the line peak each time by observing the signal recorded on the chart and setting the detector at the maximum output position. Serious errors could have been incurred in the determination of the corrections for lines lying close together, e.g. 6215Å and 6212Å, both of which were broadened to such an extent that their wings overlapped. Errors of 10% in the correction could easily have been incurred here through not setting the detector when integrating the line, in the position at which the correction was calculated. However, as the correction to the total emission was only of the order of 25% this involved a total error of only 2.5% in the final value.

The process of Abel inversion, since a digital method was used, must have incurred some error. The co-ordinates of a circle were fed into the Abel inversion programme as a check on its accuracy; the output reproduced a straight line to 0.5%. However, errors were bound to be incurred in the process of curve fitting and smoothing the intensity profiles for Abel inversion.

Since, after correction for the quartz tube refraction effects, the line intensity profiles across the discharge in one or two cases showed an assymmetry of 5%, i.e. maximum percentage difference in the integrated intensity profile from one side of the discharge to the other, a possible error of 2.5% could be present here.

8.7 Temperature Error

Now the estimated error of the temperature determination was about 2%. This meant that the relative values of transition probabilities had an accuracy of:-

$$2 \times \frac{W_1 - W_2}{kT} \%$$

with respect to each other, for lines of excitation energy W_1 and W_2.

However, absolute transition probability values have an error

$$2 \times \frac{W}{kT} \%$$

which is considerably greater and varies from 34% to 40% depending on the upper energy level W.

Thus, this error, in the case of the absolute values completely swamps all the above errors, whereas, for the relative values, the error must be calculated by the user for any ratio of lines used.

8.8 Conclusion

These transition probability results are reasonably accurate for use in relative measurements such as the relative line intensity method for determining temperature since a complete 'spectrum' of values has been obtained. Previous authors have tended to confine themselves to one transition array only and any relative line intensity method must, for accuracy, involve an energy spread of upper levels at least equal to the discharge temperature in eV. For example, to accurately measure a temperature of approximately 1eV , the lines used in a relative line intensity measurement should have an energy spread of at least 8,000 wave numbers, i.e. cover at least two transition arrays. It is hoped that this set of transition probabilities, by being the most comprehensive, will facilitate such measurement.

By altering the load matching of the generator and operating it at higher power levels, the discharge can be operated in oxygen or nitrogen. Consequently, transition probabilities in these gasses, which are not very well documented at present could be obtained in a similar manner.

During the course of the preliminary work on the discharge, it was found that at pressures of the order of 1 mm. a glow discharge could be produced in an enclosed quartz tube, which, on increasing the power to the R-F coil suddenly transformed to a bright discharge similar to the atmospheric pressure discharge. This 'glow-to-arc' transition was accompanied by a sudden increase in current drawn from the generator and suggested that the discharge formed was of an 'arc' nature and possibly in a near thermal equilibrium state. Difficulties were encountered in trying to stabilise the discharge within the quartz tube since no containing gas flows were possible at this pressure and consequently the discharge soon attacked the walls of the quartz vessel and damaged them. If a means of controlling this discharge could be found, it would be extremely suitable for measuring transition probabilities of gasses such as neon, krypton and zenon, which are too expensive to be used in the atmospheric pressure flowing gas discharge.

It is therefore suggested that future work could be carried out on stabilising and diagnosing this low pressure "plasmoid" with a view to further transition probability measurements.

During the course of the work described here, measurements of the temperature of a similar R-F discharge in argon at atmospheric pressure were made by Hughes and Wooding (ref. 64). Their results agree

extremely well with those reported here. Work on an R-F discharge has also been reported by Pettit (ref. 65) who maintained that there was no central dip in the radial temperature profile and that the effect observed was due to "defocussing" of the outer edges of the discharge when making a scan of line intensity distribution across the discharge. Pettit used an optical system with an f2 aperture and, no doubt, ran into serious difficulties of interpretation since the process of Abel inversion assumes that parallel slabs of discharge are being observed. Thus he has probably overcorrected for a poor optical arrangement. Since the central drop in temperature is of the order of 200^{o}K, this means that there should, when viewed end on, be an easily detectable drop in luminosity ($\sim$30%) in the centre of the discharge. This effect has been observed on a film taken looking down an R-F atmospheric pressure discharge. (Hughes private communication).

From considerations of the skin-depth nature of the R-F heating, (using the formula of Spitzer (ref. 66) a skin depth in argon of 1 cm. isobtained) it would seem likely that the centre region of the discharge was field-free and the heating in this region purely through diffusion.

8.9 Acknowledgements

To the following the author is indebted for valuable assistance. To Professor W.R.S. Garton for his supervision, help, and guidance at all times throughout this work; to Drs. D.D. Burgess and R.C.M. Learner for useful discussions on the techniques used in determining the discharge characteristics; to Mr. S.E. Budd for his help with the theoretical transition probability calculations; to Mr. D.S. Widmer for assistance in carrying out the preliminary work on the discharge; and to all members of the Spectroscopy Group for their help.

Thanks are also due to Dr. D.E. Roberts for his partnership in the joint project of determining the electron density in the discharge.

None of this work would have been possible without a grant awarded by the D.S.I.R. and later the S.R.C. throughout the three years of this work.

Thanks are also due to the Central Research Fund who bought the R-F Generator.

Appendix 1

Error analysis of reversal method

The measurements made are J_f, the intensity of the flash tube as determined by the monitoring photomultiplier, J_T, the total intensity measured at the line centre due to the line emission and the flash tube intensity attenuated by absorption, and J_p, the absolute line intensity.

The transmission of the plasma, $w_\nu(x)$ at a given position x, is given by

$$w_\nu(x) = \frac{J_T - J_p}{J_f}$$

Since the measurements of the absorbed intensity were taken from the oscilloscope traces, the base line from which the peak height of each trace was measured was the deflection corresponding to J_p. Hence the value of $w_\nu(x)$ measured, is given by

$$w_\nu(x) = \frac{J_{T(x)}}{J_f}$$

Therefore the error in $w_\nu(x)$ due to inaccuracies in measuring the oscilloscope traces and the inaccuracies caused by shot noise is

$$\frac{dw_\nu(x)}{w_\nu(x)} = \frac{dJ_{T(x)}}{J_{T(x)}} \quad \frac{-dJr}{Jf}$$

Now $$k_\nu(r) = \frac{1}{\pi r} \quad \frac{d}{dr} \int_r^R \log_e w_\nu(x) \quad \frac{x}{\sqrt{x^2 - r^2}}\, dx$$

To be able to make a simple error analysis, spatial homogeneity will be assumed from here on, and an additional error introduced later to account for inaccuracies in converting observed profiles into radial profiles by the Abel inversion technique.

i.e. $$k_\nu = \log_e \frac{1}{w_\nu}$$

Therefore the error in the computed value of K_ν due to an error in w_ν is given by

$$\frac{dk}{k_\nu} = \frac{dw}{w_\nu \log w_\nu}$$

Now the first approximation to the emission coefficient j_ν determined from the absolute measurement of Jp the line intensity, is given by $j_{\nu_0} = I_\nu$ where I_ν is the value of Jp put on to an absolute scale, inhomogeneity has been again ignored.

i.e. the error in j_ν , dj_ν is given by

$$\frac{dj_\nu}{j_\nu} = \frac{dI_\nu}{I_\nu} \frac{-1}{2} \frac{dw_\nu}{w_\nu}$$

In the second approximation to the emission coefficient, the correction to the first is given by

$$j_{\nu_1} = j_{\nu_0} (1 - \text{Cosh } G) \doteq j_{\nu_0} \frac{G^2}{2}$$

where G is directly related to k_ν and Cosh $G \doteq 1 - G^2/2$

Thus the error in the correction is approximately equal to twice the error in j_{ν_0}, however, as j_{ν_1} is only a few per cent of j_{ν_0} in this case, this error is completely negligible.

Now the Planck function is given by the ratio $\frac{j_\nu}{k_\nu}$, so the error in this will be

$$\frac{dP}{P} = \sqrt{\left(\frac{dI_\nu}{I_\nu}\right)^2 + \left(\frac{1}{2}\frac{dw_\nu}{w_\nu}\right)^2 + \left(\frac{dw_\nu}{w_\nu \log w_\nu}\right)^2}$$

However this does not yet give us the temperature error, we have yet to differentiate the Planck function to find the error in T due to these measurement errors.

Now $P = \dfrac{c_1}{\lambda^5(\exp(c_2/\lambda T) - 1)}$ where c_1 & c_2 are constants.

so $\frac{dP}{P} = \frac{C_2}{\lambda T} \frac{\exp(C_2/\lambda T)}{(\exp(C_2/\lambda T)-1)} \frac{dT}{T}$

at 9000°K, $\frac{dP}{P} = 2.4 \frac{dT}{T}$

Therefore $\frac{dT}{T} = \frac{1}{2.4}\sqrt{\left(\frac{dI_\nu}{I_\nu}\right)^2 + \left(\frac{1}{2}\frac{dw_\nu}{w_\nu}\right)^2 + \left(\frac{dw_\nu}{w_\nu \log w_\nu}\right)^2}$

Now, accounting for the spatial inhomogeneity, two principal Abel inversions are made, in determining j_ν and in determining k_ν. Hence we can add two error terms of $\frac{dA}{A}$ onto the above expression to account for errors made in the drawing of smooth curves through the obseÿved profiles and for the errors made in the process of inversion.

i.e. $dT/T = \frac{1/2.4\sqrt{(dI_\nu/I_\nu)^2 + (1\ dw_\nu/2\ w_\nu)^2}}{+(dw_\nu/w_\nu \log \frac{1}{w_\nu})^2 + (2dA/A)^2}$

If we take all the measurements to be of 2% accuracy and an inversion accuracy of 2% this gives, for a value of $w_\nu = .65$,

$dT/T = \frac{1/2.4\sqrt{(dI_\nu/I_\nu)^2 + ((dJ_r/2J_T)^2 + (dJ_f/Jf)^2)}}{\times(1 + 4/(\log^1/w_\nu)) + (2dA/A)^2}$

i.e. $\frac{dT}{T} \doteq 3\%$.

Appendix 2

Error analysis of Hβ method

Basically this method involves the solution of a composite Saha's equation with an assumption of pressure balance and, besides the measured electron density, a value of the local concentration ratio of argon and hydrogen.

$N_{e\ TOTAL}$ is measured and $= N_{eH} + N_{eA}$

i.e. $$N_{e\ TOTAL} = \sqrt{N_{oH} K \frac{U_{iH}(T)}{U_{oH}(T)}}\ T^{\frac{3}{4}} \exp(-W_{iH}/2kT) + \sqrt{N_{oH} LK \frac{U_{iA}(T)}{U_{oA}(T)}}$$

$$\times \exp((-W_{iA} + \Delta W_{iA})/2kT)\ T^{\frac{3}{4}}$$

where $K = 2\left(\frac{2\pi mk}{h^3}\right)^{3/2}$

and $L = \frac{N_{OA}}{N_{OM}}$ the ratio of the ground states, and, at these temperatures and pressures, the total neutral density.

ΔW_{iH} and ΔW_{iA} are the ionisation level depressions.

Now, since at the peak temperature of the discharge, the Saha equations for argon and hydrogen have similar values of $\frac{N_e N_i}{N_o}$

and assuming that hydrogen is being added to the discharge in small quantity only, we need only consider for the purposes of this analysis the electrons contributed from argon,

i.e. $$\frac{dne}{n_e} = \frac{1}{2}\frac{dn_{OA}}{n_{OA}} + \frac{dT}{T}\left[\frac{3}{4} \frac{(w_i - \Delta W_i)_A}{kT}\right]$$

There is the additional error in the choice of ΔW_i to be considered; the following values have been calculated according to the different theories proposed, assuming $T \simeq 9000^{\circ}K$ and $n_e = 4 \times 10^{15}$ e/cc.

Debye-Hückel	gives	0.019 eV
Unsöld	gives	0.111 eV
Ecker-Weizel	gives	0.122 eV
Brummer	gives	0.207 eV

Now the ionisation potential of argon is 15.755 eV so the variety of choice, less than 2% of the ionisation potential would cause an equal error in the value of T determined.

i.e. $$dT = 2 \sqrt{\frac{(dn_e/n_e)^2 + (dn_{oA}/2n_{oA})^2}{(3/4 + (W_i - \Delta W_i)_A/kT)}}$$

Thus $\frac{dT}{T}$ = 2.5% assuming a 5% error has been made in the assumption of pressure balance.

This method is therefore comparable in accuracy to the reversal method.

Appendix 3

Error analysis of slit width criteria in the reversal method

Because of the finite resolution of the dispersive system used in the reversal method, the transmission of the spectral line to the flash tube was not measured at a precise frequency, but integrated over the spectral slit width.

The transmission of the discharge at a frequency and a position x from the axis of symmetry is given by

$$w_\nu(x) = \exp\left[-2\int_x^R \frac{k_\nu(r)p(r)\ r\,dr}{\sqrt{r^2 - x^2}} \right] \qquad (1)$$

where $k_\nu(r)p(r)$ is the volume absorption coefficient and R the discharge radius.

On taking logarithms of both sides of this equation, it can be put into the form of an Abel integral equation giving the absorption coefficient.

$$\text{i.e. } k_\nu(r)p(r) = \frac{-1}{\pi r}\frac{d}{dr}\int_r^R \left[\log\frac{1}{w_\nu(x)}\right]\frac{x\ dr}{\sqrt{x^2 - r^2}} \qquad (2)$$

However, the quantity measured is not w_ν at a precise frequency, say w_{ν_0} but

$$\frac{1}{\Delta\nu}\int_{-\frac{\Delta\nu}{2}}^{\frac{\Delta\nu}{2}} w_\nu(x)\ d\nu$$

where $\Delta\nu$ is the spectral slit width over which the transmission is integrated.

Equation 2 is valid if it can be written

$$\frac{1}{\Delta\nu}\int_{-\frac{\Delta\nu}{2}}^{\frac{\Delta\nu}{2}} k_\nu(r)p(r)dr = \frac{-1}{\pi r}\frac{d}{dr}\int_r^R \left[\log\left(\frac{1}{\Delta\nu}\int_{-\frac{\Delta\nu}{2}}^{\frac{\Delta\nu}{2}} w_\nu(x)d\nu\right)^{-1}\right]\frac{x}{(x^2-r^2)^{1/2}}dx \qquad (3)$$

The left hand side of this equation is the quantity deduced in all absorption experiments, not $k_\nu(r)p(r)$ at the line centre. However, the emission coefficient $j_\nu(r)p(r)$ is also measured as

$$\frac{1}{\Delta\nu}\int_{-\frac{\Delta\nu}{2}}^{\frac{\Delta\nu}{2}} j_\nu(r)p(r)d\nu$$

and since the frequency dependence of the emission and absorption coefficients is identical the ratio of the two canoels out the frequency dependence.

To be able to write equation 3 requires that

$$\frac{1}{\Delta\nu}\int_{-\frac{\Delta\nu}{2}}^{\frac{\Delta\nu}{2}} \log\frac{1}{w_\nu(x)}\,d\nu = \log\left[\frac{1}{\Delta\nu}\int_{-\frac{\Delta\nu}{2}}^{\frac{\Delta\nu}{2}} w_\nu(x)d\nu\right]^{-1}$$

Consequently the fraotional error in $k_\nu(r)p(r)$ due to a finite spectral slit width will be

$$\frac{\frac{1}{\Delta\nu}\int_{-\frac{\Delta\nu}{2}}^{\frac{\Delta\nu}{2}} \log\frac{1}{w_\nu(x)}\,d\nu - \log\left[\frac{1}{\Delta\nu}\int_{-\frac{\Delta\nu}{2}}^{\frac{\Delta\nu}{2}} w_\nu(x)d\nu\right]^{-1}}{\frac{1}{\Delta\nu}\int_{-\Delta\nu/2}^{\Delta\nu/2} \log\frac{1}{w_\nu(x)}\,d\nu}$$

$$= 1 - \frac{\log\frac{1}{\Delta\nu}\int_{-\frac{\Delta\nu}{2}}^{\frac{\Delta\nu}{2}} w_\nu(x)d\nu}{\frac{1}{\Delta\nu}\int_{-\frac{\Delta\nu}{2}}^{\frac{\Delta\nu}{2}} \log w_\nu(x)d\nu} \qquad (4)$$

Since the spatial inhomogeneity plays no part in this error treatment the functional dependence on position will be emitted for clarity.

Now $w_\nu = \exp\left[-k_\nu \right]$ (5)

where for a Gaussian absorption profile

$$k_\nu = k_o' \exp\left[\frac{-2(\nu - \nu_o)\sqrt{\log 2}}{\Delta\nu_D} \right]^2 \quad (6)$$

and for a dispersive profile

$$k_\nu = k_o \left[1 + (2(\nu - \nu_o)/\Delta\nu_s)^2 \right]^{-1} \quad (7)$$

where $\Delta\nu_D$ and $\Delta\nu_s$ are the appropriate half-widths of the profiles. Equation (4) can now be solved by expanding the logarithm in the numerator using the expansion

$$\log y = \sum_{n=1}^{\infty} \frac{(-1)^{n+1}(y-1)^n}{n} \quad \text{where } 0 < y < 2$$

since $0 < \frac{1}{\Delta\nu} \int_{\Delta\nu/2}^{w} d\nu < 1$

On expanding w_ν and integrating, the following expressions for the error are obtained:-

For the Gaussian profile where $x = \frac{\Delta\nu}{\Delta\nu_D}$

Error is

$$1 + \frac{1}{\operatorname{erf} \frac{x}{\sqrt{2}}} \sum_{n=1}^{\infty} \frac{(-1)^{n+1}}{n} \left[\frac{k_o}{2x}\sqrt{\frac{\pi}{\log 2}} \right]^n - 1 \left[\sum_{m=1}^{\infty} \frac{(-1)^m}{m!} \frac{k_o^{m-1}}{\sqrt{m}} \operatorname{erf} \frac{x}{\sqrt{2}} \sqrt{\log 2x2m} \right]^n$$

and for the dispersive profile where $x = \frac{\Delta\nu}{\Delta\nu_s}$

Error is

$$1 + \frac{1}{\operatorname{Tan}^{-1} x} \sum_{n=1}^{\infty} \frac{(-1)^{n+1}}{n} \left[\frac{k_o}{2x} \right]^n - 1 \left[\sum_{m=1}^{\infty} \frac{(-1)^m}{m!} (k_o)^{m-1} \beta \left\{ \frac{x^2}{1+x^2} \left(\tfrac{1}{2}, m - \tfrac{1}{2} \right) \right\} \right]^n$$

where $\beta\ (x^2/(1+x^2))(\frac{1}{2}, m - \frac{1}{2})$ is an incomplete beta function. (ref. 76).

For a value of k_o, the absorption coefficient at the line peak, of 0.43 (the value obtained in the experiment described here), the two error curves are plotted in figure 1, where it can be seen that, in this case a spectral slit width less than the line half-width will not cause any significant error.

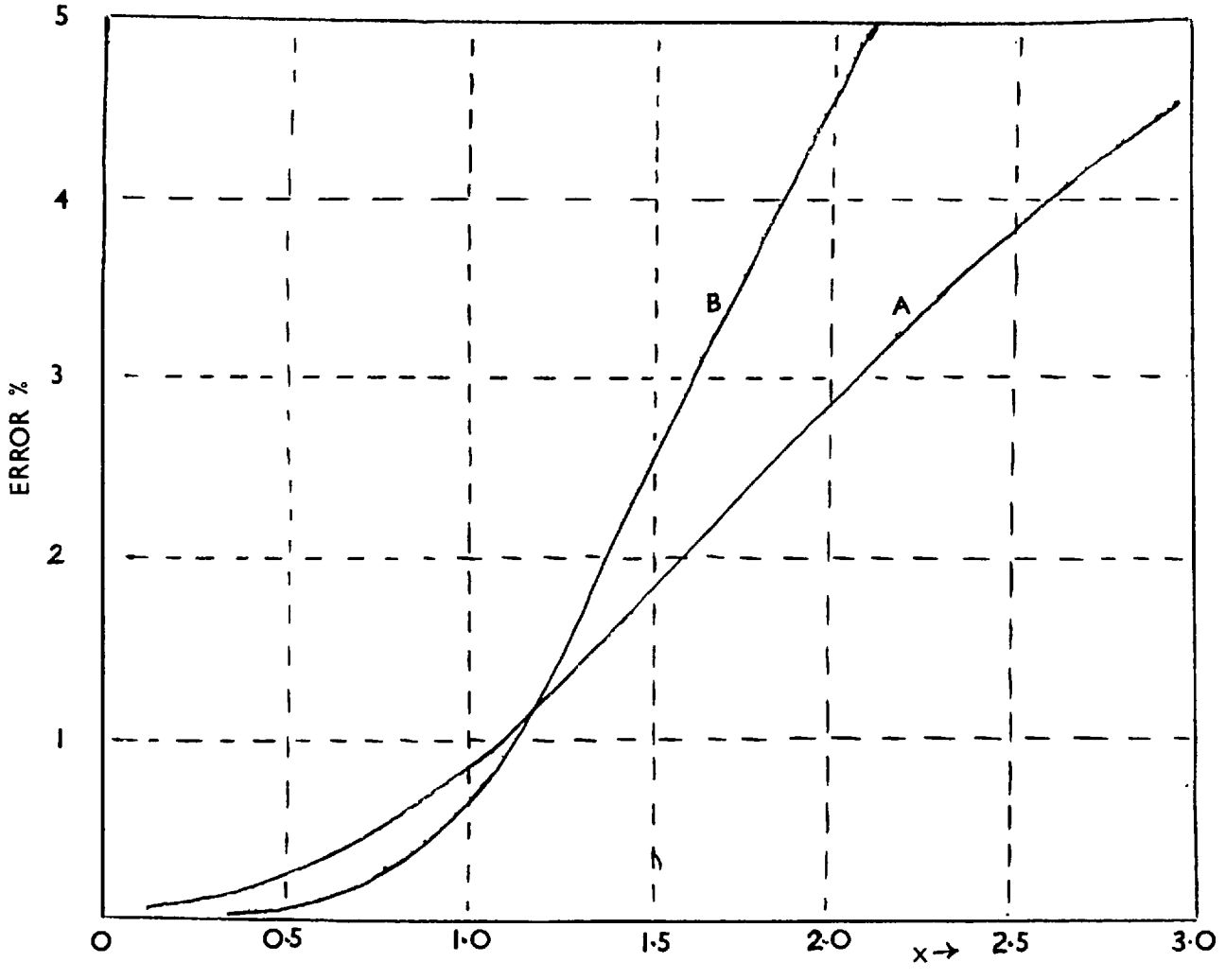

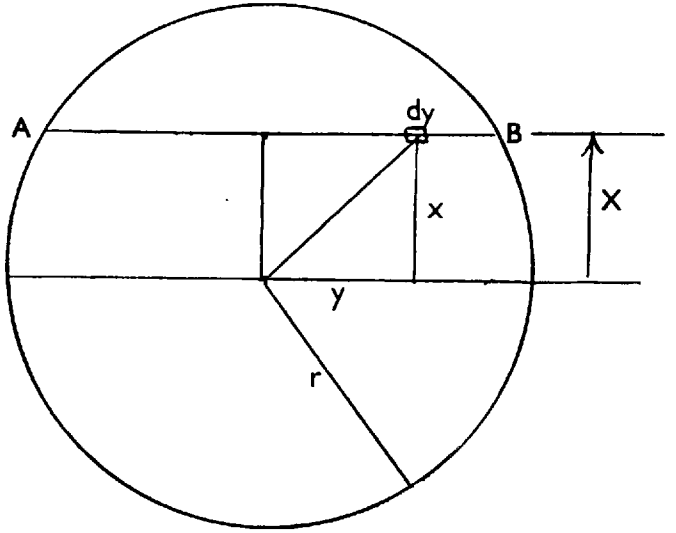

INTEGRATION IS MADE ALONG LINE OF SIGHT A — B

FIG 1&2. PERCENTAGE ERROR PLOTTED AGAINST X, THE RATIO OF OF SPECTRAL SLIT WIDTH TO LINE WIDTH.
A DISPERSIVE PROFILE.
B GAUSSIAN " .

Appendix 4

Simplification of the reiteration in the reversal method

Because of self-absorption the measured intensity of the 7635Å line does not give the true emission coefficient. As explained in chapter 5, the correction to the emission coefficient obtained in a first approximation, is calculated by an iterative process. In this case, the first correction contributes only a few per cent so that the second correction is entirely negligible. Consequently instead of using a numerical method of solution which involves a long complicated IBM 7090 programme involving magnetic disc storage (Elder Jerrick and Birkeland, private communication), the first calculation can be calculated analytically to a reasonable accuracy. Since the correction is only of the order of a few per cent, large inaccuracies in the correction (25-50%) could be tolerated; however this analytic method is accurate to several per cent.

Now the emission coefficient is written as

$$j_\nu(r) = j_{\nu_0}(r) + j_{\nu_1}(r) + j_{\nu_2}(r) + \ldots \quad (1)$$

where $$2\int_x^R j_{\nu_0}(r)\,\frac{dr}{r^2}\frac{}{x^2} = \frac{I_\nu(x)}{\sqrt{w_\nu(x)}} \quad (2)$$

$\rho(r)$ has been omitted since it plays no part in this analysis, in fact it has been absorbed into $j_\nu(r)$.

Now $$\int_x^R j_{\nu_1}(r)\,\frac{r}{\sqrt{r^2 - x^2}}\,dr = -\int_x^R j_{\nu_0}(r)\left\{1 - \text{Cosh } G_\nu(xr)\right\}\frac{r}{(r^2 - x^2)^{1/2}}\,dr \quad (3)$$

Now $\text{Cosh } G(xr) \underset{r}{\doteq} 1 - \frac{G^2_\nu(xr)}{2}$ (to 1% for transmissions $\geqslant$ 20%).

$$G(xr) = \int_x \frac{k(r)dr}{r^2 - x^2} \quad (4)$$

By fitting a polynominal in r to $k_\nu(r)$ and $j_{\nu_o}(r)$, which have already been obtained by Abel inversions of observed quantities, the RHS of equation 3 can be solved for values of from 1 to 25 (R = 25) to give 25 numbers which can then be Abel inverted to give $j_{\nu_1}(r)$.

If we let $k_\nu(r) = a + br^2 + cr^4$

then $G_\nu(xr) = \int_x^r \frac{(a + br^2 + cr^4)r\,dr}{\sqrt{r^2 - x^2}}$

$$= \sqrt{r^2 - x^2}\left[a + \frac{b(r^2 + 2x^2)}{3} + c\left\{\frac{(r^2 - x^2)^2}{5} + \frac{2}{3}x^2(r^2 - x^2) + x^4\right\}\right]$$

$$\left[\frac{G_\nu(xr)}{2}\right]^2 = \frac{(r^2 - x^2)}{2}\left\{r^8\left(\frac{c^2}{25}\right) + r^6x^2\left(\frac{8c^2}{125}\right) + r^6\left(\frac{2bc}{15}\right) + r^4\left(\frac{b^2}{9} + \frac{2ac}{5}\right)\right.$$

$$+ r^4x^4\left(\frac{64c^2}{225}\right) + r^2x^6\left(\frac{64c^2}{225}\right) + r^2x^2\left(\frac{4b^2}{9} + \frac{8ac}{15}\right) + x^4r^2\frac{32bc}{45}$$

$$+ r^4x^2\left(\frac{4bc}{9}\right) + r^2\left(\frac{2ab}{3}\right) + x^8\left(\frac{64c^2}{225}\right) + x^6\left(\frac{32bc}{45}\right)$$

$$\left. x^4\left(\frac{4b^2}{9} + \frac{16ac}{15}\right) + \frac{x^2 4ab}{3} + a^2\right\}$$

If we fit a similar polynominal to j_o, i.e.

$$j_c = d + er^2 + fr^4$$

then $$\int_x^R j_o \frac{G_\nu^2(xr)}{2} \frac{r}{\sqrt{r^2 - x^2}}\,dr = \int_x^R \frac{\sqrt{r^2 - x^2}}{2} \times r \times (d + er^2 + fr^4) \times \{\}\,dr$$

where the quantity in curly brackets is the eighteen term bracket above.

If this is now integrated we end up with a 177 term equation in diminishing powers of $(r^2 - x^2)^{n/2}$, where the maximum value of n is 15.

i.e. $$\int_x^R j_o \frac{G_\nu^2(xr)}{2} \frac{r}{\sqrt{r^2 - x}}\,dr = (RL1) \times (RR1) + (RL2) \times (RRZ)$$

$$+ (RL3 \times RR3) \ldots (RL7) \times (RR7)$$

where $RR1 = \frac{(r^2 - x^2)^{15/2}}{15} + \frac{6x^2(r^2 - x^2)^{13/2}}{13} + \frac{5x^4(r^2 - x^2)^{\frac{1}{2}}}{11} \ldots\ldots$

$\ldots\ldots \frac{1}{3} x^{12}(r^2 - x^2)^{3/2}$

$RR2 = \frac{(r^2 - x^2)^{13/2}}{13} + \frac{5x^2(r^2 - x^2)^{11/2}}{11} + \ldots\ldots$

$\ldots\ldots \frac{1}{3} x^{10}(r^2 - x^2)^{3/2}$

$\vdots$

$RR7 = \frac{1}{3}(r^2 - x^2)^{3/2}$

$RL1 = \frac{1}{2} \frac{fc^2}{25}$

$RL2 = \frac{1}{2} \left(\frac{8fc^2x^2}{125} + \frac{2fbc}{15} + \frac{5c^2}{25} \right)$

$\vdots$

etc.

This calculation was performed for integral values of x from 1 to 25 on an IBM 7090 computer. The resulting 25 values when Abel inverted gave the correction jy_1 to be applied to $j\nu_o$ to give the true emission coefficient.

This procedure, while still maintaining an accuracy better than the experimental accuracy, is considerably shorter than that used by Elder Jerrick and Birkeland, their method, involving magnetic disc storage requires several hours of IBM 7090 time; the above calculation takes less than one minute on the same computer.

The polynomial fitting was made in even powers of r only since the profile of the calculated absorption coefficient and first emission coefficients were obtained by folding procedures where the asymmetry of the discharge was averaged out. The polynomial was taken to the 4th power since both the coefficients

showed slight central dips in their profiles, although a 2cnd order polynomial might still be a good approximation. For measurements made in discharges where the absorption and emission is a monatonic function and does not exhibit central dips, and where the transmission is $\gtrsim 50\%$, the above analysis could be simplified without significant loss of accuracy by a parabolic curve fit.

Appendix 5

Abel Inversion Procedure

In side-on observations of any circularly symmetric inhomogeneous discharge, the measurement made is an integration through the discharge down the line of sight. To obtain the true radial profile of the observable across the discharge diameter, the following procedure is required.

Referring to figure 2 the measured observable is, for example in the case of intensity measurements,

$$I(x) = \int_{-\sqrt{R^2 - x^2}}^{\sqrt{R^2 - x^2}} E(r)\, dy$$

where $E(r)$ is the local emission coefficient.

This equation can be written

$$I(x) = 2\int_{x}^{R} \frac{E(r)\, r dr}{\sqrt{r^2 - x^2}}$$

To obtain $E(r)$ an Abel transform is made, i.e.

$$E(r) = \frac{-1}{\pi r} \frac{d}{dr} \int_{r}^{R} \frac{I(x)\, dx}{\sqrt{x^2 - r^2}}$$

Various methods of solving this equation for a set of observables $I(x)$ across the discharge have been proposed. One method is to divide the cross-section of the arc into narrow rings in which $E(r)$ is assumed constant. The contribution from each ring is then summed step by step beginning from the outer edge. Thus from a set of transverse measurements, the true emission of a line or a band of continuum can be obtained by use of a simple computer programme (ref. 67 - 69). Another method is to fit a least squares polynomial to $I(x)$ and solve

the differentio-integral equation analytically.

An analogue computer on-line from the recording instrument, (e.g. a photomultiplier) to automatically record I(x), convert it to E(r), and trace out the resulting profile would be the most convenient and preferable system (ref. 70).

The method used throughout the experiments described in the preceding chapters was the first. Twenty-five measurements were made of each observable across the discharge and then, using Pearce's area parameters (ref. 69) the differentio-integral equation was solved using an Elliott 803 computer. Since it is assumed that the inhomogeneity can be resolved into 25 homogeneous annuli it would be expected that these would be a considerable loss of accuracy; however, when the ordinates of a circle are "Abel inverted" by this procedure, the resulting 25 points of the radial profile deviate by a mean value of 1% from a straight line. This method was therefore considered quite adequate.

REFERENCES

1. Babat G.I. 1947, J.Inst.Elec.Eng. 94, 1.

2. Reed T.B. 1961, J.Appl.Phys., 32, 5.

3. Reed T.B. 1961, J.Appl.Phys., 32, 12.

4. Olsen H.N 1959, Phys. Fluids, 2, 6.

5. Galtier F. 1962, Comptes Rendus. Acad. Sci. 255, 20.

6. Reboux Y. 1963, Ingrs. et Techniciens 166, 109.

7. Marynowski & Monroe C.W. 1963, Int. Symp. on High Temp. Technology, Stanford.

8. Mironer A. & Hushfar F. 1963, Amer. Inst. Aero. and Astro. Elec. Propulsion Conf., Colorado Springs.

9. Clement M. & Consoli T. 1963, 6th Int. Conf. on Ionis. Phenom. in Gases, Paris.

10. Moore C.E. 1949, N.B.S. Circular 467, Vol. I.

11. Steers E.B.M. 1959, PhD. Thesis, University of London.

12. Dymshits B.M. & Koretskii Y.P. 1965, Sov. Phys. Tech. Phys. 9, 9.

13. Unsold A. 1938, Ann. Physik. 33, 607.

14. Olsen H.M. 1963, J.Q.S.R.T. 3, 59.

15. Gericke W.E. 1961, Z.fur Astro. 53, 68.

16. Drawin H.W. 1956, Z. fur Physik. 146, 295.

17. Olsen H.N. 1961, Phys. Rev. 124, 6.

18. Popenoe C.H. & Shumaker J.B., Jnr. 1965, J.Res. N.B.S., 69A, 6.

19. J.I.L.A. Rept. 79, 1966, Proc. of Workshop Conf. on the Lowering of Ionisation Potential, Boulder, Colorado.

21. Unsold, A. Physik der Sternathmospheren, (Springer-Verlag, Ohg Berlin).

22. Ecker G. & Weizel W. 1956, Ann. Physik. 17, 126.

23. Brunner J. 1960, Z.Physik. 159, 288.

24. Olsen H.N. 1963, J.Q.S.R.T. 3, 59.

25. Griem H.R. 1964, Plasma Spectroscopy, (McGraw-Hill Book Co., New York).

26. Roberts D.E. 1967, PhD. Thesis, University of London.

27. Wilson R. 1962, Culham Lab. Paper CLM-p9.

28. Reed T.B. 1962, Int. Sci. & Technology, June.

29. Reed T.B. 1961, J.Appl.Phys.,32,821.

30. Garstang R. & Blerkom J. 1965, J. Opt. Soc. Amer. 55, 9.

31. Doherty L.R. 1961, Thesis University of Michigan.

32. Thorne A.P. & Chamberlain J. 1963, Proc. Phys. Soc. 82, 133.

33. Schon K. 1937, Ann. Physik 5, 28.

34. Kuhn W. 1925, Z. Physik 33, 408.

35. Rozdehstvensky D. 1912, Ann. Physik 39, 307.

36. Rozdhestvensky D. & Penkin N.P. 1960, J. Phys. U.S.S.R. 5, 1941.

37. Ostrovskii Y.I. & Penkin N.P. 1960, Optics & Spectroscopy 9, 371.

38. Lochte-Holtgreven W. 1958, Rep. Prog. Phys. 12, 312.

39. Dickerman P.J. & Alpiner B.P. 1962, J.Q.S.R.T. 2

40. Olsen H.N. 1959, Bull. Amer. Phys. Soc. 5, 121.

41. Razumovskaya L.P. 1963, Optics & Spectroscopy 14, 98.

42. Richter J. 1965, Z. Astrophysik 61.

43. Griem H.R. 1962, Phys. Rev. 128, 997.

44. Bates D.R. & Damgaard A. 1949, Phil. Trans. Roy. Soc. A. 242, 101.

45. McLean E.A. 1962, Temperature, Its Meas. & Control in Sci. & Industry (Reinhold Pub. Co., New York).

46. Robinson D. & Lenn P.D. 1967, Appl. Optics, 6.

47. Garton W.R.S. 1964, Sci. Rept. No. 2, Harvard Coll. Obs.

48. Freeman M.P. & Katz S. 1960, J. Opt. Soc. AM. 50, 8.

49. Elder P., Jerrick T., & Birkeland J.W. 1965, Appl. Optics 4.

50. Weise W.L. & Shumaker J.B. 1961, J. Opt. Soc. Am. 51, 937.

51. Burgess D.D. & Cooper J. 1965, Proc. Phys. Soc. 85.

52. Cooper J. 1965, Some Notes on Optical Thickness of Spectral Lines (Internal Pub. Imperial College, London).

53. Parkinson W.H. & Reeves E.M. 1961, Proc. Roy. Soc. A. 262, 409.

54. Garton W.R.S. 1961, Proc. Vth Int. Conf. on Ionis. Phenomena in Gases, Munick.

55. Wheaton J. 1964, Appl. Optics 3, 11.

56. Dieke G.H. & Crosswhite H.M. 1954, Spectrum of Argon I - Ordnance Project TB 2-0001, J. Hopkins University, Maryland.

57. Brewer L.E. & McGregor W.K. 1963, Proc. VIth Int. Conf. on Ionis. Phenomena in Gases, Paris.

58. Condon E.V. & Shortley G.H. 1963, Theory of Atomic Spectra (Cambridge University Press)

    a) pp. 266.

    b) pp. 197, 268, 269, 298, 299.

    c) pp. 271, 307, 313.

    d) pp. 385.

59. Garstang R.H. 1954, Mon. Not. R. Astr. Soc. 114, 118.

60. Wybourne B.G. 1965, Spectroscopic Properties of Rare Earths (N.Y. Interscience) pp. 85, 86, 89.

61. Rotenburg M., Bevins R., Metropolis N., Wooton J. 1959, The 3-j and 6-j Symbols (Technology Press, M.I.T.).

62. Busz G., & Finkelnburg W., 1954, Z. Physik 139, 212.

63. DeVos J.C. 1954, Physica 20, 690.

64. Hughes D.W. & Wooding E.R., 1967, Phys. Letters 24A 70.

65. Pettitt. M.Sc. Thesis. University of Florida, 1966

66. Spitzer L. 1962, Physics of Ionised Gases, (N.Y. Interscience).

67. Bockasten K. 1961, J. Opt. Soc. Am. 51, 943.

68. Edels H., Hearne K. & Young A. 1962, J. Maths & Phys. 41, 1.

69. Pearce W. 1961, Optical Spectrometric Measurements of High Temperatures (Univ. of Chicago Press).

70. Shumaker J.B. & Yokley C.R. 1964, Appl. Optics 8, 83.

71. Grieg J. 1962, PhD. Thesis, University of London.

72. Cooper J. & Greig J. 1963, J. Sci. Inst. 40.

73. Allen C.W. 1964, Astrophysical Quantities (University of London, Athlone Press).

74. Posener D.W. 1959, Aust. J. Phys. 12, 184.

75. Garton W.R.S. & Rajaratnam A. 1955, Proc. Phys. Soc. A68, 1107.

76. Pearson K. 1934, Tables of the Incomplete Beta Function (London, Biometrika Office, University College).

PROC. PHYS. SOC., 1967, VOL. 92. PRINTED IN GREAT BRITAIN

Calculation of argon I transition probabilities in intermediate coupling

P. D. JOHNSTON†
Physics Department, Imperial College of Science and Technology, London
MS. received 20th July 1967

Abstract. Previous calculations of neutral argon transition probabilities have been extended to higher energy levels. The transformation to intermediate coupling was carried out from the LS and the J_1j coupling schemes. The line strengths were put on an absolute scale using the Coulomb approximation.

1. Introduction

The determination of temperature in light sources such as plasma jets, arcs and shock tubes can be simply made by measuring the relative intensities of spectral lines from the neutral species, since the temperature is inversely proportional to the logarithm of the ratio of the total intensities I of lines arising from different energy levels E_n, provided local thermodynamic equilibrium exists between the levels involved in the transitions. A graph of E_n against $\log(I\lambda/gA_{nm})$, where g is the statistical weight of E_n, and A_{nm} is the transition probability from E_n to a lower level E_m, gives a straight line whose slope is inversely proportional to the temperature. Lack of local thermodynamic equilibrium would be apparent by a deviation of the graph from a straight line.

Theoretical transition probabilities in neutral argon have been calculated for the two principal transitions, 5p → 4s and 4p → 4s in LS, J_1j and intermediate coupling (Garstang and Van Blerkom 1965). Experimental measurements have also been made for these arrays (Doherty 1961, Drawin 1956, Gericke 1961, Olsen 1963, Thorne and Chamberlain 1963). Few measurements have been made on transitions other than these.

These two groups of transitions have small energy spreads within themselves and, owing to difficulties of experimental determinations and the inherent inaccuracy of theoretical values, the two groups behave like two large diffuse points on the temperature determination graph, thus masking any deviations from local thermodynamic equilibrium. With transition probabilities available for higher energy levels any deviations from linearity of the graph would become apparent and the accuracy of the temperature determination increased owing to the larger energy spread and greater number of lines involved.

It is, therefore, the purpose of this paper to extend the range of existing transition probabilities in neutral argon. Since neutral argon deviates seriously from LS coupling, and J_1j coupling is not completely satisfactory, the transition probabilities have been calculated in intermediate coupling for the following arrays:

4p → 4s	6s → 4p	4d → 4p
5p → 4s	7s → 4p	5d → 4p
6p → 4s		6d → 4p.

2. Method of calculation

The process of calculating intermediate coupling (IC) line strengths has been described before (Garstang 1954) and a brief outline only is given here. The electrostatic and spin–orbit parameters were constructed in LS coupling (Condon and Shortley 1963, pp. 197, 268, 269, 298, 299) and J_1j coupling (Condon and Shortley 1963, p. 271, 307, 313) using the phase rules (Condon and Shortley 1963, p. 270) in terms of Slater and spin–orbit parameters which were found by a least-squares fitting of the calculated eigenvalues of the total energy matrix to the observed energy levels (Moore 1949). Trial values of these parameters were put into an IBM 7090 least-squares fitting programme and treated as adjustable, and the

† Now at Electricity Council Research Centre, Capenhurst, Cheshire.

iterative procedure of parameter adjustment and energy level calculation terminated at a tolerance where there was no significant change in the parameters. The resulting eigenvectors of the energy matrix determine the mixing of the states involved, and form the transformation matrix from the initial line strength matrix to the intermediate coupling line strength matrix.

The eigenvectors obtained from the LS coupling representation showed substantial mixing between the states and thus one would expect the eigenvectors to be sensitive to the adopted parameters. Consequently the process was also carried out from the J_1j coupling representation. This also served as a check on the phase determination of the electrostatic and spin–orbit matrices, and on the line strength matrices, since the parameters in the first case and the intermediate line strengths in the second case should be approximately the same when obtained from both coupling schemes. This revealed eight significant discrepancies in previously calculated J_1j transition probabilities, summarized by Garstang and Van Blerkom (1965), due possibly to incorrect line strength determinations.

Table 1. Mixing of energy levels (%) in LS and J_1j coupling for 4p, 5p and 6p, $J = 2$

	E_n (cm^{-1})	$^3D_2$	$^1D_2$	$^3P_2$	$\frac{3}{2}\,\frac{3}{2}$	$\frac{3}{2}\,\frac{1}{2}$	$\frac{1}{2}\,\frac{3}{2}$
4p	107289	25	30	45	5	6	89
	106238	9	37	54	90	3	7
	105617	66	32	2	4	92	4
5p	118469	43	35	22	0.1	0.5	99.4
	117184	3	22	75	95	5	0
	116999	54	42	4	5	95	0
6p	122635	47	35	18	0	0	100
	121271	2	23	75	97	3	0
	121192	52	42	6	3	97	0

In table 1, the mixing of states, given by the square of the eigenvectors, is shown for the 4p, 5p and 6p levels in LS and J_1j coupling. The inability of the LS coupling scheme to describe the levels unambiguously is clearly shown and it can also be seen that J_1j coupling, though not perfect, is a far better approximation.

The Slater and spin–orbit parameters adopted here are given in table 2 for the various configurations. The calculated and observed energy levels are given in table 3. The line strength matrices were calculated in terms of Racah 6–j symbols (Rotenburg *et al.* 1959) using the following formulae (Wybourne 1965) for transitions $l^Nl' \rightarrow l^Nl''$. The transition probability is defined as

$$A(\alpha J;\, \alpha' J') = \frac{1}{2J+1}\,\frac{64\pi^4\sigma^3}{3h}\,\mathscr{L}(\alpha J;\, \alpha' J')$$

where, in LS coupling, the line strength $\mathscr{L}(\alpha J;\, \alpha' J')$ is given by

$$\begin{aligned}\mathscr{L}^{1/2}(\alpha J;\, \alpha' J') &= \mathscr{L}^{1/2}(\alpha SLJ;\, \alpha' SL'J') \\ &= (-1)^{J+L'+S+L_1+L+l''+s}[LL'][JJ']\begin{Bmatrix} J1J' \\ L'SL \end{Bmatrix}\begin{Bmatrix} L1L' \\ l''L_1l' \end{Bmatrix} l_>{}^{1/2}s\end{aligned}$$

and in J_1j coupling

$$\begin{aligned}\mathscr{L}^{1/2}(\alpha J;\, \alpha' J') &= \mathscr{L}^{1/2}(\alpha_1 J_1 jJ;\, \alpha_1 J_1 j'J') \\ &= (-1)^{J+J_1+j'+j+l''+s+g}[JJ'][jj']\begin{Bmatrix} J1J' \\ j'J_1j \end{Bmatrix}\begin{Bmatrix} j1j' \\ l''sl' \end{Bmatrix} l_>{}^{1/2}s;\end{aligned}$$

σ is the wave number of the transition, the transition moment s is given by

$$s(n'l';\, n''l'') = -e\int_0^\infty rR(n'l')R(n''l'')\,dr$$

$$g = \tfrac{1}{2}(l''-l'+1)$$

Table 2. Slater and spin–orbit parameters (cm^{-1})

Parameter	Level								
	4s	6s	7s	4p	5p	6p	4d	5d	6d
F_0	94339·7	120221·1	122943·8	106035·5	117450	121654·3	119572	122544	124172·6
F_2	—	—	—	177·5	48·1	19·4	81·5	36·3	29·3
G_0	—	—	—	693·4	217·9	97·3	—	—	—
G_1	725·1	67·3	26·0	—	—	—	68·9	44·3	14·9
G_2	—	—	—	41·6	13·3	6·4	—	—	—
G_3	—	—	—	—	—	—	6·1	3·2	1·8
ξ_{3p}	938·5	951·3	950·8	920·7	946·9	945·0	894·7	888·1	927·3
ξ_{4p}	—	—	—	24·4	—	—	—	—	—
ξ_{5p}	—	—	—	—	14·6	—	—	—	—
ξ_{6p}	—	—	—	—	—	9·8	—	—	—
ξ_{4d}	—	—	—	—	—	—	−2·9	—	—
ξ_{5d}	—	—	—	—	—	—	—	9·9	—
ξ_{6d}	—	—	—	—	—	—	—	—	−4·7

the notation

$$[XY] = \{(2X+1)(2Y+1)\}^{1/2}$$

and $l_>$ is the larger value of l involved in the transition.

Table 3. Comparison of observed and calculated energy levels (cm^{-1})

$3p^54s$			$3p^56s$			$3p^57s$		
Obs.	Calc.	Diff.	Obs.	Calc.	Diff.	Obs.	Calc.	Diff.
93144	93145	−1	119683	119678	5	122440	122442	−2
95399	95399	0	121161	121153	8	123882	123887	−4
93751	93749	2	119760	119765	−5	122479	122477	2
94553	94553	0	121097	121105	−8	123873	123869	4
$3p^54p$			$3p^55p$			$3p^56p$		
Obs.	Calc.	Diff.	Obs.	Calc.	Diff.	Obs.	Calc.	Diff.
105463	105410	53	116943	116936	7	121165	121167	−2
107289	107267	22	118469	118466	3	122635	122631	4
106238	106264	−26	117184	117189	−5	121271	121273	−2
105617	105607	10	116999	116999	0	121192	121194	−2
107496	107520	−24	118459	118469	−10	122610	122616	−6
107132	107122	10	118407	118394	13	122601	122592	9
106087	106091	−4	117151	117155	−4	121257	121255	2
104102	104128	−26	116660	116666	−6	121069	121070	−1
108723	108719	4	118871	118878	−7	122791	122798	−7
107054	107073	−19	117563	117554	9	121470	121464	6
$3p^54d$			$3p^55d$			$3p^56d$		
Obs.	Calc.	Diff.	Obs.	Calc.	Diff.	Obs.	Calc.	Diff.
119023	118959	64	122036	122037	−1	123653	123646	7
120754	120719	35	123557	123555	2	125150	125158	−8
119566	119619	−53	122330	122349	−19	123833	123874	−41
119213	119174	39	122160	122132	28	123774	123734	40
120619	120674	−55	123506	123488	18	125113	125126	−13
120601	120561	40	123373	123434	−61	125067	125115	−48
119445	119445	0	122282	122255	27	123827	123851	−24
118907	118913	−6	122087	122059	28	123809	123677	132
121012	121035	−23	123816	123773	43	125286	125220	66
119848	119827	21	122514	122560	−46	123822	123847	−25
118651	118668	−17	121933	121910	23	123468	123555	−87
118512	118559	−47	121794	121831	−37	123509	123511	−2

The calculated line strengths were then placed on an absolute scale in terms of s^2, the square of the transition moment, values of which were obtained using the Coulomb approximation (Bates and Damgaard 1949). Separate values were obtained for levels with different parentage by averaging the effective quantum numbers for each parent of each quantum level. The values of s^2 used are given in table 4.

Landé g factors were also calculated in intermediate coupling (Condon and Shortley 1963, p. 385) and are compared with LS, J_1j and observed values in tables 5 and 6.

Table 4. Values of the square of the transition moment, s^2 (A.U.)^2

Transition	s^2	Transition	s^2	Transition	s^2
$4p(\frac{1}{2})$–$4s(\frac{1}{2})$	9·0	$6s(\frac{1}{2})$–$4p(\frac{1}{2})$	0·45	$4d(\frac{1}{2})$–$4p(\frac{1}{2})$	0·045
$4p(\frac{3}{2})$–$4s(\frac{3}{2})$	9·0	$6s(\frac{3}{2})$–$4p(\frac{3}{2})$	0·52	$4d(\frac{3}{2})$–$4p(\frac{3}{2})$	0·063
$5p(\frac{1}{2})$–$4s(\frac{1}{2})$	0·90	$7s(\frac{1}{2})$–$4p(\frac{1}{2})$	0·083	$5d(\frac{1}{2})$–$4p(\frac{1}{2})$	0·049
$5p(\frac{3}{2})$–$4s(\frac{3}{2})$	0·95	$7s(\frac{3}{2})$–$4p(\frac{3}{2})$	0·12	$5d(\frac{3}{2})$–$4p(\frac{3}{2})$	0·034
$6p(\frac{1}{2})$–$4s(\frac{1}{2})$	0·013			$6d(\frac{1}{2})$–$4p(\frac{1}{2})$	0·027
$6p(\frac{3}{2})$–$4s(\frac{3}{2})$	0·015			$6d(\frac{3}{2})$–$4p(\frac{3}{2})$	0·022

Table 5. Comparison of Landé *g* factors

	$3p^5 4s$				$3p^5 6s$				$3p^5 7s$			
Level (cm^{-1})	93144	95399	93751	94553	119683	121161	119760	121097	122440	123882	122479	123873
Desig.	$1s_5$	$1s_2$	$1s_4$	$1s_3$	$3s_5$	$3s_2$	$3s_4$	$3s_3$	$4s_5$	$4s_2$	$4s_4$	$4s_3$
LS	1·500	1·000	1·500	0·000	1·500	1·000	1·500	0·000	1·500	1·000	1·500	0·000
J_1j	1·500	1·333	1·167	0·000	1·500	1·333	1·167	0·000	1·500	1·333	1·167	0·000
IC	1·506	1·102	1·404	0·000	1·500	1·271	1·184	0·000	1·506	1·296	1·164	0·000
Obs.	1·500	1·1014	1·399	0·000	1·500	1·311	1·189	0·000	1·500	1·325	1·175	0·000

	$3p^5 4p$									
Level (cm^{-1})	105463	107289	106238	105617	107496	107132	106087	104102	108723	107054
Desig.	$2p_9$	$2p_3$	$2p_6$	$2p_8$	$2p_2$	$2p_4$	$2p_7$	$2p_{10}$	$2p_1$	$2p_5$
LS	1·333	1·000	1·500	1·167	1·500	1·000	0·500	2·000	0·000	0·000
J_1j	1·333	1·167	1·333	1·167	0·666	1·500	1·333	1·500	0·000	0·000
IC	1·338	1·260	1·305	1·112	1·380	0·819	0·838	1·985	0·000	0·000
Obs.	1·333	1·265	1·282	1·119	1·362	0·877	0·786	1·975	0·000	0·000

	$3p^5 5p$									
Level (cm^{-1})	116943	118469	117184	116999	118459	118407	117151	116660	118871	117563
Desig.	$3p_9$	$3p_3$	$3p_6$	$3p_8$	$3p_2$	$3p_4$	$3p_7$	$3p_{10}$	$3p_1$	$3p_5$
LS	1·333	1·167	1·500	1·000	1·500	0·500	1·000	2·000	0·000	0·000
J_1j	1·333	1·167	1·333	1·167	0·666	1·500	1·333	1·500	0·000	0·000
IC	—	1·18	1·42	1·09	1·45	0·61	1·01	1·90	0·000	0·000
Obs.	1·333	1·180	1·378	1·109	1·456	0·645	1·007	1·892	0·000	0·000

	$3p^5 6p$									
Level (cm^{-1})	121165	122635	121271	121192	122610	122601	121257	121069	122791	121470
Desig.	$4p_9$	$4p_3$	$4p_6$	$4p_8$	$4p_4$	$4p_2$	$4p_7$	$4p_{10}$	$4p_1$	$4p_5$
LS	1·333	1·167	1·500	1·000	1·500	1·500	1·000	2·000	0·000	0·000
J_1j	1·333	1·167	1·333	1·167	0·666	1·500	1·333	1·500	0·000	0·000
IC	—	—	—	—	—	—	—	—	—	—
Obs.	1·333	1·170	1·378	1·119	1·502	0·626	1·032	1·839	0·000	0·000

Table 6. Comparison of Landé *g* factors

	$3p^5 4d$											
Level (cm^{-1})	119024	120754	119566	119213	120619	120601	119445	118907	121012	119848	118651	118512
Desig.	$4d_4'$	$4s_1''$	$4d_1'$	$4d_4$	$4s_1'''$	$4s_1''$	$4d_1''$	$4d_3$	$4s_1'$	$4d_2$	$4d_5$	$4d_6$
LS	1·250	1·000	1·333	1·083	1·167	0·667	1·000	1·500	0·500	1·000	1·500	0·000
J_1j	1·250	1·111	1·240	1·067	1·290	0·767	1·067	1·211	0·833	1·100	1·066	0·000
IC	1·255	1·133	—	1·077	0·987	1·057	0·908	1·437	0·877	0·768	1·467	0·000
Obs.	1·250	1·141	1·194	1·081	1·169	0·866	0·869	1·429	0·783	0·758	1·459	0·000
	$3p^5 5d$											
Level (cm^{-1})	122036	123557	122330	122160	123506	123373	122282	122087	123816	122514	121933	121794
Desig.	$5d_4'$	$5s_1''$	$5d_1'$	$5d_4$	$5s_1'''$	$5s_1''$	$5d_1''$	$5d_3$	$5s_1'$	$5d_2$	$5d_5$	$5d_6$
LS	1·250	1·000	1·333	1·083	1·167	0·667	1·000	1·500	1·000	0·500	1·500	0·000
J_1j	1·250	1·111	1·240	1·067	1·290	0·767	1·067	1·211	0·833	1·100	1·066	0·000
IC	1·253	1·127	1·199	1·076	0·802	1·265	0·941	1·387	0·846	0·813	1·400	0·000
Obs.	1·250	1·119	1·209	1·087	1·232	0·794	0·934	1·374	0·831	0·756	1·413	0·000
	$3p^5 6d$											
Level (cm^{-1})	123653	125150	123833	123774	125113	125067	123827	123809	125286	123822	123468	123509
Desig.	$6d_4'$	$6s_1''$	$6d_1'$	$6d_4$	$6s_1'''$	$6s_1''$	$6d_1''$	$6d_3$	$6s_1'$	$6d_2$	$6d_5$	$6d_6$
LS	1·250	1·000	1·333	1·083	1·167	0·667	1·000	1·500	0·500	1·000	1·500	0·000
J_1j	1·250	1·111	1·240	1·067	1·290	0·767	1·067	1·211	0·833	1·100	1·066	0·000
IC	1·256	1·098	1·245	1·052	0·777	1·264	1·107	1·206	—	—	1·233	0·000
Obs.	1·250	1·122	1·228	1·066	1·204	0·826	0·950	1·354	0·770	0·810	1·420	0·000

3. Results and conclusions

The calculated transition probabilities are listed in tables 7, 8 and 9, the wavelengths being given *in vacuo*. Experimental measurements only exist (in any quantity) for the 4p → 4s and 5p → 4s transitions and these have already been compared with the theoretical values (Garstang and Van Blerkom 1965). Few experimental measurements have been published for the other transitions and consequently no comparison is possible yet. The author has measured 120 representative transition probabilities from these calculated arrays and the results will be published at a later date.

Table 7. Transition probabilities for 6s → 4p, 7s → 4p ($\times 10^{-7}$ sec^{-1})

J value									
Upper	Lower	λ_{vac}(6s–4p)	*LS*	IC	J_1j	λ_{vac}(7s–4p)	*LS*	IC	J_1j
2	3	7032·3	0·43	0·43	0·43	5890·3	0·17	0·17	0·17
2	2	8068·4	—	0·022	—	6600·2	—	0·0096	—
2	2	7437·7	0·19	0·16	0·12	6172·1	0·078	0·066	0·052
2	2	7109·3	0·073	0·081	0·15	5944·2	0·029	0·034	0·059
2	1	8205·5	0·048	0·016	—	6691·6	0·020	0·0070	—
2	1	7967·5	—	0·0034	—	6532·5	—	0·0014	—
2	1	7355·1	0·0045	0·021	0·14	6115·1	0·0018	0·0089	0·054
2	1	6418·1	0·14	0·17	0·040	5453·2	0·052	0·066	0·016
1	2	7208·8	—	0·36	0·40	6026·6	—	0·12	0·13
1	2	6701·1	0·13	0·043	—	5667·6	0·039	0·012	—
1	2	6433·4	0·43	0·013	—	5475·0	0·13	0·0053	—
1	2	8018·6	0·34	0·00042	—	6583·3	0·14	—	—
1	2	7395·4	—	0·13	0·22	6157·3	—	0·055	0·089
1	2	7070·6	—	0·35	0·25	5930·5	—	0·14	0·098
1	1	7318·0	0·058	0·13	0·077	6102·8	0·018	0·042	0·025
1	1	7128·1	—	0·076	0·17	5970·1	—	0·024	0·054
1	1	6633·9	0·13	0·014	—	5619·6	0·041	0·0056	—
1	1	5862·0	0·15	0·045	—	5055·6	0·044	0·014	—
1	1	8153·9	—	0·0033	—	6674·2	—	0·0020	—
1	1	7918·9	0·21	0·028	—	6515·9	0·088	0·013	—
1	1	7313·7	—	0·19	0·045	6100·5	—	0·076	0·018
1	1	6386·5	—	0·059	0·33	5441·8	—	0·022	0·13
1	0	8039·9	—	0·047	0·059	6596·7	—	0·016	0·020
1	0	7088·7	0·086	0·018	—	5942·5	0·027	0·0062	—
1	0	9060·4	0·047	0·0097	—	7269·6	0·022	0·0050	—
1	0	7870·3	—	0·057	0·072	6483·0	—	0·024	0·030
0	1	7352·4	0·23	0·20	0·46	6106·1	0·075	0·066	0·15
0	1	7160·8	—	0·40	0·25	5973·4	—	0·13	0·081
0	1	6662·2	0·51	0·11	—	5622·4	0·16	0·033	—
0	1	5884·1	0·15	0·073	—	5057·9	0·044	0·022	—

Apart from the discrepancies in the J_1j values mentioned above, the 4p → 4s and 5p → 4s arrays agree with those previously calculated, the difference of a few percent, which is insignificant, being due to a different choice of s^2.

It will be noticed that some of the transition probabilities of the 4d → 4p array are smaller than those of the 5d → 4p array, owing to the value of s^2 increasing for those levels of parentage $\frac{1}{2}$, together with the inverse wavelength cubed dependence of the transition probability. This implies that the 5d levels with parentage $\frac{1}{2}$ are being perturbed, causing their quantum defect to be larger rather than smaller than the 4d values. This is also reflected in the Landé *g* values where, apart from the s_1'''' and s_1'' levels which have parentage $\frac{1}{2}$, the agreement between intermediate coupling and observation is better than that of the other coupling schemes. (No configuration interaction effects have been considered here although their presence can be seen by the decreasing accuracy of the energy level fit with increasing energy (table 3). Because of this, an expected accuracy among the intermediate coupling transition probabilities from the higher energy levels of better than a factor of 2 would be optimistic and unlikely.)

Table 8. Transition probabilities for 4p → 4s, 5p → 4s, 6p → 4s ($\times 10^{-7}$ sec^{-1})

J value Upper	J value Lower	λ_{vac}(4p–4s)	LS	IC	J_1j	λ_{vac}(5p–4s)	LS	IC	J_1j	λ_{vac}(6p–4s)	LS	IC	J_1j
3	2	8117·5	3·33	3·33	3·33	4201·9	0·26	0·26	0·26	3568·8	0·066	0·066	0·066
2	2	7069·6	—	0·55	—	3948·7	—	0·0017	—	3390·9	—	0·020	—
2	2	7637·1	3·08	2·48	2·02	4159·7	0·20	0·19	0·13	3555·3	0·051	0·046	0·033
2	2	8017·3	0·88	0·97	1·74	4192·0	—	0·076	0·13	3565·3	—	0·023	0·033
2	1	8410·4	3·03	2·12	3·02	4334·6	—	0·17	0·22	3671·6	—	0·0043	0·053
2	1	7386·6	—	0·86	—	4045·6	0·022	0·058	—	3462·1	0·055	0·015	—
2	1	9225·9	—	0·57	—	4590·3	—	0·17	—	3865·2	—	0·0036	—
2	1	8008·3	0·89	0·49	1·71	4267·5	0·061	0·052	0·12	3633·7	0·016	0·017	0·031
2	1	9786·7	—	0·094	—	4629·6	0·18	0·022	—	3877·0	0·046	0·0056	—
2	1	8427·4	2·27	2·04	1·50	4301·4	—	0·14	0·12	3644·2	—	0·034	0·031
1	2	6967·7	2·24	0·73	—	3950·2	0·13	0·0098	—	3393·7	0·033	0·0006	—
1	2	7149·0	—	0·14	—	3958·4	0·0086	—	—	3394·8	0·0022	—	—
1	2	7726·2	0·11	0·53	—	4165·5	—	0·040	0·044	3557·1	—	0·0094	0·011
1	2	9125·8	1·33	1·67	1·98	4252·4	0·14	0·21	0·21	3581·0	0·038	0·056	0·055
1	1	8266·5	—	1·70	2·12	4336·5	—	0·10	0·15	3675·0	—	0·021	0·035
1	1	7275·4	1·19	0·19	—	4047·3	0·072	0·024	—	3465·1	0·019	0·0064	—
1	1	8523·0	2·92	1·25	0·97	4346·3	—	0·083	0·073	3676·2	—	0·023	0·018
1	1	7473·3	—	0·040	—	4055·8	0·012	0·015	—	3466·2	0·030	0·0069	—
1	1	9356·3	—	0·060	—	4597·3	0·19	0·027	—	3867·3	0·046	0·008	—
1	1	8106·4	1·43	2·42	2·81	4273·5	—	0·17	0·20	3635·6	—	0·044	0·053
1	1	11490·3	—	0·017	—	4703·4	—	0·00028	—	3895·6	—	0·0004	—
1	1	9660·9	0·67	0·46	0·33	4365·1	0·077	0·039	0·038	3660·6	0·021	0·0082	0·010
1	0	7726·2	1·30	1·14	1·30	4183·1	0·082	0·10	0·081	3564·2	0·020	0·031	0·019
1	0	7949·8	—	1·91	2·39	4192·2	0·13	0·14	0·16	3565·3	0·033	0·027	0·039
1	0	8670·0	1·54	0·32	—	4425·2	—	0·00095	—	3744·8	—	—	—
1	0	10472·3	0·18	0·085	—	4523·5	0·022	0·0025	—	3771·3	0·0055	—	—
0	1	7505·3	4·30	4·30	4·30	4260·4	0·24	0·22	0·24	3650·7	—	0·047	0·054
0	1	6679·1	—	0·0046	—	3980·9	—	0·022	—	3443·5	0·076	0·010	—
0	1	8580·0	—	0·0019	—	4511·8	—	0·014	—	3835·7	0·047	0·0065	—
0	1	7517·1	4·24	4·23	4·22	4199·6	0·26	0·24	0·26	3607·6	—	0·056	0·065

Table 9. Transition probabilities for 4d → 4p, 5d → 4p, 6d → 4p ($\times 10^{-7}$ sec^{-1})

J value		λ_{vac}(4d–4p)	LS	IC	J_1j	λ_{vac}(5d–4p)	LS	IC	J_1j	λ_{vac}(6d–4p)	LS	IC	J_1j
Upper	Lower												
4	3	7374·6	0·19	0·19	0·19	6033·9	0·18	0·18	0·18	5497·5	0·16	0·16	0·16
3	3	6539·8	—	0·0027	—	5526·7	—	0·00098	—	5079·5	—	0·00058	—
3	3	7090·7	0·047	0·034	0·043	5928·7	0·044	0·031	0·040	5443·7	0·037	0·034	0·033
3	3	7272·7	0·022	0·032	0·027	5989·1	0·022	0·034	0·026	5461·2	0·018	0·021	0·022
3	2	7426·7	0·13	0·13	0·13	6147·0	0·25	0·24	0·25	5598·8	0·18	0·17	0·18
3	2	6889·0	—	0·0051	—	5774·0	—	0·018	—	5287·6	—	0·0012	—
3	2	6606·3	—	0·00022	—	5574·1	—	0·0036	—	5119·5	—	0·0046	—
3	2	8145·3	—	0·0013	—	6648·5	—	0·0036	—	6044·5	—	0·0033	—
3	2	7503·0	0·13	0·14	0·15	6214·3	0·13	0·12	0·14	5683·4	0·11	0·10	0·12
3	2	7169·0	0·0057	0·016	—	5983·4	0·0054	0·019	—	5489·7	0·0045	0·0052	—
3	2	8386·4	—	—	—	6724·5	—	0·0014	—	6066·1	—	0·0015	—
3	2	7707·1	—	0·0022	0·0056	6280·6	—	0·0021	0·0056	5702·6	—	—	0·0049
3	2	7355·1	0·17	0·16	0·16	6044·9	0·17	0·15	0·16	5507·5	0·14	0·14	0·13
2	3	6598·0	0·03	0·0011	—	5542·3	0·39	0·00048	—	5089·1	0·27	0·00026	—
2	3	6605·9	0·00087	0·00033	—	5583·5	0·0015	—	—	5101·0	0·0010	—	—
2	3	7152·1	—	0·0039	0·0097	5945·7	—	0·0033	0·0092	5445·4	—	0·0035	0·0077
2	3	7438·3	0·0043	0·0076	0·0037	6015·4	0·0045	0·0093	0·0038	5450·8	0·0038	0·0073	0·0033
2	2	7501·9	—	0·010	0·013	6166·4	—	0·022	0·025	5610·4	—	0·028	0·017
2	2	6953·6	0·031	0·017	—	5791·1	0·055	0·015	—	5298·0	0·039	0·0096	—

Table 9 (cont.)

J value Upper	*J* value Lower	λ_{vac}(4d–4p)	*LS*	IC	J_1j	λ_{vac}(5d–4p)	*LS*	IC	J_1j	λ_{vac}(6d–4p)	*LS*	IC	J_1j
2	2	6665·8	0·032	0·0021	—	5590·0	0·056	0·0029	—	5129·3	0·040	0·0020	—
2	2	7512·0	—	0·014	0·020	6217·4	—	0·028	0·037	5624·9	—	0·0092	0·026
2	2	6962·3	—	0·0004	—	5836·0	—	0·0026	—	5311·0	—	0·00027	—
2	2	6673·8	0·029	0·0021	—	5631·9	0·053	—	—	5141·4	0·035	—	—
2	2	8226·4	0·034	0·00039	—	6669·8	0·035	0·0012	—	6046·7	0·030	0·0016	—
2	2	7571·7	—	0·0023	0·012	6232·9	—	0·00093	0·011	5685·4	—	0·0020	0·0097
2	2	7231·7	—	0·063	0·084	6000·6	—	0·062	0·080	5491·5	—	0·053	0·067
2	2	8607·3	—	0·012	—	6757·7	—	0·010	—	6053·3	—	0·0080	—
2	2	7893·3	0·049	0·052	0·055	6309·5	0·051	0·065	0·058	5691·2	0·045	0·058	0·052
2	2	7524·5	0·00074	0·011	—	6071·6	0·00078	0·0026	—	5496·9	0·00067	0·0012	—
2	1	7620·2	0·070	0·094	0·11	6246·1	0·14	0·19	0·22	5676·3	0·095	0·12	0·15
2	1	7414·5	—	0·0035	—	6107·2	—	0·0066	—	5561·4	—	0·0025	—
2	1	6881·4	0·0064	0·0022	—	5740·9	0·012	0·0039	—	5256·0	0·0080	—	—
2	1	6054·4	—	0·0051	—	5153·6	—	0·029	—	4759·4	—	0·022	—
2	1	7630·7	—	0·00087	0·0021	6298·4	—	0·00075	0·0040	5691·2	—	0·0074	0·0028
2	1	7424·5	—	0·12	0·11	6157·3	—	0·20	0·21	5575·7	—	0·15	0·15
2	1	6889·9	0·14	0·0057	—	5785·0	0·26	0·030	—	5268·7	0·18	0·27	—
2	1	6061·0	—	—	—	5189·1	—	—	—	4769·9	—	0·0011	—
2	1	8368·9	—	—	—	6763·2	—	—	—	6123·3	—	—	—

Table 9 (cont.)

J value		λ_{vac}(4d–4p)	LS	IC	J_1j	λ_{vac}(5d–4p)	LS	IC	J_1j	λ_{vac}(6d–4p)	LS	IC	J_1j
Upper	Lower												
2	1	8121·5	0·11	0·00091	—	6600·7	0·11	0·0085	—	5989·8	0·094	0·0086	—
2	1	7486·2	—	0·12	0·076	6174·7	—	0·10	0·074	5637·0	—	0·086	0·061
2	1	6517·6	—	—	0·015	5500·6	—	—	0·013	5069·7	—	—	0·011
2	1	8763·5	0·017	0·00017	—	6853·5	0·012	0·0015	—	6130·1	0·012	0·0023	—
2	1	8492·6	—	0·0023	—	6686·7	—	0·0018	—	5996·3	—	0·0018	—
2	1	7800·3	0·000045	0·0055	—	6250·0	0·000047	0·0046	—	5642·7	0·000041	0·0073	—
2	1	6754·5	0·14	0·11	0·16	5560·2	0·13	0·10	0·15	5074·3	0·11	0·083	0·13
1	2	7287·0	—	0·0022	0·0039	6050·7	0·0052	0·0054	0·0075	5556·5	—	0·0039	0·005
1	2	6768·6	0·0037	0·0025	—	5688·9	—	0·0030	—	5249·9	0·0044	0·0013	—
1	2	6495·6	0·012	0·0057	—	5494·8	—	0·00025	—	5084·1	0·015	0·00087	—
1	2	7962·4	0·0042	0·00021	—	6568·1	—	—	—	6048·5	0·0039	0·00068	—
1	2	7347·5	—	0·00025	0·0096	6144·0	0·0054	—	0·0089	5687·0	—	0·00058	0·0073
1	2	7026·9	—	0·010	—	5918·2	0·018	0·0077	—	5493·0	—	0·0085	—
1	2	8801·3	—	0·0038	—	6828·7	—	0·0041	—	6180·9	—	0·0031	—
1	2	8056·1	0·025	0·022	0·013	6371·5	0·028	0·025	0·014	5803·8	0·024	0·021	0·012
1	2	7672·2	0·0035	0·0067	0·024	6129·0	0·0037	0·0085	0·025	5601·9	0·0032	0·0051	0·021
1	1	7398·6	0·043	0·038	0·019	6127·5	—	0·068	0·036	5621·1	0·053	0·046	0·024
1	1	7204·6	—	0·018	0·041	5993·8	0·081	0·039	0·077	5508·4	—	0·021	0·051
1	1	6700·2	0·035	0·0030	—	5640·5	—	0·0026	—	5208·6	0·041	0·0088	—

Table 9 (cont.)

J value Upper	*J* value Lower	λ_{vac}(4d–4p)	*LS*	IC	J_1j	λ_{vac}(5d–4p)	*LS*	IC	J_1j	λ_{vac}(6d–4p)	*LS*	IC	J_1j
1	1	5913·7	—	0·00079	—	5072·5	—	0·0049	—	4720·5	—	0·0067	—
1	1	8095·9	—	0·00031	—	6501·1	—	0·0075	—	6125·2	—	—	—
1	1	7864·1	0·065	0·0098	—	6087·5	0·050	0·069	—	5991·6	0·052	0·011	—
1	1	7266·9	—	0·076	—	5431·2	—	0·0019	0·12	5638·6	—	0·055	—
1	1	6350·8	—	—	0·13	6756·3	—	0·0022	—	5071·0	—	0·0012	0·092
1	1	8964·6	0·011	0·0059	—	6310·7	0·0011	0·0046	0·11	6261·0	0·011	0·0093	—
1	1	8681·3	—	0·0019	—	5608·2	0·13	0·15	0·0052	6121·4	—	0·00034	—
1	1	7959·2	0·0011	0·0018	0·11	6658·7	0·064	0·00035	—	5753·4	0·00097	0·00075	0·097
1	1	6873·3	0·13	0·15	0·0052	6926·6	0·013	0·0093	—	5163·7	0·11	0·12	0·0043
1	0	8137·4	—	0·048	0·056	6625·6	0·079	0·10	0·11	6037·6	—	0·060	0·078
1	0	7164·4	0·062	0·010	—	5965·9	—	0·016	—	5484·9	0·079	0·027	—
1	0	8988·8	0·058	0·0085	—	7251·1	—	0·0066	—	6623·0	0·051	0·012	—
1	0	7816·2	—	0·066	0·080	6468·3	0·092	0·069	0·077	5963·7	—	0·044	0·063
1	0	10072·5	—	0·000065	—	7570·0	—	—	—	6782·0	—	0·00068	—
1	0	8622·9	0·016	0·0082	0·0066	6720·9	0·019	0·0049	0·0076	6092·4	0·016	0·0093	0·0067
0	1	9077·7	0·043	0·014	—	6994·0	0·051	0·016	—	6244·9	0·046	0·015	—
0	1	8787·3	—	0·0030	—	6820·4	—	0·0035	—	6106·1	—	0·0032	—
0	1	8048·3	0·0041	0·020	0·12	6366·6	0·0044	0·022	0·13	5739·9	0·0039	0·019	0·12
0	1	6939·6	0·13	0·16	0·038	5652·3	0·13	0·16	0·038	5152·8	0·11	0·14	0·033

Acknowledgments

The author would like to express his gratitude to Professor W. R. S. Garton for his supervision, Mr. S. E. Budd for his help with the computations and the Science Research Council for a research studentship during which this work was carried out.

References

BATES, D. R., and DAMGAARD, A., 1949, *Phil. Trans. Roy. Soc.* A, **242**, 101–22.

CONDON, E. U., and SHORTLEY, G. H., 1963, *Theory of Atomic Spectra* (New York: Cambridge University Press).

DOHERTY, L. R., 1961, *Thesis*, University of Michigan.

DRAWIN, H. W., 1956, *Z. Phys.*, **146**, 295–313.

GARSTANG, R. H., 1954, *Mon. Not. R. Astr. Soc.*, **114**, 118–33.

GARSTANG, R. H., and VAN BLERKOM, J., 1965, *J. Opt. Soc. Am.*, **55**, 1054–7.

GERICKE, W. E., 1961, *Z. Astrophys.*, **53**, 68–79.

MOORE, C. E., 1949, *Nat. Bur. Stand. Circ.*, No. 467, Vol. 1 (Washington: U.S. Govt Printing Office).

OLSEN, H. N., 1963, *J. Quant. Spectrosc. Radiat. Transfer*, **3**, 59–76.

ROTENBURG, M., BIVINS, R., METROPOLIS, N., and WOOTON, J., 1959, *The 3–j and 6–j Symbols* (Cambridge, Massachusetts: Massachusetts Institute of Technology).

THORNE, A. P., and CHAMBERLAIN, J., 1963, *Proc. Phys. Soc.*, **82**, 133–41.

WYBOURNE, B. G., 1965, *Spectroscopic Properties of Rare Earths* (New York: Interscience), pp. 85, 86, 89.

BRIT. J. APPL. PHYS. (J. PHYS. D), 1968, SER. 2, VOL. 1. PRINTED IN GREAT BRITAIN

Determination of temperature in a radio-frequency discharge using a reversal technique

P. D. JOHNSTON†

Department of Physics, Imperial College, London

MS. received 25th July 1967, *in revised form 7th November* 1967

Abstract. An absorption technique for determining the temperature in a circularly symmetric discharge has been developed by Elder, Jerrick and Birkeland, and applied by them to a low-temperature discharge using a tungsten ribbon background source. This technique has been extended here to a higher temperature radio-frequency discharge in argon at atmospheric pressure using a condenser discharge background source. The measured off-axis temperature maximum of 9200°K is in agreement with previous measurements. The error introduced by the finite resolution of the spectrograph used is discussed.

1. Introduction

For the determination of atomic parameters from a discharge, such as transition probabilities and continuum intensity correction factors, a complete knowledge of the discharge conditions must be obtained. If local thermodynamic equilibrium (LTE) exists in the discharge, as it does with certain d.c. arcs and arc jets (Olsen 1959) and radio-frequency torch discharges (Johnston 1966), the problem becomes simply that of measuring the temperature of the discharge, whence populations, electron number density, etc. can be deduced.

An absorption method for temperature determination which is independent of any atomic parameter and only requires the existence of LTE between the states involved in the transition has been developed by Elder *et al.* (1965), and has been used by them to measure the temperature of a sodium seeded nitrogen discharge. This discharge was found to have a maximum temperature of 2600°K and a tungsten ribbon lamp was used as a background source. The experiment described here applies their technique to an atmospheric pressure radio-frequency discharge in argon of maximum temperature approximately 9000°K using a 'Garton-type' flash tube (Garton 1962) as the background source.

2. Theory

The theory has been described before (Elder *et al.* 1965) and will only be briefly outlined here. Two sets of measurements are made across the discharge. The first measurement is of the peak intensity of a suitable spectral line emitted by the discharge and the second is of this line intensity with a background source. The transmission of the discharge can then be obtained by subtracting the two measurements and dividing by the intensity of the background source. Once the radial profile of the absorption coefficient has been calculated by an Abel inversion procedure from the observed transmission the radial profile of the emission coefficient can be determined. If the states involved in the transition are in LTE with respect to each other, the ratio of the emission and absorption coefficients is equal to the Planck function, thus giving the temperature.

Because of the finite resolution of the dispersive system used the transmission is not measured at a precise frequency but integrated over the spectral slit width.

† Now at Electricity Council Research Centre, Capenhurst, Cheshire.

The transmission of the discharge at a frequency ν and a position x from the axis of symmetry is given by

$$\omega_\nu(x)=\exp\left(-2\int_x^R \frac{k_\nu(r)\,\rho(r)\,dr}{(r^2-x^2)^{1/2}}\right) \tag{1}$$

where $k_\nu(r)\,\rho(r)$ is the volume absorption coefficient and R the discharge radius.

By taking logarithms of both sides of this equation it can be put into the form of an Abel integral equation whence the absorption coefficient can be determined:

$$k_\nu(r)\,\rho(r)=-\frac{1}{\pi r}\frac{d}{dr}\int_r^R \left[\ln\frac{1}{\omega_\nu(x)}\right]\frac{x\,dr}{(x^2-r^2)^{1/2}}. \tag{2}$$

However, the quantity measured is not ω_ν at a precise frequency, say ω_{ν_0}, but

$$\frac{1}{\Delta\nu}\int_{-\Delta\nu/2}^{\Delta\nu/2}\omega_\nu(x)\,d\nu$$

where $\Delta\nu$ is the spectral slit width over which the transmission is integrated.

Equation (2) is valid if it can be written

$$\frac{1}{\Delta\nu}\int_{-\Delta\nu/2}^{\Delta\nu/2}k_\nu(r)\,\rho(r)\,d\nu=-\frac{1}{\pi r}\frac{d}{dr}\int_r^R\left\{\ln\left(\frac{1}{\Delta\nu}\int_{-\Delta\nu/2}^{\Delta\nu/2}\omega_\nu(x)\,d\nu\right)^{-1}\right\}\frac{x\,dx}{(x^2-r^2)^{1/2}}. \tag{3}$$

The left-hand side of this equation is the quantity deduced in all absorption experiments, not $k_\nu(r)\,\rho(r)$ at the line centre. However, the emission coefficient $j_\nu(r)\,\rho(r)$ is also measured as

$$\frac{1}{\Delta\nu}\int_{-\Delta\nu/2}^{\Delta\nu/2}j_\nu(r)\,\rho(r)\,d\nu$$

and since the frequency dependence of the emission and absorption coefficients is identical, the ratio of the two becomes j_ν/k_ν at the line centre.

To be able to write equation (3) requires that

$$\frac{1}{\Delta\nu}\int_{-\Delta\nu/2}^{\Delta\nu/2}\ln\frac{1}{\omega_\nu(x)}\,d\nu=\ln\left(\frac{1}{\Delta\nu}\int_{-\Delta\nu/2}^{\Delta\nu/2}\omega_\nu(x)\,d\nu\right)^{-1}.$$

Consequently the fractional error in $k_\nu(r)\,\rho(r)$ due to a finite spectral slit width will be

$$\left\{\frac{1}{\Delta\nu}\int_{-\Delta\nu/2}^{\Delta\nu/2}\ln\frac{1}{\omega_\nu(x)}\,d\nu-\ln\left(\frac{1}{\Delta\nu}\int_{-\Delta\nu/2}^{\Delta\nu/2}\omega_\nu(x)\,d\nu\right)^{-1}\right\}\left(\frac{1}{\Delta\nu}\int_{-\Delta\nu/2}^{\Delta\nu/2}\ln\frac{1}{\omega_\nu(x)}\,d\nu\right)^{-1}$$

$$=1-\ln\left(\frac{1}{\Delta\nu}\int_{-\Delta\nu/2}^{\Delta\nu/2}\omega_\nu(x)\,d\nu\right)\left(\frac{1}{\Delta\nu}\int_{-\Delta\nu/2}^{\Delta\nu/2}\ln\omega_\nu(x)\,d\nu\right)^{-1}. \tag{4}$$

Since the spatial inhomogeneity plays no part in this error treatment the functional dependence on position will be omitted for clarity.

Now

$$\omega_\nu=\exp(-k_\nu) \tag{5}$$

where for a Gaussian absorption profile

$$k_\nu=k_0\exp\left(\frac{-2(\nu-\nu_0)\,(\ln 2)^{1/2}}{\Delta\nu_D}\right)^2 \tag{6}$$

and for a dispersive profile

$$k_\nu = k_0 \left\{1 + \left(\frac{2(\nu-\nu_0)}{\Delta\nu_S}\right)^2\right\}^{-1} \tag{7}$$

where $\Delta\nu_D$ and $\Delta\nu_S$ are the appropriate half-widths of the profiles. Equation (4) can now be solved by expanding the logarithm in the numerator using the expansion

$$\ln y = \sum_{n=1}^{\infty} \frac{(-1)^{n+1}(y-1)^n}{n} \qquad \text{where} \qquad 0<y<2$$

since

$$0 < \frac{1}{\Delta\nu} \int_{-\Delta\nu/2}^{\Delta\nu/2} \omega_\nu d\nu < 1.$$

On expanding ω_ν and integrating the following expressions for the error are obtained:

$$1 + \frac{1}{\operatorname{erf}(x/\sqrt{2})} \sum_{n=1}^{\infty} \frac{(-1)^{n+1}}{n} \left(\frac{k_0\pi}{2x \ln 2}\right)^{n-1} \left[\sum_{m=1}^{\infty} \frac{(-1)^m (k_0)^{m-1}}{m!\sqrt{m}} \operatorname{erf}\left\{\frac{x}{\sqrt{2}}(2m \ln 2)^{1/2}\right\}\right]^n$$

for the Gaussian profile where $x = \Delta\nu/\Delta\nu_D$
and

$$1 + \frac{1}{\tan^{-1}x} \sum_{n=1}^{\infty} \frac{(-1)^{n+1}}{n} \left(\frac{k_0}{2x}\right)^{n-1} \left\{\sum_{m=1}^{\infty} \frac{(-1)^m}{m!} (k_0)^{m-1} \beta\left(\frac{x^2}{1+x^2}(\tfrac{1}{2}, m-\tfrac{1}{2})\right)\right\}^n$$

for the dispersive profile where $\beta(\{x^2/(1+x^2)\}(\frac{1}{2}, m-\frac{1}{2}))$ is an incomplete beta function (Pearson 1934) and $x = \Delta\nu/\Delta\nu_S$.

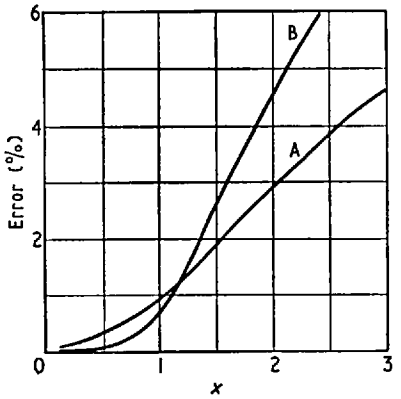

Figure 1. Percentage error plotted against x, the ratio of spectral slit width to spectral line width. Curve A, dispersive profile, curve B, Gaussian profile.

For a value of k_0, the absorption coefficient at the line peak, of 0·43 (the value obtained in the experiment described here), the two error curves are plotted in figure 1, where it can be seen that, in this case, a spectral slit width less than the line half-width will not cause any significant error.

3. Experimental procedure

Previous measurements of the radio-frequency discharge operating at 4·5 MHz (Johnston 1966) indicated that LTE prevailed, that the discharge temperature reached an off-axis maximum of about 9500°K and that the the $1s_5$–$2p_6$ 7635 Å line exhibited self-absorption. Consequently, this transition was chosen for the absorption measurement. The $1s_4$–$2p_5$ 7514 Å line was also used since the $1s_5$ level is metastable, and, despite the collision domination of LTE, the population of this level could be greater than one would expect from a Boltzmann distribution, causing an anomalously high value of absorption from this level.

The above error analysis suggests that a resolution equal to or better than the half-width of the spectral line is required to avoid any significant error in the measured absorption coefficient. The approximate conditions already found for this discharge indicate a half-width for the 7635 Å line of 0·11 Å due to Stark broadening (0·0235 Å half half-width) and Doppler broadening (0·0493 Å half 1/e width). In fact the line half-width will be slightly increased due to self-absorption. A resolution of the order of 3×10^5 is therefore required to resolve easily less than the half-width and so that the instrument width imposed by the grating does not influence the line width. This resolution was obtained by using a 6 in. 30 000 line/in. grating in the second order. At the wavelength involved, the angle of incidence of the grating was such that the focal plane was at a distance from the grating less than half its radius of curvature, i.e. for a 10 ft grating, the focus of the 7635 Å line in the second order would be approximately 4 ft from the grating. Since grating focusing mechanisms in most spectrographs do not operate up to such short distances from the exit plane, a 21 ft radius of curvature grating with the above specification was chosen and used in a 10 ft normal-incidence Eagle spectrograph. Incorrect focal plane curvature was of no consequence since focus was required over such a small spectral width as to be well within the depth of focus. With the plate holder at its maximum angle of 45° and an exit slit of 200 μm the bandwidth accepted by the detector was 0·09 Å.

A 'Garton-type' flash tube (Garton 1962) was used as the background source. This source gives a short intense pulse of continuum radiation, produced by the discharge of a 10 kv low-inductance capacitor through a ceramic capillary, which approximates a black body of approximately 29 000°K (Parkinson and Reeves 1961). The gate output of a Tektronix 551 oscilloscope triggered a thyratron circuit which in turn gave a 300 v pulse to a coaxial transformer which fired the flash tube. Since the intensity of the spectral lines from the radio-frequency discharge was observed to fluctuate at 300 Hz, the measurements of emission and transmission were made at the same point in the cycle by means of a synchronous chopper, driven by the same power supply as the radio-frequency generator and placed in front of the entrance slit of the spectrograph. Since previous measurements (Johnston 1966, Hughes and Wooding 1967) were made over a period of many cycles and thus gave some average temperature, and the temperature had been shown to vary by approximately ± 250degK over the cycle (Johnston, to be published), the mid-point of the cycle was chosen for these measurements (i.e. maximum negative gradient) so that a comparison with the previous work could be made. A pea-bulb and photomultiplier were placed either side of the chopper disk and the signal generated used to trigger the oscilloscope beams and gate output.

An RCA 7102 photomultiplier was chosen for detecting the signal since this had a AgOCs cathode surface which had the highest quantum efficiency at the wavelength concerned. The photomultiplier was cooled with liquid oxygen to reduce the cathode dark current and an extension glass tube sealed on to the photomultiplier envelope and terminated by a window 6 in. in front of the cathode and liquid-oxygen jacket to prevent icing over of the cathode window. The photomultiplier was mounted in the exit plane of the spectrograph behind a 200 μm slit and an EMI 9664B photomultiplier accepting a spectral bandwidth of 2·4 Å was mounted adjacent to it to monitor the flash-tube intensity, since the discharge continuum was transparent to the flash-tube continuum. The two output signals were displayed on the oscilloscope and recorded on 35 mm film using a Shackman camera mounted vertically to permit a greater number of exposures to be taken on a length of film.

The radio-frequency discharge apparatus has been described before (Johnston 1966), the only modification here being to the power input coil which was wound so that the coil planes were horizontal and the displacement from one turn to the next occurred at the side of the vertically mounted discharge tube, enabling a slit height on the spectrograph of 1 cm, equal to the spacing between the coils, to be used when scanning across the tube, since a one-to-one optical imaging system was used. The argon flow rate was increased from 60 to 70 l. min^{-1} so that wall heating during the long operating times ($\sim$1 hour) would not be serious.

The emission intensities of the 7635 and 7514 Å lines were transferred to an absolute

scale using a calibrated tungsten black-body lamp. Part of the optical scanning arrangement could be rotated through 180° so that the spectrograph and photomultiplier accepted the same solid angle of light from the tungsten lamp as from the discharge whilst retaining the mirrors and lenses of the optical system at the same angle. This output signal was measured on an Ecko vibrating-reed electrometer whose input resistor was calibrated with a standard cell and potentiometer bridge.

The effects of refraction and scattering of the light emitted from the discharge owing to striations and blemishes in the quartz discharge tube were measured by suspending an electrically heated wire down the centre of the tube, scanning the tube from side to side and measuring the intensity variation of the hot wire with position.

4. Results

The transmission of the 7635 Å line was measured twenty times in twenty-five positions and the 7515 Å line sixteen times in fifty positions across the discharge. The mean values of the absorption across the discharge for each of the lines were then calculated and the values Abel-inverted to give the radial profiles of the absorption coefficient. The calculation of the emission coefficients from the observed intensities requires a long iterative procedure involving the absorption coefficient to correct for self-absorption, and this necessitates magnetic disk storage on an IBM 7090 computer (J. W. Birkeland 1966 private communication). Details of the mathematics involved are given by Elder *et al.* (1965). However, in cases of small absorption, i.e. transmission not less than 80%, no iterative procedure is necessary and for transmissions not less than 60% only one iteration is required, and this only affects the first approximation to the emission coefficient by a few per cent. Consequently, the correction to the emission coefficient was simply calculated by curve fitting the calculated absorption and emission coefficients and solving analytically without any significant loss of accuracy but with considerable saving of computer time. The absorption and emission profiles across the discharge for both spectral lines are given in figure 2.

The temperature profiles obtained from the two lines are shown in figure 3 and the results agree well with previous measurements (Johnston 1966, Hughes and Wooding 1967). The steeper fall-off in temperature towards the walls compared with these previous measurements was caused by having a higher argon flow rate (70 l. min^{-1} as opposed to 60 l. min^{-1}). The largest error involved, that of calibration of the emission intensity (~5%), in this temperature régime would produce an error in the final temperature of about 2½%. By

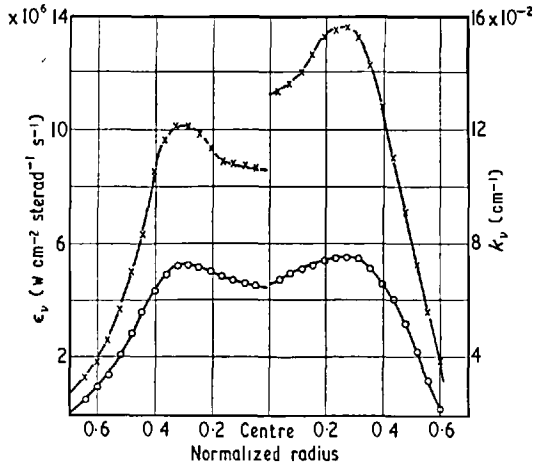

Figure 2. Absorption k_ν and emission ϵ_ν coefficients plotted against normalized tube radius. × 7635 Å, ○ 7514 Å.

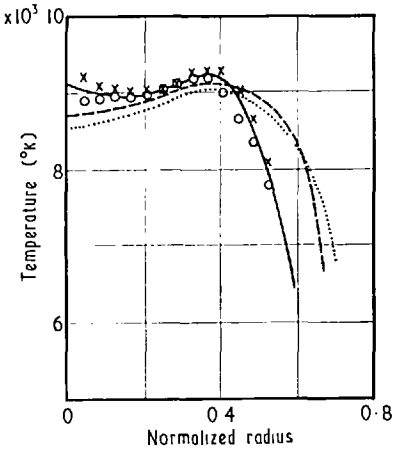

Figure 3. Temperature plotted against normalized tube radius. × from 7635 Å line, ○ from 7514 Å line; broken curve, Johnston (1966); dotted curve, Hughes and Wooding (1967).

using two different lines with different emission coefficients it is hoped that the final error in the averaged temperature distribution will be less than this. The errors caused by integration over the spectral slit width and the reiteration process in the data reduction are negligible compared with the above error.

5. Conclusions

The temperature obtained by absorption from the $1s_5$ metastable level agrees within the limits of error with that obtained from the non-metastable $1s_4$ level, indicating that under the conditions of LTE the metastable population in this discharge is what would be expected from a Boltzmann distribution.

This method of determining temperature distributions in dense inhomogeneous LTE discharges is extremely attractive from the point of view of high accuracy and independence of transition probability values, although it does not seem to be widely used. In fact, the 'reversal' method has even been erroneously dismissed as 'inapplicable' to inhomogeneous discharges (Griem 1964, Robinson and Lenn 1967).

Acknowledgments

The author would like to express his gratitude to Professor W. R. S. Garton for suggesting this work and to him and Dr. D. D. Burgess for useful discussions. Thanks are also due to the Science Research Council for a research studentship, during the tenure of which this work was carried out, and to the Central Research Fund for purchasing the radio-frequency generator.

References

ELDER, P., JERRICK, T., and BIRKELAND, J. W., 1965, *Appl. Optics*, **4**, 589–92.

GARTON, W. R. S., 1962, *Proc. 5th Int. Conf. on Ionization Phenomena in Gases, Munich*, 1961, Vol. 2 (Amsterdam: North-Holland), pp. 1884–8.

GRIEM, H. R., 1964, *Plasma Spectroscopy* (New York: McGraw-Hill).

HUGHES, D. W., and WOODING, E. R., 1967, *Phys. Letters*, **24A**, 70–1.

JOHNSTON, P. D., 1966, *Phys. Letters*, **20**, 499–501.

OLSEN, H. N., 1959, *Phys. Fluids*, **2**, 614–23.

PARKINSON, W. H., and REEVES, E. M., 1961, *Proc. Roy. Soc.* A, **262**, 409–19.

PEARSON, K., 1934, *Tables of the Incomplete Beta Function* (London: Biometrika Office, University College).

ROBINSON, D., and LENN, P. D., 1967, *Appl. Optics*, **6**, 983–1000.

TEMPERATURE AND ELECTRON DENSITY MEASUREMENTS IN AN R.F. DISCHARGE IN ARGON

P.D.JOHNSTON
Spectroscopy Department, Imperial College, London

Received 9 February 1966

Results of measurements of temperature and electron density distribution within an electrodeless discharge in argon at atmospheric pressure are briefly presented. The temperature is found to exhibit an off-axis peak of 9500°K.

This paper presents some results obtained during preliminary steps of research on the spectral and radiative characteristics of an electrodeless radio-frequency discharge in argon.

The discharge was excited in a continuously flowing stream of argon, fed into one end of a fused-quartz tube of two-inch internal diameter and about twelve inches long, the other end being open to the atmosphere. A five-turn coil of water cooled copper tubing was wound about the central four inches of the quartz tube and supplied with radio-frequency power from a "Radyne" 4-7 Mc/s, 15 kW oscillator. In the experiment reported here the oscillator was operated at 4.5 Mc/s and 6 kW. By arranging the argon gas inlet eccentrically, stability of the plasma and avoidance of excessive wall heating were achieved.

The discharge temperature was determined from the relative intensities of lines or argon I [1]. Two photomultipliers were used with a 10 foot normal-incidence Eagle spectrograph to record the intensities of the $3p^54s$ - $3p^54p$ and $3p^54s$ - $3p^55p$ line groups in the blue and the red. The intensities were measured at 20 positions across a diameter of the discharge between the radio-frequency coils. The measured intensities $I(y)$ were converted into radial intensities $I(r)$ by means of an Abel inversion [1]. If a Boltmann distribution of population in the excited states of neutral argon exists (see below), the graph of $\log I\lambda/gA$ versus E, (the excitation energy of the upper level of the line is a straightline with a slope inversely proportional to temperature. A typical result, in which the temperature is seen to reach a maximum value of 9500°K well off-axis is shown in graph I.

However, when the Fowler-Milne method [2, 9] was applied to the red 7635 Å line, an *on-axis* peak temperature of 16500°K was obtained. This

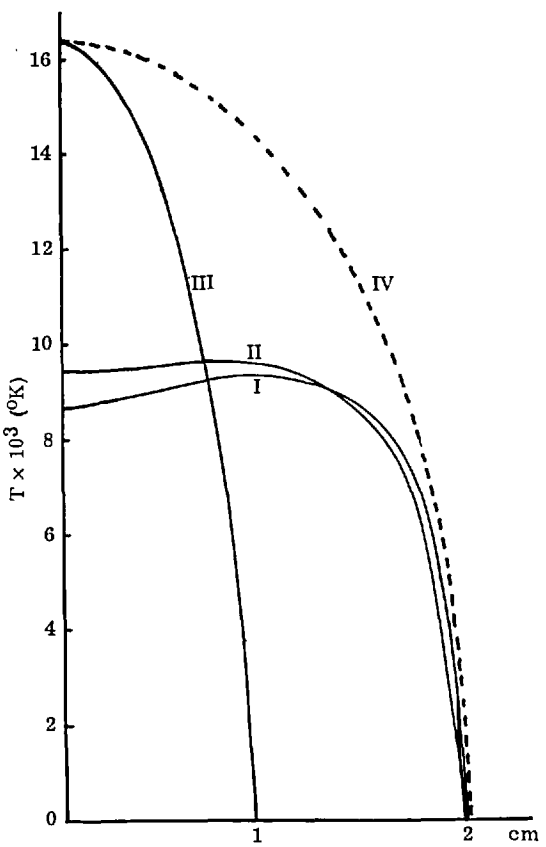

Fig. 1.

method depends on the fact that the intensity of a spectral line from a given ionisation stage (in this case the neutral atom) will increase with temperature, reach a maximum, and then decrease at higher temperatures due to removal of atoms from that ionisation stage to a higher one. It is assumed that the excited state used is in local thermodynamic equilibrium with the free-electrons.

The intensity distribution of the 7635 Å line across the discharge was measured and converted to a radial distribution. Off-axis peaks in intensity were obtained. (Off-axis peaks in intensity were also obtained for all the radial intensity distributions used in the relative line intensity temperature measurements) On identifying the off-axis intensity peaks with the line intensity maximum which occurs at 15 000°K for the 7635Å line, a temperature profile was obtained, graph IV. This was in excellent agreement with previous measurements [3] obtained on a similar discharge in argon of smaller size and lower power input, with the same line. The fact that no argon II lines could be seen in emission lends support to the lower temperature measurement.

The degree of local thermodynamic equilibrium was then determined by measuring the electron density. This was evaluated across the discharge from the Stark-broadened half-widths of the neutral argon lines. A scanning Fabry-Perot interferometer was used to measure the half-widths [4]. The Doppler half-width was estimated from the relative intensity temperature measurement, the instrument function was measured and these two contributions to the total half-width subtracted from it. The electron density was then obtained from the Stark broadening parameters [5a]. As the accuracy of these measurements was not expected to be high in view of uncertainties in the parameters, and as the temperature profile from the relative intensity measurements was reasonably flat-topped no attempt was made to convert the electron density measurements into a radial distribution.

The value obtained was 4.4×10^{15} electrons/cc in the centre of the discharge. It was also found that the 7635Å line had a slightly greater half-width in the centre of the discharge than that expected, indicating self-absorption. On applying the usual equation for the calculation of optical depth e.g. [6], with the measured values of electron density and temperature, it was found that this line should have an optical depth of about 0.3 corresponding to a drop in intensity of the line peak through re-absorption of about 7%.

Using the validity criteria for local thermodynamic equilibrium in an inhomogeneous time-independent plasma [5b] it was found that all the excited states of neutral argon were in equilibrium with the continuum, and the ground state, if not in complete local thermodynamic equilibrium was not far from it.

When the value of electron density together with the pressure balance condition was substituted into Saha's equation, the temperature obtained was 9000 ±500°K in agreement with the relative line intensity temperature measurement.

The line to continuum ratio was measured across a diameter of the plasma since, with substitution of Saha's equation, this ratio is a function of temperature only. Use of the Unsold-Kramers theory for the continuum intensity showed that a correction factor of 4.8 to the theoretical continuum intensity was needed to bring the temperature obtained by this method into agreement with the relative line intensity temperature measurements. This agrees well with the correction factor of 5 experimentally determined by Olsen [7] using a d.c. thermal arc running in argon. Graph II shows the temperature distribution using the correction factor of 5 suggested by Olsen.

We conclude that the off-axis peaks in line intensity after Abel inversion were not due to the maximum intensity temperature of the line being reached, and in the centre exceeded, previously as [3] concluded but due to the nature of the radio-frequency heating which occurs within a certain skin depth dependent on the frequency applied. The central portion of the discharge is heated only by radiation and thermal diffusion. The slight self-absorption of the 7635Å line would also enhance the central dip in inverted intensity of this line.

Recent Russian work on enclosed radio-frequency discharges [8] is in agreement with the above temperature measurements and shape of the temperature profile, obtained from the relative intensity measurements.

In conclusion it should be said that the Fowler Milne method cannot be used in this type of discharge, only when the distribution of two different ionisation stages of the same element can be examined [9].

The author would like to express his gratitude to Professor W.R.S.Garton for suggesting this topic and for his helpful supervision.

References

1. W.Pearce, Optical spectrometric measurements of high temperatures (University of Chicago Press 1961) p. 125.
2. R.H.Fowler, Statistical mechanics (Cambridge University Press, New York 2nd edition) chap. XV.

3. T. B. Reed, J. Apl. Phys. 32 no. 5 (1961).
4. J. Cooper and J. R. Grieg, J. Sci In. 40 (1963).
5. H. R. Griem. Plasma spectroscopy (Mc Graw Hill 1964) a) p. 495 b) chap. 6.
6. D. D. Burgess and J. Cooper, Proc. Phys. Soc. 85 (1965). 85.
7. H. N. Olsen, Phys. Rev. 124 no. 6 (1961).
8. B. M. Dymshits and Y. P. Koretskii Sov. Phys. Techn. Phys. 9 no. 9 (1965).
9. H. N. Olsen, Phys. Fluids 2 No. 6 (1959).

* * * * *